論文 / 著書情報
Article / Book Information

題目(和文)	ランダム量子スピン系の実空間くりこみ群による解析
Title(English)	Real-Space Renormalization-Group Analysis of Random Quantum Spin Systems
著者(和文)	宮崎涼二
Author(English)	Ryoji Miyazaki
出典(和文)	学位:博士(理学), 学位授与機関:東京工業大学, 報告番号:甲第9382号, 授与年月日:2014年3月26日, 学位の種別:課程博士, 審査員:西森 秀稔,斎藤 晋,田中 秀数,古賀 昌久,西田 祐介
Citation(English)	Degree:Doctor (Science), Conferring organization: Tokyo Institute of Technology, Report number:甲第9382号, Conferred date:2014/3/26, Degree Type:Course doctor, Examiner:,,,,
学位種別(和文)	博士論文
Type(English)	Doctoral Thesis

Dissertation

Real-Space Renormalization-Group Analysis of Random Quantum Spin Systems

Ryoji Miyazaki

Department of Physics, Tokyo Institute of Technology

February, 2014

Abstract

The present thesis investigates phase transitions and critical phenomena in the random transverse-field Ising models by means of a real-space renormalization-group method. The analysis is intended to examine the presence of infinite-randomness fixed points in the models in a renormalization-group picture.

Infinite-randomness fixed points are concerned with peculiar critical phenomena, which have been established in a study of the one-dimensional random transverse-field Ising model. Subsequent studies have conjectured the presence of the fixed point in some cases. The thesis mainly examines such two cases: the two- and three-dimensional Ising spin glasses in a transverse field and the one-dimensional Ising spin glass with the power-law interaction in a transverse field. The latter is not directly tackled. Instead, we introduce and analyze the hierarchical model which is expected to show similar critical phenomena.

A real-space renormalization-group method is exploited in the thesis. We develop the method in a model without randomness first. The method reproduces some previously known results of transition points and critical exponents in pure and disordered cases. The spin-glass models mentioned above are investigated with the method. We find evidence of the presence of infinite-randomness fixed points in these cases as a result, which supports the conjectures.

Acknowledgments

I would like to express my gratitude to my supervisor Prof. Hidetoshi Nishimori for his guidance and encouragement. His approach to unsolved problems on physics is embedded in all my studies. I am so deeply grateful to Dr. Kazutaka Takahashi for his thought-provoking comments on my studies. In particular, one of his suggestions led to the study of the hierarchical model in this thesis. I would like to thank the current and previous members of the Nishimori group for stimulating discussions, especially Dr. Masayuki Ohzeki for his support during my days as a graduate student. I am greatly indebted to Prof. Gerardo Ortiz for his idea of a real-space renormalization-group method. Without the idea, the studies in this thesis would have never started. I would like to thank Prof. Ferenc Iglói for giving me an explanation of the strong-disorder renormalization group. Many thanks to all colleagues who have shared the room 343 in the main building at Tokyo Institute of Technology for cheerful mood and good coffee. I acknowledge the financial support from the Global Center of Excellence Program by MEXT, Japan through the "Nanoscience and Quantum Physics" Project of Tokyo Institute of Technology and the financial support provided through the Research Fellowship of the Japan Society for the Promotion of Science. Finally, I would like to thank my family for continuing support.

List of publications

Publications on which this thesis is built

1. R. Miyazaki and H. Nishimori, "Real-space renormalization-group approach to the random transverse-field Ising model in finite dimensions," Phys. Rev. E **87**, 032154 (2013).

2. R. Miyazaki, H. Nishimori, and G. Ortiz, "Real-space renormalization group for the transverse-field Ising model in two and three dimensions," Phys. Rev. E **83**, 051103 (2011).

Other publications

1. R. Miyazaki, "Frustration and Transition Point of Ising Spin Glasses," Interdisciplinary Information Sciences **19**, 43 (2013). Proceedings of The 4th Young Scientist Meeting on Statistical Physics and Information Processing in Sendai.

2. R. Miyazaki, "Frustration in Vicinity of Transition Point of Ising Spin Glasses," J. Phys. Soc. Jpn. **82**, 094001 (2013).

Contents

Chapter 1

Introduction

This thesis presents an analysis of phase transitions and critical phenomena in quantum spin systems with randomness by means of a real-space renormalization-group method. We start with a review of random quantum spin systems. The first section outlines elementary concepts for the subsequent discussion. The next section discusses effects of randomness on critical phenomena. We classify the effects into three types. One of the classes contains systems exhibiting critical phenomena governed by an infinite-randomness fixed point, which is the main subject in the present thesis. Effects of rare regions on critical phenomena, which is one of the features in random systems, are also described. Section 1.3 introduces the random transverse-field Ising model, which has an infinite-randomness fixed point and is hence the basic model in the thesis. We review the properties of this model. In addition, Sec. 1.4 gives short surveys of understandings of other systems in this field. This chapter is closed with the overview of the present thesis.

1.1 Phase transitions, critical phenomena, and renormalization group

We all surely have seen popular examples of phase transitions that ice melts or water evaporates. The phase transition of water is an everyday phenomenon. We have no question about it in our daily life. In a theoretical viewpoint, nevertheless, phase transitions are difficult issues. A lot of physicists have been attracted to this topic. Let us explore this exciting field.

We first introduce some terms for subsequent theoretical arguments. The most fundamental concept in this thesis is phase. When we determine some parameters characterizing a system, for example, temperature, volume, and fields, the system lies in some phase. Phases are distinguished by their macroscopic properties. For example, spatial symmetries of systems distinguish the gas, liquid, and solid phases. The macroscopic properties suddenly change in phase transitions. This sudden change is described as a singularity in the free energy of the system.

A phase transition often accompanies another fascinating phenomenon, namely a critical phenomenon. This phenomenon makes phases indistinguishable and causes interesting singularities in physical quantities. Typical examples of the singularities

in magnetic materials are found in specific heat C, magnetization m, susceptibility χ, correlation function $G(r)$ with two spins separated by distance r, and correlation length ξ. In case that the critical phenomenon is driven by the change of temperature T or an external field h, they are represented with critical exponents $\alpha, \beta, \ldots$ as [1]

$$C \sim |t|^{-\alpha} \quad (T > T_c), \quad |t|^{-\alpha'} \quad (T < T_c), \tag{1.1}$$
$$m \sim |t|^{\beta} \quad (T < T_c), \tag{1.2}$$
$$\chi \sim |t|^{-\gamma} \quad (T > T_c), \quad |t|^{-\gamma'} \quad (T < T_c), \tag{1.3}$$
$$m \sim |h|^{1/\delta} \quad (T = T_c), \tag{1.4}$$
$$G(r) \sim e^{-r/\xi} \quad (T \neq T_c), \tag{1.5}$$
$$\xi \sim |t|^{-\nu} \quad (T > T_c), \quad |t|^{-\nu'} \quad (T < T_c), \tag{1.6}$$
$$G(r) \sim r^{-d+2-\eta} \quad (T = T_c), \tag{1.7}$$

where $t = (T - T_c)/T_c$ with the critical temperature T_c, and d is for the spatial dimension of the system. The symbol "$\sim$" expresses the most singular contribution of the left hand side near the critical point.

Critical exponents show a strong universality. Systems have the same set of critical exponents if they share only three things in common: the symmetry of the Hamiltonian, the dimensionality, and the type of interactions [2]. Systems with the same set of critical exponents constitute a universality class. The universality in critical phenomena has been one of the central themes in statistical physics.

A system at a critical point has another significant feature that fluctuations of all length scales exist. In a magnetic material, a system at a critical point has various sizes of domains which consist of parallel spins. This property leads to the scale invariance of a system at the critical point, and the invariance is a clue to investigate critical phenomena with renormalization group.

It is an apparently impracticable attempt to explore macroscopic phenomena such as phase transitions and critical phenomena, with microscopic Hamiltonians. Renormalization group [3] is one of the powerful tools (or concepts) to tackle the problem. In the framework of renormalization group, we first focus on the smallest scale in a system and calculate the influence of the scale on the objective physical quantities such as the free energy or the partition function. For concreteness, let us consider the one-dimensional Ising model with the Hamiltonian

$$H = -J \sum_i S_i S_{i+1}, \tag{1.8}$$

where i denotes a site of the chain and $S_i = \pm 1$. We first take the partial trace, for example, calculations of only spins on even number sites, of the partition function. Taking the effect into the larger scales, we reconstruct the system without the smallest scale. We then rescale the system to have the same scale as the original one. The resulting function has the *renormalized* parameters shifted through this transformation. This process is illustrated in Fig. 1.1. In the Ising model, the parameter is the product of coupling constant and inverse temperature, and it is shifted through this transformation. Moreover, new parameters are also produced in general. Iterating this transformations, we ought to reach a macroscopic scale.

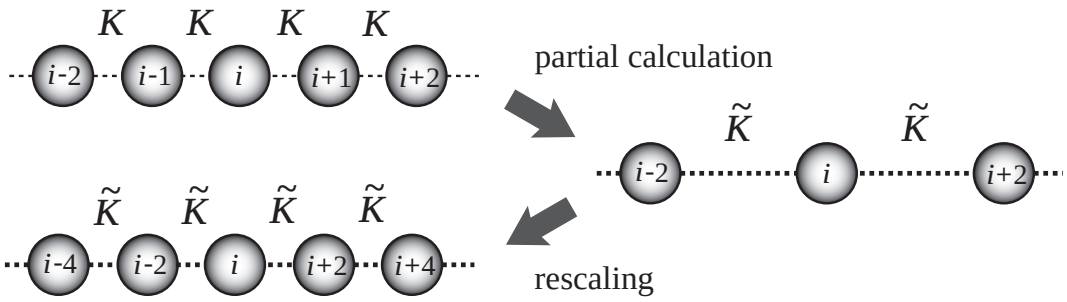

Figure 1.1: Renormalization-group procedure in a one-dimensional system. In the example, the spin degrees of freedom depicted as circles on alternate sites are traced out. The systems is then rescaled as the distance between neighboring sites takes the original value. The symbol K denotes the product of coupling constant and temperature, which is shifted to $\tilde{K}$ through the transformation.

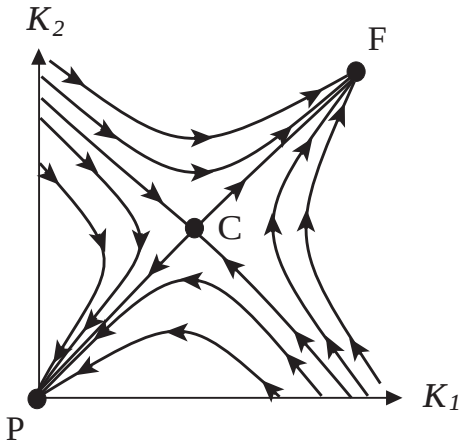

Figure 1.2: An example of renormalization-group flow in the parameter space (K_1–K_2 plane). This flow has two stable fixed points denoted by P and F, and an unstable fixed point denoted by C.

We trace the change of parameters, and then draw the flow of renormalization group in the parameter space as in Fig. 1.2. The flow has fixed points, which represent the coarse-grained macroscopic states. In general, stable ones correspond to phases, whereas unstable ones to critical points or transition points. The correspondence of unstable fixed points with critical points is due to the scale invariance at the critical points. To estimate critical exponents, we observe the flow in the vicinity of the critical point. With the scaling theory for free energy and other observables, we deduce the critical exponents from the flow. This framework of renormalization group will be elaborated in Sec. 2.1.

Although the concept of renormalization group is clear, we have no general prescription to execute calculations in specific problems. The generation of additional parameters through the transformations leads to an especially awkward problem. To get over or get around the hurdle, various approximate methods have been developed [1,2].

Our strategy in this thesis will be explained in Sec. 2.4.

1.2 Effects of randomness

As a consequence of long studies, phase transitions and critical phenomena in uniform systems have been substantially understood. Unfortunately, our world is not so clean as the ideal models employed in the studies. Usually, systems include uncontrollable impurities which distribute randomly. The impurities and the resulting randomness can change the nature of systems and trigger new problems. Fortunately, they also give a glimpse of elegant universalities. Systems with randomness, which we refer to as random systems hereafter, show unique critical phenomena. This section reviews the relationship between randomness and critical phenomena.

1.2.1 Classification of critical phenomena in random systems

One of the elementary problems on random systems is whether the presence of impurities or randomness changes macroscopic properties of the systems. In particular, we are interested in the influence on critical phenomena. The criterion on this issue has been derived [4]. To suppress the effects of randomness on critical phenomena, a pure system, which has no randomness, needs to satisfy the inequality about the critical exponent ν, which is called the Harris criterion,

$$d\nu > 2, \tag{1.9}$$

with the spatial dimension d of the system.

The Harris criterion is intuitively understood as follows [1]. Let us consider a magnet, where spins interact each other with a coupling constant J. Randomness is introduced as the perturbation in the interactions as $J \to J + \delta J(\boldsymbol{r})$. We can interpret this perturbation as the change of local temperature, since coupling constants appear as the product with inverse temperature in statistical mechanical calculations. Thus, we should examine how the system responds to the change of temperature. Specific heat then plays an important role. If the critical exponent α is positive, the specific heat diverges at the critical point. The perturbation in local temperatures, or in interactions, induces a sudden change in local energies accordingly. Consequently, randomness destabilizes the system if $\alpha > 0$. This argument results in the Harris criterion with an equation of hyperscaling, $\alpha = 2 - d\nu$, which is derived from the scaling theory of the correlation function [1]. We should note that the Harris criterion is a necessary condition, and is not a sufficient condition, to suppress the effects of randomness.

If $d\nu \leq 2$, the randomness influences critical phenomena. We can find two types of the influence [5,6], which are described below. Thus, with the case that the randomness is suppressed, critical phenomena of random systems are categorized into three types [5, 6]. The classification is based on the behavior of disorder strength through coarse-graining processes. We classify random systems according to critical phenomena in a renormalization-group picture:

1. Systems whose critical phenomena are not influenced by randomness
2. Systems which keep their inhomogeneities at all length scales with finite strength of randomness
3. Systems where the magnitude of randomness is unlimitedly amplified under coarse-graining processes.

In the first class, critical exponents of the systems satisfy the Harris criterion $d\nu > 2$. The strength of randomness decreases through the coarse-graining processes. In other words, the width or the variance of the distribution of physical quantities or parameters in the system vanishes. Hence, the randomness is irrelevant in a renormalization-group picture. The width of distributions of macroscopic observables vanishes as a result [7,8]. The critical fixed point is the same as in the corresponding pure system. An example in this class is the three-dimensional classical Heisenberg model, where $\nu \simeq 0.698$ [9]. We can find the inequality $d\nu > 2$ in this case.

In the second class, inhomogeneities in the systems do not vanish through coarse-graining processes. They affect critical phenomena, and critical exponents are shifted from those in the pure system. The width of distributions of macroscopic observables approaches a finite size-independent value [7, 8]. This class includes the three-dimensional classical Ising model. The pure system shows $\nu \simeq 0.627$ [10], which does not fulfill the Harris criterion, and the diluted model has the different value $\nu \simeq 0.684$ [11].

In the third class, the magnitude of randomness is infinitely amplified through renormalization, which means that the width of distributions of observables grows indefinitely (in the logarithmic scale). The fixed point is referred to as an *infinite-randomness fixed point* [12], and it represents broad distributions of physical quantities. As a consequence, rare regions in the system, which are usually expected not to affect macroscopic properties, strongly influence some of the behavior of the system. The effects of rare regions in random systems are elaborated in the next subsection. In addition, at the critical point, the scaling-law is not the conventional power-law scaling but an exponential scaling, which is often called the activated scaling. The first example in this class is the McCoy-Wu model [13–16]. This model is a descendant of the two-dimensional classical Ising model and will be explained in the next subsection.

The third class is our main objective in this thesis. This class is the most fascinating. In this class, the randomness infinitely grows through renormalization, and extremely affects the system as a result. The strong randomness seems to spoil the universal aspects of critical phenomena. Contrary to the intuition, systems in this class share peculiar scaling relations. We can find in this class the universality generated by the randomness, which is one of the goals of studies on random systems. The characteristic features of the third class are considered to originate from the influence of rare regions, the mechanism of which is discussed in the next subsection.

1.2.2 Rare regions

As mentioned in the last subsection, rare regions in a random system can influence macroscopic properties. This phenomenon is the feature not only in the third class,

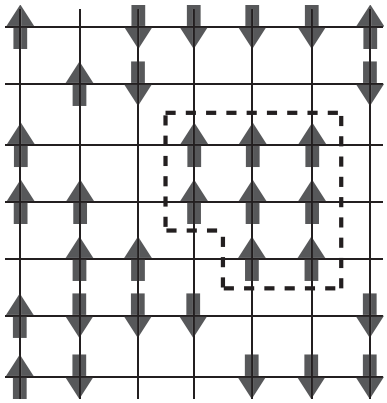

Figure 1.3: Two-dimensional site-diluted Ising system and a cluster. Spins depicted as arrows sit on vertexes of a lattice drawn by solid lines. Some sites are vacant. The dashed line encloses a region. The spins in the region do not interact with spins outside of the dashed line and build a cluster.

where the randomness is infinitely amplified through a coarse-graining process. We can find the effects of rare regions in the systems in the second class, although the effects are very weak. The rare regions, thus, play an important role which produces differences from pure systems and interesting behavior of random systems. We review studies on effects of rare regions.

Let us consider a system with parameters randomly taken from some distribution. Imagine random variable interactions J_{ij} between spins i and j. The parameters take various values, but parameters in most regions have values in the vicinity of the average of the distribution, and the regions with parameters of large deviated values are rare. Thus, it is natural to expect that the nature of the system is mainly governed by the typical values of the parameters. In some cases, however, rare regions affect the macroscopic properties. Their effects cause singularities in physical quantities. These singularities have been explicitly pointed out by Griffiths [17] and McCoy and Wu [13–16], and called the Griffiths singularity or the Griffiths-McCoy singularity.

Griffiths investigated the site-diluted Ising ferromagnet [17]. This is a model for a magnetic material with partial substitution of nonmagnetic impurities for magnetic ions. The system consists of spins residing on a regular two- or three-dimensional lattice and their nearest-neighbor ferromagnetic interactions. The difference from the standard Ising ferromagnet is that only a fraction p of sites on the lattice are occupied by spins and the rest sites are vacant or occupied by nonmagnetic impurities, as depicted in Fig. 1.3. When $p = 1$, this system reproduces the standard Ising ferromagnet and has spontaneous magnetization at lower temperatures than the critical temperature $T_c(p = 1)$. With $p < 1$, the critical temperature $T_c(p)$ is lower than $T_c(1)$. With the concentration below a particular boundary p_c, the system has no finite spontaneous magnetization at any finite temperatures. The phase diagram is shown in Fig. 1.4.

The singular behavior is found in the magnetization (or susceptibility) for $p < 1$ at any lower temperatures than $T_c(1)$. This is an essential singularity, that is, the magnetization at low temperatures is infinitely differentiable but non-analytic. This

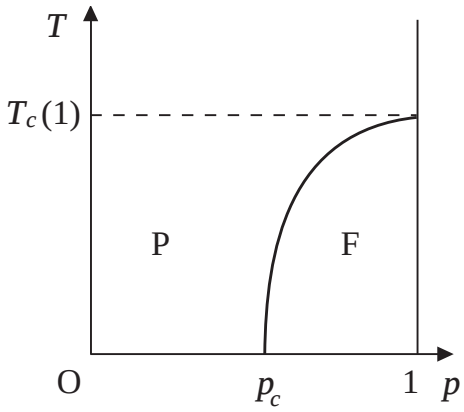

Figure 1.4: Phase diagram of the two-dimensional site-diluted Ising ferromagnet. The symbols p and T denote fraction of sites occupied by spins and temperature, respectively. The phase boundary between the ferromagnetic (F) and paramagnetic (P) phases is drawn as a solid curved line. The critical temperature of the pure Ising ferromagnet and the critical fraction at zero temperature are denoted by $T_c(1)$ and p_c, respectively. A dashed line represents $T = T_c(1)$.

surprising feature results from effects of rare regions as follows. When $p < 1$, the system has vacant sites. Interactions are lost accordingly. Consequently, clusters which are isolated from other parts are generated as illustrated in Fig. 1.3. The concentration of a cluster of volume V is $p^V = \exp(-\tilde{p}V)$ with $\tilde{p} = -\log p$ (> 0). As the volume of a cluster grows, the probability for finding the cluster exponentially decreases, which shows the fact that large clusters are rare. Clusters behave as rather small Ising ferromagnetic systems. Hence, at low temperatures, some clusters have local magnetization and show properties which are seen in the ferromagnetic phase of the pure Ising model, while the whole system lies in the paramagnetic phase. These small Ising systems cause the essential singularities in a range of low temperatures, which is known as the Griffiths region or the Griffiths phase. The singularities, however, are very weak so that an experimental verification is difficult [18].

McCoy and Wu studied a random system produced by modification of the two-dimensional Ising model [13–16], which we refer to as the MW model hereafter. The MW model was proposed as a prototype to study the effects of randomness in the Ising model. The randomness is introduced in interactions indicated in Fig. 1.5. Interactions between neighboring spins in a direction, say, the horizontal direction, are uniform. On the other hand, interactions in the vertical direction take different random values from column to column. These interactions seem artificial. However, this model is analytically accessible due to the artificial symmetry in the vertical direction, although disordered models are regarded as an awkward subject usually. Note that the MW model is the first model with an infinite-randomness fixed point as mentioned in the last subsection, although the concept of the infinite-randomness fixed point has been established [12, 19, 20] a quarter of a century after this work.

McCoy and Wu revealed the presence of singularities in physical observables such as the specific heat. This singularity is also a kind of the Griffiths type explained above.

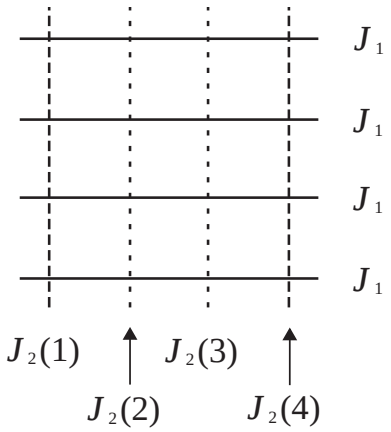

Figure 1.5: Interactions in the MW model. Interactions in the horizontal direction are denoted by J_1, and interactions in the vertical direction in jth column are denoted by $J_2(j)$.

The specific heat is an infinitely differentiable function of temperature, but diverges at a critical point. Although the MW model shows the Griffiths singularity, the model has no isolated cluster, which plays an important role as small Ising models in the diluted model. What plays the role of the cluster is the perfectly correlated randomness. In the MW model, the randomness in the vertical interactions perfectly correlates with each other in the vertical direction.

The singularities in the two examples belong to the Griffiths-McCoy singularity, but the latter example shows stronger effects on critical phenomena. The difference is considered to be qualitatively derived from the size of rare regions [21]. The diluted model with small p below p_c has only finite-size clusters, or finite-size rare regions. On the other hand, the MW model has one-dimensional infinite-size rare regions which infinitely extend to the vertical direction. Both the models are based on the Ising models, where the lower critical dimension is one. Hence, the rare regions in the MW model are regarded as systems in the lower critical dimension, whereas those in the diluted model are only zero-dimensional systems. Physical quantities in systems exactly at the lower critical dimension usually shows exponential divergence [1] as the distance from a critical point in a renormalization-group picture decreases. The inverse of system size is expected to be the distance. The exponentially strong effect of rare regions is comparable with the exponentially small concentration of a rare region. The stronger effects on critical phenomena are found in the MW model as a result.

The occurrence of the strong Griffiths singularity is considered to be a consequence of the presence of an infinite-randomness fixed point [6], which is a fixed point in a renormalization-group picture and controls the characteristic scaling instead of the conventional power-law scaling [12]. Indeed, the MW model has the fixed point, which has been established in the equivalent quantum spin model to the MW model [12,19,20]. As this phenomenon, infinite-randomness fixed points signal the strong effects of rare regions. Physics originated from the fixed points is one of the examples that rare events extremely affect the whole system.

1.3 Random transverse-field Ising chain

The characteristic critical behavior of infinite-randomness fixed points is produced by strong effects of the peculiar randomness as seen in the MW model. The fixed point, hence, seems an artificial or pathological consequence of the artificial randomness. However, a change of the viewpoint yields a natural random system. After a mapping of the MW model onto the one-dimensional quantum spin model [22], we obtain an equivalent quantum spin chain with natural randomness, namely the random transverse-field Ising chain. This fact suggests that the presence of an infinite-randomness fixed point is a natural consequence in quantum spin systems with randomness. This section reviews the random transverse-field Ising models, whose critical phenomena we investigate in this thesis.

1.3.1 Pure model

Before discussion on the random transverse-field Ising model, we should gain intuition about the transverse-field Ising model without randomness

$$H = -J \sum_{\langle i,j \rangle} \sigma_i^z \sigma_j^z - \Gamma \sum_i \sigma_i^x, \tag{1.10}$$

where $\{\sigma_i^\alpha\}$ are the Pauli matrices. We assume $J > 0$. This model has ferromagnetic interactions only between z-component of the nearest-neighbor spins, and a transverse-field is applied. The term "transverse" expresses that the direction of the field, x direction, transverses the direction of the interactions, z direction. The transverse field generates quantum effects.

We first consider the one-dimensional case. The transverse-field Ising chain has the ferromagnetic phase and the paramagnetic phase as illustrated in Fig. 1.6 (a). The former exists only at zero temperature. The chain exhibits a quantum phase transition and critical phenomenon. The word "quantum" highlights that they are induced by the transverse field, namely the origin of quantum effects. If the strength of the field Γ is larger than the strength of the interaction J, the expectation value of σ^z vanishes. That means the system lies in the paramagnetic phase. If Γ becomes smaller than J, the system has a finite expectation value of σ^z, and then the system enters the ferromagnetic phase. The phase boundary is located at $\Gamma = J$ [23–25]. The reason why we focus on the expectation value of σ^z rather than σ^x is that the phase transition accompanies a spontaneous symmetry breaking concerning the Z_2 symmetry in the Hamiltonian [Eq. (1.10)] under the transformation $\sigma^z \to -\sigma^z$.

The phase boundary in the one-dimensional model can be deduced from the self-duality of this model [26]. A transformation on spin variables from σ to new Pauli matrices τ,

$$\tau_i^x = \sigma_i^z \sigma_{i+1}^z, \quad \tau_i^z = \prod_{j \le i} \sigma_i^x \tag{1.11}$$

yields a transverse-field Ising chain

$$H = -J \sum_i \tau_i^x - \Gamma \sum_i \tau_i^z \tau_{i+1}^z, \tag{1.12}$$

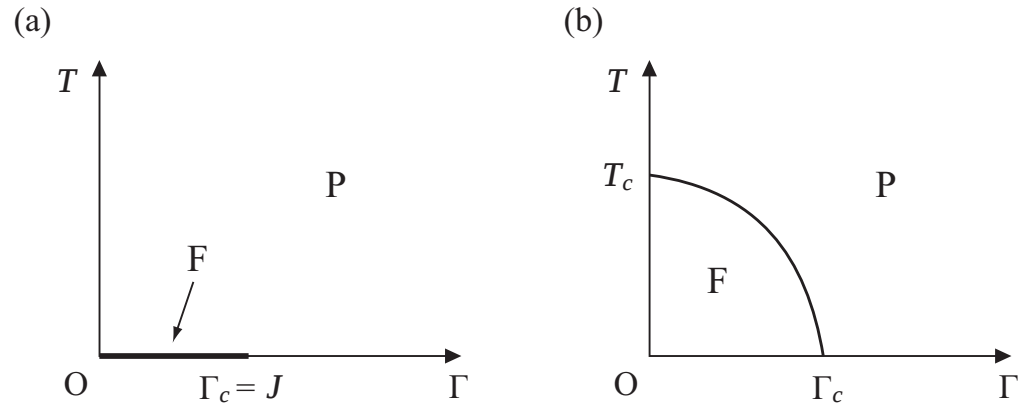

Figure 1.6: Phase diagrams of the transverse-field Ising models (a) in one dimension and (b) in higher dimensions. The models have the ferromagnetic (F) and paramagnetic (P) phases. The ferromagnetic phase is shown in low transverse fields, $\Gamma < \Gamma_c$, in general. In the one-dimensional model, the phase exists only at zero temperature, $T = 0$, whereas the phase extends to finite temperatures in the higher-dimensional models. The phase transition in one dimension occurs at $\Gamma = J$, where the magnitude of the transverse field is equal to the coupling constant.

with the role of J's and Γ's interchanged. To be precise, the resulting Hamiltonian depends on the boundary condition, which is ignored here. Note that this transformation preserves the form of the model only in one dimension. The invariance of the form of the Hamiltonian, namely self-duality, is used to deduce the transition point. In general, parameters in the Hamiltonian take particular values on transition points, where the physical quantities can have singularities. If the system has the unique transition point, the parameters, for example the coupling constant, in the original and transformed Hamiltonians take the same values on the transition point. Hence, the transition point of the transverse-field Ising chain is determined as $\Gamma = J$. The self-duality will be exploited in our renormalization-group scheme in Chap. 3.

A quantum critical phenomenon occurs around the transition point [24, 25]. Physical quantities show singularities or divergence as functions of Γ, represented by the same expression as the relations (1.1)–(1.7) but the temperature T is replaced by the transverse field Γ. The quantum critical phenomenon has another critical exponent z, which expresses the singularity of the energy gap Δ between the ground state and the first excited state as [24, 25]

$$\Delta \sim (\Gamma - \Gamma_c)^{\nu z}. \tag{1.13}$$

The energy gap represents a characteristic energy scale, and the zero gap is a signal of quantum phase transition. The two relations (1.6) and (1.13) lead to the relation between energy and length,

$$\Delta \sim \xi^{-z}. \tag{1.14}$$

Values of critical exponents are listed in Table. 1.1. The exponents except for z take the

Table 1.1: Critical exponents α, β, γ, δ, ν, η, and z of the transverse-field Ising chain [1, 24]. The exponents except for z take the same values as those of the two-dimensional Ising model. The exponent z is defined for quantum systems with an energy gap.

Exponents	α	β	γ	δ	ν	η	z
Values	0	$\frac{1}{8}$	$\frac{7}{4}$	15	1	$\frac{1}{4}$	1

same values as those of the two-dimensional Ising model. This fact is a consequence of the equivalence [22] between the thermodynamic (static) properties in the two models. This equivalence is generalized to the equivalence between the MW model and the random transverse-field Ising chain.

In higher dimensions [24, 25, 27], the ferromagnetic phase extends to finite temperatures. The phase transitions at finite temperatures accompany critical phenomena, but these are classical ones.

1.3.2 Random model and material

The random transverse-field Ising model is governed by the Hamiltonian

$$H = -\sum_{\langle i,j \rangle} J_{ij}\sigma_i^z\sigma_j^z - \sum_i \Gamma_i\sigma_i^x. \tag{1.15}$$

Interactions J_{ij} and transverse fields Γ_i are random variables taken from identical independent distributions, respectively. Specifically, interactions are distributed according to $P_J(J_i)$ and transverse fields according to $P_\Gamma(\Gamma_i)$. Although a uniform field is natural in experiments, we consider the random transverse fields. This is because the uniform-field model belongs to the same universality class as the random-field model, which means that the randomness in interactions makes the field random after renormalization-group transformations. This model is the simplest quantum spin model with randomness.

The one-dimensional model at zero temperature has ferromagnetic and paramagnetic phases as in the pure case. The phase boundary is determined by the equation [28]

$$\sum_i \log J_i = \sum_i \log \Gamma_i. \tag{1.16}$$

In short, the interactions and fields share the same average in the logarithmic scale at the phase-transition point in one dimension. This condition includes the pure case. The system exhibits critical phenomena, which will be reviewed in the next subsection.

The equivalence between the MW model and the random transverse-field Ising chain is based on a particular mapping [22]. The horizontal interactions in the MW model are mapped onto the interactions in the chain, and the vertical interactions onto the transverse fields. Intuitively, the mapping vertically presses the two-dimensional

model into the horizontal chain. This mapping can be performed only when the two-dimensional system has the (discrete) translational symmetry in the vertical direction. Hence, the symmetry in the MW model, illustrated in Fig. 1.5, is essential to the equivalence. The MW model seems to be a little artificial because of the symmetry. Accordingly, the peculiar features in the MW model appear to be pathological features in the artificial model. With the mapping, the pathological features are interpreted as interesting features in the quantum system with natural randomness.

The random transverse-field Ising model is related to a compound $LiHo_xY_{1-x}F_4$ [29–32]. This compound has a body-centered tetragonal unit cell, and the dipolar-coupled Ising interactions between magnetic Ho^{3+} ions are dominant at low temperatures [33–36]. The dipolar couplings are described as

$$H_{ij} = \frac{1 - 3(\cos\theta_{ij})^2}{r_{ij}^3} J S_i S_j, \tag{1.17}$$

where S_i is the Ising variable ($S_i = \pm 1$) on site i, θ_{ij} denotes the angle formed by the Ising axis and the line connecting sites i and j, and r_{ij} is the distance between the two spins. The nearest-neighbor dipolar interaction in this system is ferromagnetic, and the second-nearest-neighbor interactions are antiferromagnetic. Pure $LiHoF_4$ without yttrium is a ferromagnet at low temperatures [33–36]. However, sufficient dilution by nonmagnetic Y^{3+} ion substituted for Ho^{3+} induces the mixture of ferromagnetic and antiferromagnetic interactions and then destroys the long-range order. Consequently, the compound $LiHo_xY_{1-x}F_4$ with small x shows behavior like random spin systems at low temperatures [29]. The compound has a ground-state doublet as Ising systems. The magnetic field H_t transversing the Ising axis splits the doublet, which corresponds to an effective field $\Gamma \propto H_t^2$ in Eq. (1.15). Thus, $LiHo_xY_{1-x}F_4$ placed in the transverse field appears the random transverse-field Ising model [30–32].

Nevertheless, experiments on $LiHo_xY_{1-x}F_4$ [31] have not found quantum criticality. The origin of this unexpected result has been inferred in a theoretical study [37]. It has been concluded that the transverse field applied to $LiHo_xY_{1-x}F_4$ also induces random longitudinal fields, which smear out the quantum criticality. This statement suggests imperfect correspondence between $LiHo_xY_{1-x}F_4$ and the random transverse-field Ising model. Thus, the correspondence is controversial, and it is an open question to create magnetic materials which clearly show the quantum criticality predicted in the random transverse-field Ising model.

1.3.3 Scaling relations

Peculiar properties of the random transverse-field Ising chain has been revealed by Fisher [19, 20]. To analyze the model, he used a renormalization-group method originally proposed by Ma, Dasgupta, and Hu [38, 39]. The method is now known as the strong-disorder renormalization group [40]. By the method, we trace the change of the distributions of J_i and Γ_i. The distributions are expressed as functions of the value Ω of the strongest parameter such as $P_J(J, \Omega)$ and $P_\Gamma(\Gamma, \Omega)$. We deduce differential equations about the distributions under renormalization processes, which will be described in Sec. 2.3. We then observe how physical quantities are changed as the energy scale

Ω changes. Scaling laws are obtained as a result. One of the representative examples is the scaling relation between energy Ω and length L_Ω,

$$\log \frac{\Omega_0}{\Omega} \sim L_\Omega^\psi, \tag{1.18}$$

with the basic energy scale Ω_0 and an exponent ψ. This scaling is a peculiar one, compared with the conventional scaling where energy scales as $\Omega \sim L_\Omega^{-z}$ with the dynamical exponent z. The derivation of the above relation will be elaborated in Sec. 2.3.2. This subsection surveys other scaling relations [12, 19, 20, 41] between physical quantities without detailed derivations.

At the critical point, the average correlation function $C_{\rm av}(r) = [\langle \sigma_i^z \sigma_{i+r}^z \rangle]$, where $\langle \cdot \rangle$ denotes the standard thermal average and $[\cdot]$ the average of the distribution of randomness, between widely separated spins at the critical point is expressed as

$$C_{\rm av}(r) \sim r^{-2+\phi}. \tag{1.19}$$

with an exponent $\phi = (\sqrt{5}+1)/2$. Although this form is similar to the conventional style, this is not a trivial result, since the typical, not average, correlation function is

$$-\log C(r) \sim r^\psi \tag{1.20}$$

in contrast. The difference between these scalings is considered to arise from the effect of rare regions. Typically, the observable is not affected by the rare regions, but the effect is found in the average.

If the system lies slightly off the critical point by δ, the correlation length ξ yields

$$\xi \sim |\delta|^{-\nu} \tag{1.21}$$

with an exponent $\nu = 2$. Here δ indicates the difference between the distributions of interactions J_i and fields Γ_i, and is approximately equal to Δ, introduced in Sec. 2.3.2, in the vicinity of the critical point. The correlation length appears in the correlation function

$$C_{\rm av}(r) \sim e^{-r/\xi}. \tag{1.22}$$

in the paramagnetic phase near the critical point, namely the weakly disordered phase. As in the case at the critical point, the average correlation function is not identical to the typical one. The form of the function is shared, but the correlation length has a difference

$$\xi_{\rm typ} \sim |\delta|^{-(1-\psi)\nu}. \tag{1.23}$$

It is natural to introduce another exponent $\nu_{\rm typ} = (1-\psi)\nu$.

In the weakly disordered phase, the scaling between energy and length is given by

$$\Omega \sim L_\Omega^{-z}, \tag{1.24}$$

which appears as a conventional one. The corresponding exponent z in the conventional critical phenomena takes a constant value, for example, 1 in the pure transverse-field

Ising model, while the above exponent z is a continuous variable which diverges as $\delta \to 0$ as $z \sim \delta^{-1}$. This exponent is found in the scaling of the magnetization m as

$$m \sim h^{1/z} \tag{1.25}$$

with a longitudinal field h, and in the susceptibility χ at a low temperature T as

$$\chi \sim T^{-1+1/z}. \tag{1.26}$$

Despite the disordered phase where the system lies, singularities as the function of field and temperature occur. These relations manifest the Griffiths-McCoy singularities. In the ordered phase, similar scaling relations are found, but some logarithmic correction terms are needed. The above relations (1.25) and (1.26) are remarkable for their power-law scaling. The standard Griffiths singularities, which are found in the site-diluted Ising model, exhibit weaker singularities, for instance, as $m \sim \exp(-1/h)$.

1.4 Other systems

Fisher's work [19, 20], which has derived the relations explained in the last subsection, made an epoch in the study of critical phenomena in random quantum spin systems. His work has been numerically confirmed [42–45]. His approach, the strong-disorder renormalization group [40], is then regarded to yield the asymptotically exact result when the randomness in the system is strong. This section reviews several studies on random quantum systems mainly with the strong-disorder renormalization group, which have been developed after Fisher's work.

1.4.1 Random quantum spin chains with discrete symmetry

Random quantum spin chains with discrete symmetry, which are descendants of the random transverse-field Ising chain, have been examined. The random quantum Potts chain and the random quantum clock chain are examples of such objectives. The classical version of these models are given by

$$H_{\text{Potts}} = -\sum_{i=1}^{q} J_i \delta_{S_i, S_{i+1}}, \tag{1.27}$$

where $\delta_{x,y} = 1$ only if $x = y$, otherwise $\delta_{x,y} = 0$, and

$$H_{\text{clock}} = -\sum_{i=1}^{q} J_i \cos\left[\frac{2\pi}{q}(S_i - S_{i+1})\right]. \tag{1.28}$$

These models have q-state spin variables, $S_i = 1, 2, \ldots, q$, which also describe states as $|S_i\rangle$. The two models are identical for $q = 2, 3$, and are also equivalent for $q = 2$ to the Ising model. In the limit as $q \to \infty$, the clock model becomes the XY model. The two models are standard testing grounds in the studies of phase transitions and

critical phenomena [46]. The corresponding quantum models are produced by adding transverse-field terms

$$H_{\text{Potts,t.f.}} = -\sum_i \frac{\Gamma_i}{q} \sum_{k=1}^{q-1} M_i^k, \tag{1.29}$$

$$H_{\text{clock,t.f.}} = -\sum_i \frac{\Gamma_i}{2} (M_i + M_i^{-1}), \tag{1.30}$$

where operators M_i are defined as $M_i|S_i\rangle = |S_i + 1, \text{mod} q\rangle$.

The above quantum spin models have been investigated by means of the strong-disorder renormalization group [47,48] and the density matrix renormalization group [48, 49]. The latter is a powerful numerical technique to mainly analyze quantum spin systems, based on the variational method. Their analyses conclude that if randomness in original systems is stronger than a certain degree, critical properties of these models at zero temperature are controlled by an infinite-randomness fixed point. The critical properties are independent of the number of states q, whereas classical critical phenomena depend on the value of q [46]. Further, the fixed point is the same fixed point as in the random transverse-field Ising chain. As a consequence, the set of critical exponents of the random quantum Potts and clock models are identical to that of the random transverse-field Ising chain. This is an instance that randomness creates a new strong universality.

1.4.2 Random antiferromagnetic XXZ spin chains

The Heisenberg model

$$H = J \sum_{i,j} \boldsymbol{S}_i \cdot \boldsymbol{S}_j \tag{1.31}$$

is a standard model to describe interacting magnetic moments. This model in one dimension is generalized to the random antiferromagnetic XXZ spin chain

$$H = \sum_i J_i^{\perp} (S_i^x S_{i+1}^x + S_i^y S_{i+1}^y) + J_i^z S_i^z S_{i+1}^z \tag{1.32}$$

with anisotropy and random exchange couplings.

Let us consider at first the spin-1/2 model. The properties of this model at low temperatures have been revealed by means of the strong-disorder renormalization group [38, 39, 50–52]. The point where the averages of $J^{\perp}$ and J^z take the same value corresponds to the random antiferromagnetic Heisenberg model and is also referred to as the random antiferromagnetic XXX model. This point is an unstable fixed point in the renormalization-group picture. Renormalization-group flows are drawn from this point to the points $J^z = 0$ (the random antiferromagnetic XX model) and $J^{\perp} = 0$ (the random antiferromagnetic Ising model). The ground states of the random antiferromagnetic XX and XXX models have been dubbed the random-singlet phase [38,39,50], where pairs of spins form singlets over arbitrarily long distances as shown in Fig. 1.7.

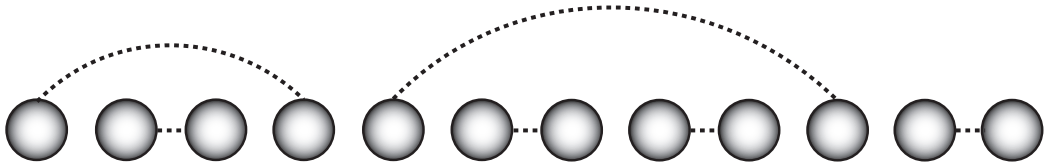

Figure 1.7: Random-singlet ground state. Pairs of spins connected by dashed lines form singlets over arbitrarily long distances.

The properties of this phase (or the corresponding fixed points) are characterized by infinite-randomness fixed points [50].

In the pure antiferromagnetic Heisenberg chain, there are drastic differences between the half-integer and integer spin chains [53]. Thus, there have been a lot of interests in investigating the random spin-1 model. One of the main interests have lain on whether the ground state is characterized by the random-singlet phase as in the spin-1/2 case. The analyses based on the strong-disorder renormalization group [54–56] have found the random-singlet phase. On the other hand, contrary results have been obtained in some direct numerical studies via exact diagonalization [57], the quantum Monte-Carlo method [58], and the density-matrix renormalization group [59]. However, a study in a larger system via the stochastic series expansion quantum Monte-Carlo has found the random-singlet phase [60]. These discrepancies are considered to result from strong finite-size effects. The random-singlet phase has been identified also in the spin-3/2 model [61, 62]

1.4.3 Higher-dimensional systems

It is a natural question whether the nature of critical phenomena found in the random transverse-field Ising chain is the peculiar feature of the one-dimensional systems. To settle this issue, higher-dimensional systems have been investigated. The strong-disorder renormalization group [40] has been numerically applied to the two- and three-dimensional random ferromagnetic Ising model in a transverse field [5, 63–69] and the same properties as in the one-dimensional case have been found. There is, however, another report with a conflicting result [70] in higher dimensions, and hence further investigations are necessary to resolve the controversy. In particular, the strong-disorder renormalization group cannot keep the lattice structure in dimension $d > 1$. To avoid this problem, other modified methods have been proposed [71–75].

1.4.4 Quantum spin glasses

Spin glasses [76, 77] have been one of the challenging themes in statistical physics. Spin-glass models have been introduced to theoretically explore spin-glass materials, for example, CuMn, where spins are randomly frozen at low temperatures. One of the representative mechanisms in spin glasses is the Ruderman-Kittel-Kasuya-Yosida

(RKKY) interaction [78–80], which is expressed as

$$J_{ij} \propto \frac{\cos(2k_{\rm F}r_{ij})}{r_{ij}^3}, \tag{1.33}$$

where $k_{\rm F}$ denotes the Fermi wave number. In CuMn, the RKKY interactions work between the magnetic impurities Mn. The sign of the coupling depends on distance r_{ij} between the two interacting magnetic moments. Random locations of the impurities, thus, lead to ferromagnetic and antiferromagnetic interactions randomly.

To investigate such systems, the Ising spin-glass model,

$$H = -\sum_{i,j} J_{ij} S_i S_j, \tag{1.34}$$

has been proposed [81]. The couplings J_{ij} are random variables, which can take both positive and negative values. The system has frustration as a result. If the product of coupling constants on a plaquette, which is a minimal loop on a lattice, is negative, there is no spin configuration, permitting all bonds to be in the lowest-energy state, and the palaquette is then regarded to be frustrated or have frustration. Further, the locations of frustrated plaquettes are randomly distributed. The frustration causes extreme degeneracy of the ground states of the whole system. Thus, it is one of the most difficult problems to unveil properties of the spin-glass models at low temperatures.

Also in the context of the studies of critical phenomena in random quantum spin systems, quantum spin-glass models are particularly important issues. There are several ways to add quantum effects to the classical spin-glass models. We here consider the Ising spin glass in a transverse field to be compared with the random ferromagnetic Ising model in a transverse field. The quantum spin-glass model has been presumed to have an infinite-randomness fixed point based on an analogy with the random ferromagnet model [5]. In this conjecture, frustration is considered not to play any important role in the system. However, the method of the strong-disorder renormalization group has not successfully settled the issue so far, since the method is not effective in the spin-glass models as explained in Sec. 2.3.1. In contrast, other (rather old) numerical estimates [82,83] have indicated results against the conjecture, but the system size used in these studies might be too small.

Furthermore, a spin-glass model with the power-law interaction in a transverse-field has been investigated with a field-theoretical approach [84]. The interaction shows the power-law decay, that is, $J_{ij} \propto r_{ij}^{-\alpha/2}$ with distance of an interacting pair r_{ij}. It is important to investigate this model, since as mentioned in Sec. 1.3.2, the random transverse-field Ising model is realized in $\mathrm{LiHo}_x\mathrm{Y}_{1-x}\mathrm{F}_4$ to a good approximation [29–32], where the dipolar interaction written in Eq. (1.17) dominates [33–36]. In addition, the RKKY interaction is a kind of the power-law interaction as seen in Eq. (1.33). The study [84] has been done only in the case of the long-range interaction, that is, small α in the above expression. Concerning the large α region, a conjecture has been stated that critical phenomena are governed by an infinite-randomness fixed point [84]. This issue will be reviewed in Chap. 5.

1.5 Overview

This thesis explores critical phenomena in random quantum spin systems. We especially focus on the critical phenomena governed by infinite-randomness fixed points. In a system with the fixed point, the magnitude of randomness is infinitely amplified through coarse-graining processes. As a consequence, rare regions in the system strongly influence some macroscopic properties of the system. This fact illustrates an unusual property of the systems with infinite-randomness fixed points. Usually, we expect rare regions or rare events not to affect the behavior of the whole system. However, the cases where we cannot ignore them because of their strong effects are often found. Critical phenomena controlled by an infinite-randomness fixed point is one of such examples in physical systems. Our study in the thesis is intended to understand the unusual strong effects of rare regions to the macroscopic properties.

Specifically, we investigate the random transverse-field Ising models. As reviewed in this chapter, critical phenomena in these models are known to be controlled by infinite-randomness fixed points. However, the presence of the fixed points is controversial in some cases. In particular, the spin-glass cases with the nearest-neighbor interaction and with the power-law (rather short-range) interaction are still not analyzed. A compound $\mathrm{LiHo}_x\mathrm{Y}_{1-x}\mathrm{F}_4$ is expected to realize the random transverse-field Ising model [29–32], and is dominated by the dipolar couplings, which is a kind of the power-law interaction. Hence, the power-law interacting model should be especially examined. We tackle these cases with a renormalization-group method. The study in this thesis is not intended to further investigate the intrinsic properties of infinite-randomness fixed points. We focus on whether the models have an infinite-randomness fixed point or not.

Let us overview the present thesis. Chapter 2 reviews the renormalization-group theory. We first describe the framework of renormalization group. After that, we present an example of renormalization-group calculations and the Gaussian model, which gives an intuition about the relation between the classical Ising model and the transverse-field Ising model. We next review the strong-disorder renormalization group [40], which has been developed to reveal the properties of the random quantum spin systems. However, this method is not effective to spin-glass models. We then employ in this thesis another real-space renormalization-group method, whose prescription is outlined in the end of this chapter.

Chapter 3 applies our real-space renormalization-group method to the pure transverse-field Ising model, which is the basic model in the thesis. In the calculation of the one-dimensional model, we find the reason why we exploit the method that our method yields the results which agree with the exact solutions in the transition point and some critical exponents. We also generalize the method to higher-dimensional models. This generalization acts as the preparation to examine random systems in the next chapter.

Chapter 4 is one of the main parts in the thesis. We investigate the random transverse-field Ising models with our renormalization-group method generalized to random systems. We first examine the one-dimensional model, where asymptotically exact results [19, 20, 28] are well known. We next tackle the higher-dimensional models, where the presence of infinite-randomness fixed points is controversial. Specifically, we examine the random ferromagnetic Ising models and the Ising spin glasses

in a transverse field in two and three dimensions. The spin-glass case is especially important, since this case has not been explicitly analyzed, and the presence of an infinite-randomness fixed point remains a conjecture inferred from the ferromagnetic case [5].

Chapter 5 is the other main part of the thesis, where the long-range interacting systems are explored. This chapter is intended to examine the spin glass in a transverse field with the power-law interaction. Avoiding the direct analysis of the model, we employ an alternative model with the hierarchical interaction, which has the similar structure to the power-law interacting model. The power-law interaction and the hierarchical interaction are reviewed at first in this chapter. After that, we perform the renormalization-group calculations in the hierarchical model without randomness and confirm the compatibility of our scheme and the hierarchical model. We move to the spin-glass case, and examine the presence of an infinite-randomness fixed point.

We summarize our findings and conclude the thesis in Chap. 6.

Author's original works constitute some parts of the thesis. Chapter 3, in particular the generalization of the method to higher dimensions, and Chap. 4 are based on the author's works [85, 86] with Hidetoshi Nishimori (Chaps. 3 and 4) and Gerardo Ortiz (Chap. 3). The material in Chap. 5 except for the review part (Sec. 5.1) is also author's original work.

Chapter 2

Renormalization group

This chapter reviews the renormalization-group theory, which our analyses in the subsequent chapters are based on. We first describe the framework of renormalization group in Sec. 2.1. Section 2.2 gives an example of renormalization-group calculations, which demonstrates that a transverse field in the transverse-field Ising model at zero temperature plays the role of temperature in the classical Ising model. Thus, the scaling relations of classical systems without randomness explained in Sec. 2.1 are found also in the transverse-field Ising model, but with temperature replaced by a transverse field. Random systems, however, are not so simple. We see this fact via the strong-disorder renormalization group [40] in Sec. 2.3. This method is one of the standard tools to examine the critical properties of a system with an infinite-randomness fixed point. However, the method is not effective to investigate spin-glass models. We then utilize another approach, a kind of real-space renormalization-group, whose basic prescription is outlined in Sec. 2.4.

2.1 Framework of renormalization group

In the renormalization-group theory, macroscopic properties of a system are deduced from changes of parameters of the system through coarse-graining processes. The renormalization-group transformation, which is the pillar of the theory, is explained in Sec. 2.1.1. Section 2.1.2 finds how this transformation illuminates the feature of singularities in physical quantities.

2.1.1 Renormalization-group transformations

Let us consider some coarse-graining process, for example, partial trace of the partition function or truncation of the Hilbert space. The change of parameters is governed by the renormalization-group equation

$$\tilde{\boldsymbol{u}} = R_b(\boldsymbol{u}), \tag{2.1}$$

where $\boldsymbol{u}$ denotes a vector representing the set of all possible parameters and $\tilde{\boldsymbol{u}}$ is the renormalized one. An example of parameters is the nearest-neighbor couplings. The function $R_b(\cdot)$ expresses the renormalization-group transformation with the scaling

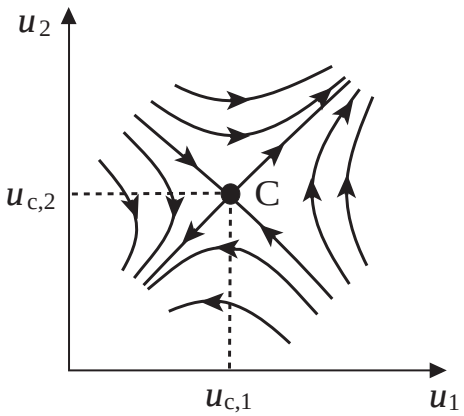

Figure 2.1: An example of renormalization-group flow concerning two parameters u_1 and u_2 in the vicinity of a fixed point $\mathrm{C}(u_{c,1}, u_{c,2})$.

factor b. It is natural that a set of two successive transformations with the scaling factors b_1 and b_2 is equivalent to the single transformation with the scaling factor $b_1 b_2$,

$$R_{b_1}\left(R_{b_2}(\boldsymbol{u})\right) = R_{b_1 b_2}(\boldsymbol{u}). \tag{2.2}$$

On iterating the renormalization group transformations, the system traces a trajectory in the parameter space. The set of all such trajectories generates a renormalization-group flow in the parameter space as illustrated in Fig. 2.1, where the flow is projected onto the u_1–u_2 plane. The flow has fixed points $\boldsymbol{u}^*$ of the transformation,

$$\boldsymbol{u}^* = R_b(\boldsymbol{u}^*), \tag{2.3}$$

which represent the coarse-grained macroscopic states.

We focus our attention on the local behavior of the renormalization-group flow in the vicinity of a fixed point. The renormalization-group transformation is expanded around the fixed point as

$$\tilde{\boldsymbol{u}} = R_b(\boldsymbol{u}^* + \delta\boldsymbol{u}) = R_b(\boldsymbol{u}^*) + \left.\frac{\partial R_b}{\partial \boldsymbol{u}}\right|_{\boldsymbol{u}^*} \delta\boldsymbol{u} + \cdots . \tag{2.4}$$

The linearized renormalization-group equation is

$$\delta\tilde{\boldsymbol{u}} = T_b(\boldsymbol{u}^*)\delta\boldsymbol{u}, \tag{2.5}$$

where

$$\delta\tilde{\boldsymbol{u}} = \tilde{\boldsymbol{u}} - \boldsymbol{u}^* = \tilde{\boldsymbol{u}} - R_b(\boldsymbol{u}^*), \tag{2.6}$$

$$T(\boldsymbol{u}^*) = \left.\frac{\partial R_b}{\partial \boldsymbol{u}}\right|_{\boldsymbol{u}^*}. \tag{2.7}$$

Components of the matrix $T_b(\boldsymbol{u}^*)$ are given by

$$\left(T_b(\boldsymbol{u}^*)\right)_{ij} = \left.\frac{\partial \tilde{u}_i}{\partial u_j}\right|_{\boldsymbol{u}^*}. \tag{2.8}$$

Although the matrix T_b is not necessarily diagonalizable, we assume that T_b is diagonalizable with real eigenvalues, which is the case in practice.

An eigenvalue of T_b is represented as a power of b,

$$\lambda_i(b) = b^{y_i}. \tag{2.9}$$

This is derived from Eq. (2.2). Eigenvalues of both sides of Eq. (2.2) are

$$\lambda_i(b_1)\lambda_i(b_2) = \lambda_i(b_1 b_2). \tag{2.10}$$

Differentiating this equation with respect to b_2, setting $b_2 = 1$,

$$\begin{aligned} \lambda_i(b_1)\frac{d\lambda_i(b_2)}{db_2}\bigg|_{b_2=1} =& \frac{d\lambda_i(b_1 b_2)}{db_2}\bigg|_{b_2=1} \\ =& b_1 \frac{d\lambda_i(b_1)}{db_1}, \end{aligned} \tag{2.11}$$

we obtain the differential equation for $\lambda_i(b_1)$,

$$\frac{d\lambda_i(b_1)}{db_1} = \frac{d\lambda_i(b_2)}{db_2}\bigg|_{b_2=1} \frac{\lambda_i(b_1)}{b_1}. \tag{2.12}$$

Note that $\lambda_i(1) = 1$ given by Eq. (2.2) setting $b_2 = 1$. Hence, the solution of Eq. (2.12) is the right hand side of Eq. (2.9).

The exponent y_i plays an important role. This fact is found in the expansion of $\delta\boldsymbol{u}$ and $\delta\tilde{\boldsymbol{u}}$ with eigenvectors $\{\boldsymbol{\phi}_i\}$ of T_b,

$$\delta\boldsymbol{u} = \sum_i g_i \boldsymbol{\phi}_i, \quad \delta\tilde{\boldsymbol{u}} = \sum_i \tilde{g}_i \boldsymbol{\phi}_i. \tag{2.13}$$

The coefficient g_i is called a scaling field, and g_i and $\tilde{g}_i$ have a relation as $\tilde{g}_i = b^{y_i} g_i$. When $g_i = 0$ for all i, the system lies at the fixed point. If $y_i < 0$, the value of g_i becomes smaller at every renormalization and finally converges to 0. On the other hand, if $y_i > 0$, the value of g_i grows and then diverges. For analysis of a fixed point, g_i for $y_i > 0$ needs to be already 0 before the renormalization-group transformation. The scaling field with positive y_i crucially influences the behavior of the system near fixed points. It is called, thus, relevant variables. The scaling field with a negative exponent is called an irrelevant variable and with $y_i = 0$ a marginal variable.

We next consider the global properties of a renormalization-group flow, which determine the phase diagram of the system. For a standard magnetic material, relevant variables for the fixed point corresponding to the critical point composed of the temperature T and magnetic field h. If we consider a quantum phase transition in the transverse-field Ising model, a transverse field should be treated as a relevant variable instead of temperature, as seen in Sec. 2.2.2. In the absence of a magnetic field, when the temperature does not take the critical value T_c, the system rapidly goes away from the fixed point through the renormalization-group transformations. All points on the line $T < T_c$ flow to the fixed point $T = 0$. There is another fixed point $T = \infty$ which attracts the flow on the line $T > T_c$. These two fixed points represent phases or the

points where the features of phases are illustrated most clearly. The fixed point $T = 0$ is the ferromagnetic phase and $T = \infty$ is the paramagnetic phase. These two fixed points are unstable for a magnetic field, and even the infinitesimal external field is enough to make flows leave for the fixed points $h = \pm\infty$. While the fixed points which have only one or no relevant variable correspond to phases, the fixed point where both two parameters are relevant usually represents a critical point.

2.1.2 Scaling law

Analyzing physical quantities under the renormalization-group transformations, we derive the relationship between critical exponents and the exponents of scaling fields. Since the partition function is kept constant by a renormalization-group transformation, the free energy density per a spin is transformed as

$$f(t, h) = b^{-d} f(b^{y_t} t, b^{y_h} h), \tag{2.14}$$

where $t = (T - T_c)/T_c$, and d is the spatial dimension, and y_t and y_h represent the exponents of the scaling fields of temperature and a magnetic field, respectively. We have to note a few remarks on this equation. Although the eigenvectors of the linearized renormalization-group transformation in this case would be linear combinations of t and h, we nevertheless assume that t and h are not mixed. We identify the scaling fields of temperature and a magnetic field with t and h, respectively. Non-singular terms which can be included in the equation are left out, because those terms do not contribute to the singularities at the critical point which we are going to study. Irrelevant variables are also not written.

After iterating the transformation n times, Eq. (2.14) becomes

$$f(t, h) = b^{-nd} f(b^{ny_t} t, b^{ny_h} h). \tag{2.15}$$

Choosing the number n such that $b^{ny_t} t = 1$ or $b^{ny_h} h = 1$, we have the scaling law,

$$f(t, h) = t^{d/y_t} f(1, h t^{-y_h/y_t}), \tag{2.16}$$

or

$$f(t, h) = h^{d/y_h} f(t h^{-y_t/y_h}, 1). \tag{2.17}$$

The relations between critical exponents and y_t and y_h are extracted from the derivative of the free energy,

$$C(t, 0) \propto \frac{\partial^2 f(t, 0)}{\partial t^2} \propto t^{d/y_t - 2}, \tag{2.18}$$

$$m(t, 0) \propto \left.\frac{\partial f(t, h)}{\partial h}\right|_{h=0} \propto t^{(d-y_h)/y_t}, \tag{2.19}$$

$$\chi(t, 0) \propto \left.\frac{\partial^2 f(t, h)}{\partial h^2}\right|_{h=0} \propto t^{(d-2y_h)/y_t}, \tag{2.20}$$

$$m(0, h) \propto \frac{\partial f(0, h)}{\partial h} \propto h^{d/y_h - 1}. \tag{2.21}$$

Compared with the relations (1.1)–(1.4), these lead to the following relations,

$$\alpha = 2 - \frac{d}{y_t}, \quad \beta = \frac{d - y_h}{y_t}, \quad \gamma = \frac{2y_h - d}{y_t}, \quad \delta = \frac{y_h}{d - y_h}. \tag{2.22}$$

We next consider the scaling law of the correlation length,

$$\xi(t, h) = b\, \xi(b^{y_t} t, b^{y_h} h). \tag{2.23}$$

Setting $h = 0$ and n to be $b^{ny_t} t = 1$, we have

$$\xi(t, 0) \propto t^{-1/y_t}. \tag{2.24}$$

This gives

$$\nu = \frac{1}{y_t}. \tag{2.25}$$

Finally, the scaling law of the correlation function $G(r, t) = \langle S(0)S(r)\rangle - \langle S(0)\rangle\langle S(r)\rangle$ is represented as

$$G(r, t) = b^{-2d+2y_h} G(b^{-1} r, b^{y_t} t). \tag{2.26}$$

The coefficient b^{-2d+2y_h} is derived from the scaling law of the magnetization m,

$$m(t, 0) = b^{-d+y_h} m(b^{y_t} t, 0). \tag{2.27}$$

This is the derivative of Eq. (2.14) with respect to h. For $t = 0$ and $b = r$, we obtain

$$G(r, 0) \propto r^{-2d+2y_h}, \tag{2.28}$$

from which the following relation is extracted,

$$\eta = d - 2y_h + 2. \tag{2.29}$$

2.2 Momentum-space renormalization group and the Gaussian model

This section reviews an example of renormalization-group calculations which is performed in the momentum-space representation [3, 87]. This review is intended to consider critical phenomena and scaling relations in quantum spin systems, in particular the transverse-field Ising model, through the common description, the Gaussian model, to classical and quantum systems. Moreover, this section is also intended to prepare for the review part in Chap. 5. The expression explained in this section has been used in previous studies [84, 88] related to our study in Chap 5. The first subsection considers the classical Ising model, and the next, the transverse-field Ising model.

2.2.1 Classical Ising model

Let us imagine the d-dimensional Ising model

$$H = -\frac{1}{2}\sum_{i,j} J(\boldsymbol{R}_i - \boldsymbol{R}_j) S_i S_j. \tag{2.30}$$

Although spin variables S_i should take ± 1, we here adopt the continuous spin model [3, 87] where the spin length is allowed to vary continuously. The continuous spins are interpreted as coarse-grained spins of neighboring Ising spins. To avoid S being too large, a sum of functions $\sum_i w(S_i)$, where

$$w(S) = \frac{1}{2}S^2 + uS^4 + \dots \tag{2.31}$$

is introduced into the partition function

$$Z = \int \Big(\prod_i dS_i\Big) \exp(\bar{H}), \tag{2.32}$$

$$\bar{H} = -\beta H + W(\{S\}), \tag{2.33}$$

where β denotes inverse temperature T^{-1}. We use a unit where $k_B = 1$.

We next introduce a momentum-space representation

$$\bar{H} = -\frac{1}{2}\left(\frac{a}{2\pi}\right)^d \int d^d q V_2(\boldsymbol{q}) \hat{S}_{\boldsymbol{q}} \hat{S}_{-\boldsymbol{q}} + \dots, \tag{2.34}$$

where

$$V_2(\boldsymbol{q}) = \frac{1}{c^2}\big[1 - \beta \hat{J}(\boldsymbol{q})\big]. \tag{2.35}$$

We have used Fourier transformed functions $\hat{S}_{\boldsymbol{q}}$ and $\hat{J}(\boldsymbol{q})$, and a denotes the lattice spacing. The coefficient c will be determined below. Although the terms of the higher orders in the spins $\hat{S}$ exist in $\bar{H}$ because of the corresponding higher-order terms in $w(S)$, we here kept only the terms bilinear in the spins $\hat{S}$. The Gaussian model is then obtained. If the terms of S^4 are considered, the model corresponds to the so-called ϕ^4 model.

The function $\hat{J}(\boldsymbol{q})$ is expanded in powers of $\boldsymbol{q}$ apart from terms $J_{\text{n.a.}}(\boldsymbol{q})$ which are non-analytic in $\boldsymbol{q}$, and then we have

$$V_2(\boldsymbol{q}) = r + q^2 - \frac{1}{j}\hat{J}_{\text{n.a.}}(\boldsymbol{q}) + O(q^4), \tag{2.36}$$

where

$$r = \frac{1}{j}\big[T - J(0)\big]. \tag{2.37}$$

with some constant j. We have determined c as $c^2 = \beta j$ to normalize the coefficient of q^2 in Eq. (2.36) to be unity.

The partition function is now written as

$$Z = \int \Big(\prod_{|\boldsymbol{q}|<\Lambda} d\hat{S}_{\boldsymbol{q}} \Big) \exp\big(\bar{H}[\hat{S}_{\boldsymbol{q}}]\big) \tag{2.38}$$

with $\bar{H}[\hat{S}_{\boldsymbol{q}}]$ given by Eq. (2.34). The range of $\boldsymbol{q}$ is restricted by $|\boldsymbol{q}| < \Lambda \propto 1/a$. The renormalization-group calculation of this model is to perform the integral in steps. We first integrate over $\hat{S}_{\boldsymbol{q}}$ with $\Lambda/b < |\boldsymbol{q}| < \Lambda$ and $b > 1$. Then, we have

$$Z = \int \Big(\prod_{|\boldsymbol{q}|<\Lambda/b} d\hat{S}_{\boldsymbol{q}} \Big) \exp\big(\bar{H}_1[\hat{S}_{\boldsymbol{q}}]\big) \tag{2.39}$$

with

$$\exp(\bar{H}_1[\hat{S}_{\boldsymbol{q}}]) = \int \Big(\prod_{\Lambda/b<|\boldsymbol{q}|<\Lambda} d\hat{S}_{\boldsymbol{q}} \Big) \exp\big(\bar{H}[\hat{S}_{\boldsymbol{q}}]\big). \tag{2.40}$$

We next bring the right hand side of Eq. (2.39) to the original form, namely the right hand side of Eq. (2.38). To this end, momentum vectors and spin variables are rescaled as

$$\boldsymbol{q}' = b\boldsymbol{q}, \quad \hat{S}'_{\boldsymbol{q}'} = b^{x_S} \hat{S}_{\boldsymbol{q}}, \tag{2.41}$$

where x_S will be determined below. By introducing these new variables, the terms bilinear in the spins $\hat{S}$ in $\bar{H}_1$ become

$$\int_{|\boldsymbol{q}|<\Lambda/b} d^d q V_2(\boldsymbol{q}) \hat{S}_{\boldsymbol{q}} \hat{S}_{-\boldsymbol{q}} = \int_{|\boldsymbol{q}'|<\Lambda} b^{-d} d^d q' V_2(b^{-1}\boldsymbol{q}') b^{-x_S} \hat{S}'_{\boldsymbol{q}'} b^{-x_S} \hat{S}'_{-\boldsymbol{q}'} \tag{2.42}$$

$$= \int_{|\boldsymbol{q}'|<\Lambda} d^d q' V_2'(\boldsymbol{q}') \hat{S}'_{\boldsymbol{q}'} \hat{S}'_{-\boldsymbol{q}'}, \tag{2.43}$$

where V_2 is rescaled as

$$V_2'(\boldsymbol{q}') = b^{-d-2x_S} V_2(b^{-1}\boldsymbol{q}'). \tag{2.44}$$

To retrieve the original form represented in Eq. (2.36), the coefficient of q^2 in Eq. (2.44), b^{-d-2x_S-2}, is normalized to be unity. We then find

$$x_S = -\frac{d+2}{2}. \tag{2.45}$$

Accordingly, we obtain

$$r' = b^2 r, \tag{2.46}$$

$$\hat{J}'_{\text{n.a.}}(\boldsymbol{q}') = b^2 \hat{J}_{\text{n.a.}}(b^{-1}\boldsymbol{q}'). \tag{2.47}$$

The above process represents the renormalization-group transformation which generates a new effective Hamiltonian $\bar{H}'[\hat{S}_{\boldsymbol{q}'}]$ $(= \bar{H}_1[\hat{S}_{\boldsymbol{q}}])$.

In the short-range-interaction case, there is no non-analytic term $\hat{J}_{\rm n.a.}(\boldsymbol{q})$, and then the single parameter r represents temperature $T - J(0)$. By using the scaling law, Eq. (2.46) identifies $y_t = 2$. Similar deduction for y_h is found by including a magnetic field in the Hamiltonian,

$$\bar{H}_h = -\sum_i h(\boldsymbol{R}_i) S_i = -\left(\frac{a}{2\pi}\right)^d \int d^d q \hat{h}_{\boldsymbol{q}} \hat{S}_{-\boldsymbol{q}}. \tag{2.48}$$

The right hand side of this equation gives the scaling relation of the magnetic field,

$$h'_{\boldsymbol{q}} = b^{-d-x_s} h_{b^{-1}\boldsymbol{q}} = b^{-(d-2)/2} h_{b^{-1}\boldsymbol{q}}. \tag{2.49}$$

Hence, we find

$$h'(\boldsymbol{R}) = b^{(d+2)/2} h(b\boldsymbol{R}), \tag{2.50}$$

and $y_h = (d+2)/2$ as a result. The values of y_t and y_h obtained from the Gaussian model, $(y_t, y_h) = (2, (d+2)/2)$, correspond to the well known mean-field values. Thus, the Gaussian model is regarded to yield the mean-field theory.

In the case of the power-law interaction, $J(\boldsymbol{R}) \propto R^{-\alpha}$, $\hat{J}_{\rm n.a.}(\boldsymbol{q})$ does not vanish. The critical exponents of the Gaussian model accordingly change from those obtained above. We will revisit this case in Chap. 5, where we study the transverse-field Ising models with the power-law interaction.

2.2.2 Transverse-field Ising model

We move to the description of quantum systems in the renormalization-group picture [89, 90]. In particular, the transverse-field Ising model

$$H = -\frac{1}{2}\sum_{i,j} J_{ij}\sigma_i^z\sigma_j^z - \Gamma\sum_i \sigma_i^x, \tag{2.51}$$

is considered, where σ denotes the Pauli matrix. To handle non-commuting spin operators, we use this expression,

$$\exp(-\beta H) = \mathscr{T} \exp(H_x)\exp(H_z), \tag{2.52}$$

where $\mathscr{T}$ is a τ-ordering prescription and

$$H_x = \Gamma\int_0^\beta d\tau \sum_i \sigma_i^x(\tau), \quad H_z = \frac{1}{2}\int_0^\beta d\tau \sum_{i,j} J_{ij}\sigma_i^z(\tau)\sigma_j^z(\tau). \tag{2.53}$$

Note that τ of an operator $\sigma(\tau)$ is only a label of the position of the operator in a product of operators, and we do not use the interaction representation.

Using a formula,

$$\exp\left(\frac{1}{2}\sum_{i,j}\sigma_i(A^2)_{ij}\sigma_j\right) = \int_{-\infty}^{\infty}\left(\prod_i \frac{ds_i}{\sqrt{2\pi}}\right)\exp\left(-\frac{1}{2}\sum_i s_i^2 + \sum_{i,j} s_i A_{ij}\sigma_j\right) \tag{2.54}$$

we obtain the partition function of the Hamiltonian Eq. (2.51)

$$Z = \mathrm{Tr}\exp(-\beta H) \propto [\mathrm{Tr}\exp(H_x)] \int_\infty^\infty \left(\prod_{i,\tau} ds_i(\tau) \right) \exp\left\{ -\frac{1}{2}\int_0^\beta d\tau \sum_i [s_i(\tau)]^2 + \sum_{n=1}^\infty \frac{1}{n!} \left\langle \left[\int_0^\beta d\tau \sum_{i,j} s_i(\tau) A_{ij} \sigma_j^z(\tau) \right]^n \right\rangle_{x,c} \right\} \tag{2.55}$$

where $\langle\cdot\rangle_x = \mathrm{Tr}[\mathscr{T}\exp(H_x)\cdot\,]/\mathrm{Tr}\exp(H_x)$ and the subscript c denotes cumulant averages. In addition, we have used $(A^2)_{ij} = J_{ij}$. Some calculations, where we use $\exp(\beta\Gamma\sigma^x) = \cosh(\beta\Gamma) + \sigma^x \sinh(\beta\Gamma)$, lead to

$$\langle \sigma_i^z(\tau) \rangle_{x,c} = 0, \tag{2.56}$$

$$\langle \sigma_i^z(\tau_1)\sigma_j^z(\tau_2) \rangle_{x,c} = \delta_{i,j} \frac{\cosh[(\beta - 2\tau_1 - 2\tau_2)\Gamma]}{\cosh(\beta\Gamma)}, \tag{2.57}$$

where we assume $\tau_1 > \tau_2$. The partition function is then written as

$$Z \propto \int_\infty^\infty \left(\prod_{i,\tau} ds_i(\tau) \right) \exp\left(-\frac{1}{2}\int_0^\beta d\tau_1 d\tau_2 \sum_{i,j} \left\{ \delta_{i,j}\delta(\tau_1 - \tau_2) - J_{ij} \frac{\cosh[(\beta - 2\tau_1 - 2\tau_2)\Gamma]}{\cosh(\beta\Gamma)} \right\} s_i(\tau_1) s_j(\tau_2) + \cdots \right). \tag{2.58}$$

After Fourier transforming, the coefficient $u_2(\boldsymbol{q}, m)$ of the terms bilinear in $\hat{s}_{\boldsymbol{q},m}$, where m labels a frequency $\omega_m = 2\pi m/\beta$, is represented as

$$u_2(\boldsymbol{q}, m) = \frac{1}{j}\left[\frac{4\Gamma^2 + \omega_m^2}{4\Gamma \tanh(\beta\Gamma)} - \hat{J}(0) \right] + q^2 + \hat{J}_{\mathrm{n.a.}}(\boldsymbol{q}) + O(q^4) \tag{2.59}$$

$$\to \frac{1}{4\Gamma j}\omega^2 + \frac{1}{j}[\Gamma - \hat{J}(0)] + q^2 + \hat{J}_{\mathrm{n.a.}}(\boldsymbol{q}) + O(q^4), \tag{2.60}$$

where we normalize the coefficient of q^2 to be unity, and the zero-temperature limit has been taken. This expression is the same form as the coefficient of the corresponding bilinear terms of the classical Ising model, Eqs. (2.36) and (2.37), apart from the term of ω^2, but with T replaced by Γ.

In the renormalization-group calculations, ω is also rescaled as

$$\omega' = b^z \omega. \tag{2.61}$$

We have the corresponding calculation to Eq. (2.43)

$$\int_0^{\beta^{-1}b^{-z}} d\omega \int_{|\boldsymbol{q}|<\Lambda/b} d^d\boldsymbol{q}\; u_2(\omega, \boldsymbol{q}) \hat{s}_{\omega,\boldsymbol{q}} \hat{s}_{\omega,-\boldsymbol{q}} \tag{2.62}$$

$$= \int_0^{\beta^{-1}} d\omega' \int_{|\boldsymbol{q}|<\Lambda} d^d\boldsymbol{q}' \left(\frac{1}{4\Gamma j} b^{-d'-2z-2x_s}\omega'^2 + \frac{1}{j} b^{-d'-2x_s} r + b^{-d'-2-x_s} q'^2 + \hat{J'}_{\mathrm{n.a.}}(\boldsymbol{q}') \right) \hat{s}'_{\omega',\boldsymbol{q}'} \hat{s}_{\omega',-\boldsymbol{q}'}, \tag{2.63}$$

where $d' = d + z$ and $r = \Gamma - \hat{J}(0)$. Normalizing the coefficient of ω'^2 and q'^2 in Eq. (2.63), $b^{-d'-2z-2x_s}$ and $b^{-d'-2-x_s}$, to be unity, we find

$$x_s = -\frac{d'+2}{2}, \tag{2.64}$$

$$z = 1. \tag{2.65}$$

Accordingly, we obtain

$$r' = b^2 r, \tag{2.66}$$

$$\hat{J'}_{\text{n.a.}}(\boldsymbol{q}') = b^2 \hat{J}_{\text{n.a.}}(\boldsymbol{q}). \tag{2.67}$$

This result demonstrates that static critical phenomena of the d-dimensional transverse-field Ising model at zero temperature are described in the same form as in the $(d+z)$-dimensional classical Ising model with $z = 1$. Moreover, the transverse field in the quantum system plays the role of temperature in the classical system. Thus, the scaling relations Eqs. (2.22), (2.25), and (2.29) are satisfied also in the transverse-field Ising model, but with T replaced by Γ. We will use these relations in Chap. 3. A different character of the quantum critical phenomena from the classical ones is shown in the dynamical exponent z, which is associated with the scaling of ω.

2.3 Strong-disorder renormalization group

This section gives a short review of the strong-disorder renormalization group [40], which has been originally proposed by Ma, Dasgupta, and Wu [38] and has been developed by Fisher [19, 20] to study the random transverse-field Ising chain

$$H = -\sum_i J_i \sigma_i^z \sigma_{i+1}^z - \sum_i \Gamma_i \sigma_i^x \tag{2.68}$$

with random positive couplings $J_i > 0$ and random positive transverse fields $\Gamma_i > 0$. We have found in the last section that the static critical phenomena of the transverse-field Ising model at zero temperature are described in the same form as in the classical Ising model at finite temperatures. However, the random transverse-field Ising chain does not belong to the same category. Randomness can drastically change the nature of critical phenomena as reviewed in Chap. 1. Indeed, the parameter $\log \Gamma$ rather than Γ is appropriate to describe the system. The strong-disorder renormalization group grasps the peculiar scalings, in particular lying between length and energy, which this section aims to explicitly show.

2.3.1 General rules of the strong-disorder renormalization group

This subsection explains the general rules of the strong-disorder renormalization group. This method treats the highest-energy part in a random system and then renormalizes the part into the lower-energy system. This rule follows the general strategy of renormalization group that to deduce the property in the objective scale, which is now the lowest-energy scale, we first treat the distant scale, namely the highest-energy

scale. Specifically, the strongest parameter among bonds J_i and transverse fields Γ_i are focused on at first.

If the strongest term is a bond, say, J_2, the fields Γ_2 and Γ_3 which are applied to the two spins linked by the bond are typically much smaller than J_2, that is, $J_2 \gg \Gamma_2$, Γ_3. Thus, the two spins 2 and 3 are almost always parallel and behave a composite spin with double momentum. In the terms in the Hamiltonian, Eq. (2.68), associated only with the two spins,

$$H_{2,3} = -J_2\sigma_2^z\sigma_3^z - \Gamma_2\sigma_2^x - \Gamma_3\sigma_3^x, \tag{2.69}$$

the field terms $-\Gamma_2\sigma_2^x - \Gamma_3\sigma_3^x$ are taken into account as a perturbation to $-J_2\sigma_2^z\sigma_3^z$. Then, an effective transverse field which the composite spin feels is calculated as

$$\tilde{\Gamma}_{2,3} \simeq \frac{\Gamma_2\Gamma_3}{J_2} \tag{2.70}$$

with the second order perturbation. As a consequence, $H_{2,3}$ is transformed into a composite spin in a field

$$\tilde{H}_{2,3} = -\tilde{\Gamma}_{2,3}\tilde{\sigma}_{2,3}^x. \tag{2.71}$$

In the above process, the two highest-energy states of $H_{2,3}$ in the second order perturbation is ignored. The validity of this ignorance is given by a large energy gap about $2J_2$ between the ignored states and the kept states.

On the other hand, if the strongest term is a field, say, Γ_2, the bonds J_1 and J_2 which are connected with spin 2 represented as

$$H_{1,2,3} = -J_1\sigma_1^z\sigma_2^z - \Gamma_2\sigma_2^x - J_2\sigma_2^z\sigma_3^z, \tag{2.72}$$

are much smaller than Γ_2, that is, $\Gamma_2 \gg J_1, J_2$. Thus, the spin is isolated from the other spins, and is regarded as a dead spin. In contrast, remaining spins are active, which concerns critical phenomena with the activated scaling. Two spins 1 and 3 are then coupled with a new coupling constant

$$\tilde{J}_{1,2} \simeq \frac{J_1J_2}{\Gamma_2}, \tag{2.73}$$

calculated with the second order perturbation. Hence, $H_{1,2,3}$ is transformed into

$$\tilde{H}_{1,2,3} = -\tilde{J}_{1,2}\sigma_1^z\sigma_3^z. \tag{2.74}$$

Also in this case, the four highest-energy states of $H_{1,2,3}$ are ignored.

We trace the change of the distributions of J_i and Γ_i. The distributions are expressed as functions of the value Ω of the strongest parameter such as $P_J(J,\Omega)$ and $P_\Gamma(\Gamma,\Omega)$. We deduce differential equations about the distributions under the renormalization process described above. We then observe how physical quantities are changed as the energy scale Ω changes.

The new parameters such as $\tilde{\Gamma}_{2,3}$ and $\tilde{J}_{1,2}$ are smaller than the original parameters. For instance, if $J_2 \gg \Gamma_2$, Γ_3, we have $\Gamma_2\Gamma_3/J_2 < J_2, \Gamma_2$, and Γ_3. Hence, these two

processes reduce the highest-energy scale $\Omega = \max\{J_i, \Gamma_i\}$ in the system. During an infinitesimal decrease of the highest-energy scale as $\Omega \to \Omega - d\Omega$, the distribution of bonds changes as

$$\begin{aligned} P_J(J, \Omega - d\Omega) = \Bigg\{ & P_J(J,\Omega) + d\Omega P_\Gamma(\Omega,\Omega) \int_0^\Omega dJ_1 \int_0^\Omega dJ_2 P_J(J_1,\Omega) P_J(J_2,\Omega) \\ & \times \left[\delta\left(J - \frac{J_1 J_2}{\Omega} \right) - \delta(J - J_1) - \delta(J - J_2) \right] \Bigg\} \\ & \times \{1 - d\Omega[P_J(\Omega,\Omega) + P_\Gamma(\Omega,\Omega)]\}^{-1}, \end{aligned} \tag{2.75}$$

by the bond decimation, where the strongest parameter is a field Γ_2. The coefficient $P_\Gamma(\Omega,\Omega)$ of the integral means that the strongest parameter is a field. The three delta functions represent the generation of a bond and the decimation of two bonds in the transformation. The last factor $\{1 - d\Omega[P_J(\Omega,\Omega) + P_\Gamma(\Omega,\Omega)]\}^{-1}$ normalizes the distribution as $\int_0^{\Omega - d\Omega} dJ P_J(J, \Omega - d\Omega) = 1$. Equation (2.75) leads to

$$\begin{aligned} \frac{\partial P_J(J,\Omega)}{\partial \Omega} = & P_J(J,\Omega)[P_\Gamma(\Omega,\Omega) - P_J(\Omega,\Omega)] \\ & - P_\Gamma(\Omega,\Omega) \int_J^\Omega dJ' P_J(J',\Omega) P_J\left(\frac{J}{J'}\Omega, \Omega \right) \frac{\Omega}{J'}. \end{aligned} \tag{2.76}$$

Similarly, the differential equation for the distribution of the fields is obtained as

$$\begin{aligned} \frac{\partial P_\Gamma(\Gamma,\Omega)}{\partial \Omega} = & P_\Gamma(\Gamma,\Omega)[P_J(\Omega,\Omega) - P_\Gamma(\Omega,\Omega)] \\ & - P_J(\Omega,\Omega) \int_\Gamma^\Omega d\Gamma' P_\Gamma(\Gamma',\Omega) P_\Gamma\left(\frac{\Gamma}{\Gamma'}\Omega, \Omega \right) \frac{\Omega}{\Gamma'}. \end{aligned} \tag{2.77}$$

It is essential in this scheme that the interactions are positive, namely the ferromagnetic interactions. When the strongest parameter is a ferromagnetic bond, we can interpret the two spins linked by the bond as a composite spin. The renormalized system is also a spin system. We can iterate the procedure as a result. However, if the strongest one is an antiferromagnetic bond, the interpretation would not be permitted. The two spins would be antiparallel represented as $|\uparrow\downarrow\rangle$ or $|\downarrow\uparrow\rangle$, which are not expressed as a single spin. Thus, the scheme stops at this step. In the one-dimensional model, this issue is not crucial, since the antiferromagnetic interactions are mapped onto the ferromagnetic interactions by the gauge transformation: $\sigma^x \to \sigma^x$, $\sigma^y \to -\sigma^y$, and $\sigma^z \to -\sigma^z$, which preserves the commutation relation of a spin, $[\sigma^x, \sigma^y] = 2i\sigma^z$. This transformation, however, cannot remove the problem in some higher-dimensional models, for example, the spin-glass models, which have both ferromagnetic and antiferromagnetic interactions randomly. Hence, the method of the strong-disorder renormalization group is not effective in the spin-glass models. To investigate the spin-glass models, we employ another procedure in this thesis.

2.3.2 Relationship between energy and length

We try to extract a relation between the energy scale and the length scale at the critical point from the renormalization-group flow. The relation represents a peculiar

feature of the critical phenomena of this model. We first carry out an intuitive argument [12]. After that, concrete calculations [20, 40, 91] based on Eqs. (2.76) and (2.77) are described.

We consider the system at the critical point. The correlation length is a characteristic length of the system, and it is the length of a cluster where all spins are correlated. The cluster results in a compound spin after the renormalization-group steps. In the renormalization-group scheme, such a cluster or compound spin is produced and grows in each step of the scheme when the strongest term is a bond. When the length of a cluster extends by a unit length, namely the distance of the neighboring spins, the effective field is the product of fields divided by a bond as shown in Eq. (2.70). Hence, an effective field $\tilde{\Gamma}_i$ is a product of some number, say, f_i, of original fields divided by $f_i - 1$ original bonds, and typical diameter L_Ω of a cluster scales as a power of f_i. Since the number f_i is similar to $\log \Omega$ rather than Ω, we write the scaling relation between energy and length as

$$\log \frac{\Omega_0}{\Omega} \sim L_\Omega^\psi, \tag{2.78}$$

with the basic energy scale Ω_0, for example the initial value of Ω, and with an exponent ψ.

This scaling is a peculiar one, compared with the conventional scaling at critical points where energy scales as $\Omega \sim L_\Omega^{-z}$ with the dynamical exponent z. The unconventional scaling is regarded as the divergence of z and shows an extremely slow dynamics. The key point yielding this scaling is that in a single step of renormalization-group process, the lengths of clusters are added while the couplings and fields are multiplied.

As mentioned above, an effective field is expressed as a product of f_i fields divided by $f_i - 1$ bonds and an effective bond is also similarly expressed. Hence, the logarithm of an effective field or bond is a sum of logarithm of several original random parameters. This fact implies that the width of the distributions of $\log \Gamma$ and $\log J$ diverges as renormalization-group calculations are iterated and $\Omega \to 0$. In short, the nature of infinite-randomness fixed point is suggested.

We move to an overview of the derivation [20, 40, 91] of the scaling relation between energy and length. A solution of Eqs. (2.76) and (2.77) is given by

$$P_J(J, \Omega) = \frac{r(\Omega)}{\Omega} \left(\frac{\Omega}{J} \right)^{1-r(\Omega)}, \tag{2.79}$$

$$P_\Gamma(\Gamma, \Omega) = \frac{p(\Omega)}{\Omega} \left(\frac{\Omega}{\Gamma} \right)^{1-p(\Omega)}, \tag{2.80}$$

where the two functions $r(\Omega)$ and $p(\Omega)$ satisfy

$$-\frac{dy(\Omega)}{d \log \Omega} + y(\Omega)^2 = \Delta \tag{2.81}$$

with $y(\Omega) = p(\Omega) - \Delta = r(\Omega) + \Delta$. Note that $d\Delta/d\Omega = 0$, and hence Δ is independent of Ω. The difference of the distributions is controlled by Δ. The critical point is

represented as $\Delta = 0$, since the two distributions should coincide with each other to produce the relation at the critical point in Eq. (1.16). However, Δ does not denote the energy gap, and we should not confuse them.

We are now interested in the critical point, $\Delta = 0$, where the two functions $p(\Omega)$ and $r(\Omega)$ have the same form as the solution to Eq. (2.81) with $\Delta = 0$,

$$y(\Omega) = p(\Omega) = r(\Omega) = \frac{1}{\log(\Omega_0/\Omega)}. \tag{2.82}$$

A characteristic length scale of the system is the typical distance between remaining spins, namely not decimated spins. At the critical point, the distance corresponds to the length of a cluster or the size of a composite spin focused on in the above intuitive argument, and also to the number of consecutive isolated spins. The distance is estimated as $L_\Omega \sim n_\Omega^{-1}$, where n_Ω denotes the fraction of remaining spins at scale Ω. With the decrease of the energy scale by an amount of $d\Omega$, a fraction of spins which are decimated out is $n_\Omega[P_J(\Omega,\Omega) + P_\Gamma(\Omega,\Omega)]$. We then have

$$\frac{dn_\Omega}{d\Omega} = n_\Omega[P_J(\Omega,\Omega) + P_\Gamma(\Omega,\Omega)]. \tag{2.83}$$

With Eqs. (2.79), (2.80), and (2.82), this is solved as

$$n_\Omega = \left(\log\frac{\Omega_0}{\Omega}\right)^{-2}. \tag{2.84}$$

We therefore obtain the scaling relation

$$\log\frac{\Omega_0}{\Omega} \sim L_\Omega^{1/2}, \tag{2.85}$$

which gives the exponent $\psi = 1/2$.

2.4 Our renormalization-group scheme

This section develops the basic idea of the real-space renormalization-group scheme for quantum spin systems which will be used in the remainder of this thesis. We confine our analysis to the description of phase transitions and critical phenomena at zero temperature. Systems are not disturbed by thermal fluctuation accordingly. Consequently, quantum effects dominantly influence the nature of systems.

Principle of our scheme is explained at first, and then its properties are discussed. Concrete calculations based on the scheme will be demonstrated in the next chapter.

2.4.1 Principle of our scheme

Our scheme starts with the division of a system into blocks. Holding only the lowest-energy states of blocks, we carry out a coarse-graining process. The present method is a conventional approach on the basis of the block-spin transformation [92] for quantum systems [93–99].

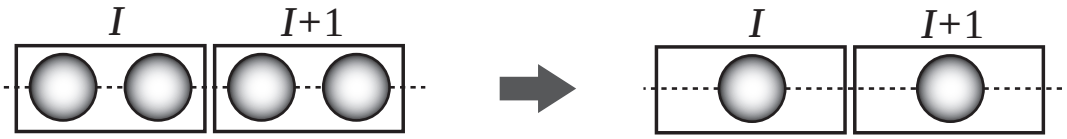

Figure 2.2: Construction of blocks and coarse-graining process in one dimension.

To illustrate the scheme, let us consider the Hamiltonian H of a quantum spin system. For example, imagine the Hamiltonian of the transverse-field Ising chain introduced in Sec. 1.3.1,

$$H = -J \sum_i \sigma_i^z \sigma_{i+1}^z - \Gamma \sum_i \sigma_i^x, \tag{2.86}$$

which is the simplest quantum spin model exhibiting a phase transition and critical phenomenon.

We start our scheme by dividing the lattice into blocks of spins, as shown in Fig. 2.2. We assume a block contains n spins. In general, the number of spins in a block is not limited to be the same as that in other blocks. In a uniform model, however, it is natural to divide the system uniformly. According to the division of the system, the Hamiltonian is also split into the intrablock part $H_I^{\rm intra}$ for couplings between spins in a block I and the interblock part $H_{I,J}^{\rm inter}$ for couplings between spins in different blocks I and J,

$$H = \sum_I H_I^{\rm intra} + \sum_{I,J} H_{I,J}^{\rm inter}. \tag{2.87}$$

The partition of the Hamiltonian is not unique. Indeed, $H^{\rm intra}$ and $H^{\rm inter}$ can have terms associated with the transverse field applied to spins on the edges of blocks, as shown in the next section for the transverse-field Ising chain. Results of the following calculations depend on the choice of the block partition.

The next step is a coarse-graining procedure carried out by using eigenstates of $H^{\rm intra}$. In the spin-s system, $H_I^{\rm intra}$ has $(2s+1)^n$ eigenstates. Note that n is the number of spins in a block. For example, if we use blocks of two spins in analyzing the transverse-field Ising chain, $H^{\rm intra}$ has four eigenstates. To truncate the Hilbert space, we focus only on the $2s+1$ lowest-lying eigenstates represented as $|1\rangle, |2\rangle, \ldots, |2s+1\rangle$. We define the projector onto a truncated system as

$$P = \bigotimes_I P_I, \tag{2.88}$$

where P_I is the projector,

$$P_I = \left(\sum_{m=1}^{2s+1} |m\rangle\langle m| \right)_I. \tag{2.89}$$

The projected Hamiltonian is PHP, which consists of $PH^{\rm intra}P$ and $PH^{\rm inter}P$. Note that $PH^{\rm intra}P$ is a diagonal matrix in the basis $|1\rangle, |2\rangle, \ldots, |2s+1\rangle$. This projection

realizes a coarse-graining process, since the dimension of the state space of a block reduces to the dimension of an original spin, $2s+1$. Moreover, these $2s+1$ vectors have properties of the original blocks effectively. Furthermore, we consider situations where the coarse-grained Hamiltonian can be expressed with the new spin operators defined as $S^z|m\rangle = m|m\rangle$ and $S^{\pm}|m\rangle = \sqrt{s(s+1) - m(m\pm 1)}|m\pm 1\rangle$. If $s = 1/2$, the Hamiltonian is necessarily so. The blocks are then transformed into spins as shown in Fig. 2.2, and the length scale grows. This is just a block-spin transformation.

According to the real-space renormalization-group framework, spatial length in the system is rescaled. More specifically, we normalize the distance between new spins to the original value. We then obtain the renormalized system.

The process described above constitutes a step of our renormalization-group transformation. The transformations change the values of parameters in the Hamiltonian and generate additional couplings. The change is drawn as a renormalization-group flow in the space of parameters, accordingly. Following the prescription of renormalization group, our scheme finishes by extracting the nature of phases, phase transitions, and critical phenomena of the system from the flow .

2.4.2 Basic properties of our scheme

The coarse-graining procedure in our scheme is expected to be effective for the study of the ground state, since we keep only the lowest-energy states of blocks and drop the others. The process, nevertheless, does not lead to the ground state of the whole system in general. If we can obtain the ground state $|\psi\rangle_{\rm gs}$ by iterating the coarse-graining procedure, $|\psi\rangle_{\rm gs}$ satisfies the following relation:

$$ {}_{\rm gs}\langle\psi|PHP|\psi\rangle_{\rm gs} = {}_{\rm gs}\langle\psi|H|\psi\rangle_{\rm gs}. \tag{2.90}$$

Possible degeneracies of the ground states apart, this equation leads to

$$ P|\psi\rangle_{\rm gs} = |\psi\rangle_{\rm gs}. \tag{2.91}$$

This means that $|\psi\rangle_{\rm gs}$ is a superposition of states such as $|m_1\rangle_1 \otimes |m_2\rangle_2 \otimes \cdots$, namely

$$ |\psi\rangle_{\rm gs} = \sum_{m_1,m_2,\ldots} c_{m_1,m_2,\ldots} \bigotimes_I |m_I\rangle_I, \tag{2.92}$$

where $c_{m_1,m_2,\ldots}$ is an amplitude. Unfortunately, the actual ground state is not necessarily such a state. States $|m\rangle$ are the lowest-energy states of blocks but derived without considerations of effects of couplings between blocks. The effects play an essential role in the determination of the ground state. Hence, we cannot always write the ground state in the form of Eq. (2.92). Our coarse-graining procedure thus does not produce the exact ground state in general.

The argument discussed above yields an intuition that blocks of bigger size are appropriate to study the ground state. This is because effects of edges of blocks reduces as the size of blocks becomes large. The effects are the origin of disagreement between states produced by our procedure and the true ground state. Indeed, we can obtain the exact ground state by using a block of infinite size though it is impossible in practice.

Of course, bigger blocks cause hard calculations in diagonalizing the intrablock Hamiltonians. We should adopt an appropriate size of blocks which allows us to execute practical calculations.

On the other hand, from a viewpoint of renormalization group, the block size should be small. We evaluate critical exponents by observing infinitesimal changes of parameters in a system through renormalization-group transformations. With a large scaling factor, the changes are not so small in general. We cannot accurately estimate the exponents as a result. Hence, small blocks are appropriate to investigate critical phenomena. Since our main interest lies on critical phenomena, we will employ small blocks in the remainder of this thesis.

Chapter 3

Real-space renormalization group for the transverse-field Ising models

This chapter performs our renormalization-group method in the transverse-field Ising models. The principle of our scheme was explained in Sec. 2.4. The first example of explicit calculations is demonstrated in the transverse-field Ising chain, which is the basic model in the present thesis, in Sec. 3.1. This example shows effectiveness of our method in analyzing phase transitions and critical phenomena in the transverse-field Ising model. The method is generalized to higher dimensions in Sec 3.2. This chapter is summarized in Sec. 3.3. The generalization in Sec. 3.2 is author's original work published in [85].

3.1 Renormalization group for the transverse-field Ising chain

This section illustrates an example of renormalization-group calculations according to our prescription in the transverse-field Ising chain [85, 99]. Since this chain is the basic model in the present thesis, we tackle it at first. We write its Hamiltonian again,

$$H = -J \sum_{i=1}^{N} \sigma_i^z \sigma_{i+1}^z - \Gamma \sum_{i=1}^{N} \sigma_i^x, \tag{3.1}$$

where N is the number of sites and is assumed to be an even number. We impose the periodic boundary condition $\boldsymbol{\sigma}_{N+1} = \boldsymbol{\sigma}_1$. In addition, we assume Γ are positive. This assumption does not lose generality, since even if Γ is negative, the Hamiltonian with positive Γ is retrieved by the following transformation: $\sigma^x \to \mathrm{sgn}(\Gamma)\sigma^x$, $\sigma^y \to \mathrm{sgn}(J)\mathrm{sgn}(\Gamma)\sigma^y$, and $\sigma^z \to \mathrm{sgn}(J)\sigma^z$, and for spins on odd sites, $\sigma^x \to \mathrm{sgn}(\Gamma)\sigma^x$, $\sigma^y \to \mathrm{sgn}(\Gamma)\sigma^y$, and $\sigma^z \to \sigma^z$. This transformation preserves the commutation relation of a spin, $[\sigma^x, \sigma^y] = 2i\sigma^z$. We consider the ferromagnet model ($J > 0$) hereafter, but it is connected to the antiferromagnetic model ($J < 0$) by the above transformation. The validity of this mapping is due to the fact that the chain with even sites is one of the bipartite lattices.

Section 3.1.1 gives our renormalization-group transformation, which is deduced from a particular block partition. A transition point and critical exponents are extracted

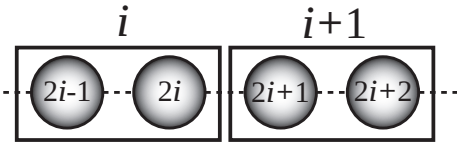

Figure 3.1: Blocks for Eqs. (3.2) and (3.3).

from the transformation in Sec. 3.1.2. The resulting values of the transtion point and critical exponents ν and α agree with the exact solutions. Section 3.1.3 examines other block partitions. Section 3.1.4 discusses our block partition employed in Sec. 3.1.1.

3.1.1 Renormalization-group transformation

We divide the system governed by Eq. (3.1) into blocks of two spins. The two-spin blocks enable us to analytically diagonalize block Hamiltonians. The next procedure is to split the Hamiltonian into intrablock and interblock Hamiltonians. We here adopt the following block Hamiltonians:

$$H_i^{\rm intra} = -J\sigma_{2i-1}^z\sigma_{2i}^z - \Gamma\sigma_{2i-1}^x, \tag{3.2}$$

$$H_{i,i+1}^{\rm inter} = -J\sigma_{2i}^z\sigma_{2i+1}^z - \Gamma\sigma_{2i}^x, \tag{3.3}$$

where spins $2i-1$ and $2i$ belong to block i, and spin $2i+1$ belongs to block $i+1$ as depicted in Fig 3.1. The label of block i runs from 1 to $N/2$. Most importantly, this particular block partition is suited to preserve the form of the Hamiltonian under the renormalization-group transformations and is the key for the success of our calculations. Other block partitions will be examined in Sec. 3.1.3, and the effectiveness of our block partition will be discussed in Sec. 3.1.4.

The eigenvalues of $H_i^{\rm intra}$ are degenerate,

$$\varepsilon^{(1)} = \varepsilon^{(2)} = -\sqrt{J^2+\Gamma^2}, \tag{3.4}$$

$$\varepsilon^{(3)} = \varepsilon^{(4)} = \sqrt{J^2+\Gamma^2}. \tag{3.5}$$

The corresponding eigenvectors are

$$|1\rangle = a^+|\uparrow\uparrow\rangle + a^-|\downarrow\uparrow\rangle, \quad |2\rangle = a^+|\downarrow\downarrow\rangle + a^-|\uparrow\downarrow\rangle, \tag{3.6}$$

$$|3\rangle = a^-|\downarrow\downarrow\rangle - a^+|\uparrow\downarrow\rangle, \quad |4\rangle = a^-|\uparrow\uparrow\rangle - a^+|\downarrow\uparrow\rangle, \tag{3.7}$$

where

$$a^\pm = \sqrt{\frac{1}{2}\left(1 \pm \frac{J}{\sqrt{J^2+\Gamma^2}}\right)}, \tag{3.8}$$

and $\{|\uparrow\uparrow\rangle, |\uparrow\downarrow\rangle, |\downarrow\uparrow\rangle, |\downarrow\downarrow\rangle\}$ is the orthonormal basis in the σ^z basis, i.e., $\sigma^z|\uparrow\rangle = |\uparrow\rangle$, $\sigma^z|\downarrow\rangle = -|\downarrow\rangle$.

We next keep the two lowest-lying energy eigenstates $|1\rangle$ and $|2\rangle$, and drop the others, $|3\rangle$ and $|4\rangle$, to perform a coarse-graining. We then replace each block with a single spin representing the $|1\rangle$ and $|2\rangle$ states as

$$\tilde{\sigma}^x = |1\rangle\langle 2| + |2\rangle\langle 1|, \quad \tilde{\sigma}^y = -i|1\rangle\langle 2| + i|2\rangle\langle 1|, \quad \tilde{\sigma}^z = |1\rangle\langle 1| - |2\rangle\langle 2|. \tag{3.9}$$

To this end, we define the projector onto the coarse-grained system as

$$P = \bigotimes_{i=1}^{N/2} P_i, \tag{3.10}$$

where P_i is the projector,

$$P_i = \left(|1\rangle\langle 1| + |2\rangle\langle 2|\right)_i. \tag{3.11}$$

The resulting coarse-grained Hamiltonian is

$$PHP = \sum_{i=1}^{N/2} P_i H_i^{\text{intra}} P_i + \sum_{i=1}^{N/2} (P_i \otimes P_{i+1}) H_{i,i+1}^{\text{inter}} (P_i \otimes P_{i+1}), \tag{3.12}$$

where $N/2+1$ means 1 in the periodic condition we assumed. The renormalized intrablock Hamiltonian is trivially represented by the identity operator 1_i on block i as

$$P_i H_i^{\text{intra}} P_i = \varepsilon^{(1)} 1_i. \tag{3.13}$$

Deriving the corresponding projection of the interblock Hamiltonian, we recall that spin $2i$ belongs to block i, and spin $2i+1$ belongs to block $i+1$. Explicitly writing this fact,

$$H_{i,i+1}^{\text{inter}} = -J(1_{2i-1} \otimes \sigma_{2i}^z) \otimes (\sigma_{2i+1}^z \otimes 1_{2i+2}) - \Gamma(1_{2i-1} \otimes \sigma_{2i}^x). \tag{3.14}$$

Let us calculate the projections of the terms in this equation. First, $1_{2i-1} \otimes \sigma_{2i}^z$ has the following property:

$$\begin{aligned} (1_{2i-1} \otimes \sigma_{2i}^z)\,|1\rangle &= (1_{2i-1} \otimes \sigma_{2i}^z)\left(a^+|\uparrow\uparrow\rangle + a^-|\downarrow\uparrow\rangle\right) && (3.15)\\ &= |1\rangle, && (3.16) \end{aligned}$$

$$\begin{aligned} (1_{2i-1} \otimes \sigma_{2i}^z)\,|2\rangle &= (1_{2i-1} \otimes \sigma_{2i}^z)\left(a^+|\downarrow\downarrow\rangle + a^-|\uparrow\downarrow\rangle\right) && (3.17)\\ &= -|2\rangle. && (3.18) \end{aligned}$$

Using these relations, we obtain

$$\begin{aligned} P_i\,(1_{2i-1} \otimes \sigma_{2i}^z)\,P_i &= \left(|1\rangle\langle 1| + |2\rangle\langle 2|\right)_i \left(1_{2i+1} \otimes \sigma_{2i+2}^z\right) \left(|1\rangle\langle 1| + |2\rangle\langle 2|\right)_i && (3.19)\\ &= \left(|1\rangle\langle 1| - |2\rangle\langle 2|\right)_i && (3.20)\\ &= \tilde{\sigma}_i^z. && (3.21) \end{aligned}$$

The corresponding calculations of $\sigma^z_{2i+1} \otimes 1_{2i+2}$ are

$$\left(\sigma^z_{2i+1} \otimes 1_{2i+2}\right)|1\rangle = \left(\sigma^z_{2i+1} \otimes 1_{2i+2}\right)\left(a^+|\uparrow\uparrow\rangle + a^-|\downarrow\uparrow\rangle\right) \tag{3.22}$$

$$= a^+|\uparrow\uparrow\rangle - a^-|\downarrow\uparrow\rangle, \tag{3.23}$$

$$\left(\sigma^z_{2i+1} \otimes 1_{2i+2}\right)|2\rangle = \left(\sigma^z_{2i+1} \otimes 1_{2i+2}\right)\left(a^+|\downarrow\downarrow\rangle + a^-|\uparrow\downarrow\rangle\right) \tag{3.24}$$

$$= -a^+|\downarrow\downarrow\rangle + a^-|\uparrow\downarrow\rangle, \tag{3.25}$$

$$P_{i+1}(\sigma^z_{2i+1} \otimes 1_{2i+2})P_{i+1} = [(a^+)^2 - (a^-)^2](|1\rangle\langle 1| - |2\rangle\langle 2|)_{i+1} \tag{3.26}$$

$$= \frac{J}{\sqrt{J^2+\Gamma^2}}\tilde{\sigma}^z_{i+1}. \tag{3.27}$$

Similarly, we have

$$\left(1_{2i-1} \otimes \sigma^x_{2i}\right)|1\rangle = \left(1_{2i-1} \otimes \sigma^x_{2i}\right)\left(a^+|\uparrow\uparrow\rangle + a^-|\downarrow\uparrow\rangle\right) \tag{3.28}$$

$$= a^+|\uparrow\downarrow\rangle + a^-|\downarrow\downarrow\rangle, \tag{3.29}$$

$$\left(1_{2i-1} \otimes \sigma^x_{2i}\right)|2\rangle = \left(1_{2i-1} \otimes \sigma^x_{2i}\right)\left(a^+|\downarrow\downarrow\rangle + a^-|\uparrow\downarrow\rangle\right) \tag{3.30}$$

$$= a^+|\downarrow\uparrow\rangle + a^-|\uparrow\uparrow\rangle, \tag{3.31}$$

$$P_i\left(1_{2i-1} \otimes \sigma^x_{2i}\right)P_i = \left(a^+a^- + a^+a^-\right)(|1\rangle\langle 2| + |2\rangle\langle 1|)_i \tag{3.32}$$

$$= \frac{\Gamma}{\sqrt{J^2+\Gamma^2}}\tilde{\sigma}^x_i. \tag{3.33}$$

Consequently, the interblock Hamiltonian is projected as

$$(P_i \otimes P_{i+1})H^{\text{inter}}_{i,i+1}(P_i \otimes P_{i+1}) = -\frac{J^2}{\sqrt{J^2+\Gamma^2}}\tilde{\sigma}^z_i\tilde{\sigma}^z_{i+1} - \frac{\Gamma^2}{\sqrt{J^2+\Gamma^2}}\tilde{\sigma}^x_i. \tag{3.34}$$

Using Eqs. (3.13) and (3.34), we express the renormalized Hamiltonian, Eq. (3.12), as

$$PHP = \varepsilon^{(1)}\sum_{i=1}^{N/2} 1_i - \tilde{J}\sum_{i=1}^{N/2}\tilde{\sigma}^z_i\tilde{\sigma}^z_{i+1} - \tilde{\Gamma}\sum_{i=1}^{N/2}\tilde{\sigma}^x_i \tag{3.35}$$

with renormalized couplings

$$\tilde{J} = \frac{J^2}{\sqrt{J^2+\Gamma^2}}, \tag{3.36}$$

$$\tilde{\Gamma} = \frac{\Gamma^2}{\sqrt{J^2+\Gamma^2}}. \tag{3.37}$$

These equations constitute our renormalization-group transformation. Note that the renormalized Hamiltonian is the Hamiltonian of the transverse-field Ising chain. In other words, our transformation preserves the form of the Hamiltonian and does not generate additional couplings under renormalization.

3.1.2 Transition point and critical exponents

To analyze phase transitions and critical phenomena in the transverse-field Ising chain, we observe the change of the transverse field normalized with the exchange coupling through the renormalization-group transformation. The transverse field is the origin of quantum effects in this model and causes a quantum phase transition. Thus, we should focus on the change of the transverse field. More specifically, we should calculate the change of the transverse field normalized by the exchange coupling, namely Γ/J, since the coupling J represents the scale of energy in this model. We then generate the renormalization-group equation from Eqs (3.35)–(3.37) with the parameter $k_\Gamma = \Gamma/J$,

$$\tilde{k}_\Gamma = k_\Gamma^2. \tag{3.38}$$

This equation has three fixed points: $k_\Gamma = 0, 1, \infty$. The fixed points $k_\Gamma = 0, \infty$ are stable ones. Indeed, k_Γ smaller than 1 is driven to 0 by the recursion of the transformation. Similarly, k_Γ larger than 1 goes to ∞. These two fixed points $k_\Gamma = 0, \infty$ represent the ferromagnetic phase and the paramagnetic phase, respectively. The other fixed point $k_\Gamma = 1$ is an unstable one and corresponds to a critical point $k_{c,\Gamma}$. In other words, the point $k_\Gamma = 1$ is the location of the transition point resulting from our renormalization-group scheme. Although our scheme includes a non-rigorous treatment of the ground state, which is ignoring the states $|3\rangle$ and $|4\rangle$ in the coarse-graining process, the resulting value $k_{c,\Gamma} = 1$ is equal to the exact transition point of the model [23].

We extract critical exponents from a renormalization-group flow around the critical fixed point $k_{c,\Gamma} = 1$. To this end, we expand the renormalization-group transformation [Eq. (3.38)],

$$\tilde{k}_\Gamma - k_{c,\Gamma} = 2(k_\Gamma - k_{c,\Gamma}) + O\left((k_\Gamma - k_{c,\Gamma})^2\right). \tag{3.39}$$

We derive an eigenvalue 2^{y_Γ}, where 2 is the scaling factor of this renormalization, from the coefficient 2 of the linear term. We thus have $y_\Gamma = 1$. This value determines the critical exponent ν for the correlation length, $\xi \sim (k_\Gamma - k_{c,\Gamma})^{-\nu}$, with the equation, $\nu = 1/y_\Gamma$, explained in Secs. 2.1.2 and 2.2.2. Hence, the value of critical exponent ν derived from our renormalization-group scheme is 1. This is a remarkable result since this value agrees with the exact one similarly to the case of the transition point.

Since critical exponents other than ν involve the renormalization-group flow caused by a longitudinal field, we need to carry out our renormalization-group scheme with additional longitudinal-field terms. The Hamiltonian of the transverse-field Ising chain written in Eq. (3.1) is extended as

$$H = -J\sum_{i=1}^{N}\sigma_i^z\sigma_{i+1}^z - \Gamma\sum_{i=1}^{N}\sigma_i^x - h\sum_{i=1}^{N}\sigma_i^z. \tag{3.40}$$

with a longitudinal field h. For this model, we use

$$H_i^{\text{intra}} = -J\sigma_{2i-1}^z\sigma_{2i}^z - \Gamma\sigma_{2i-1}^x - h\sigma_{2i-1}^z, \quad H_{i,i+1}^{\text{inter}} = -J\sigma_{2i}^z\sigma_{2i+1}^z - \Gamma\sigma_{2i}^x - h\sigma_{2i}^z, \tag{3.41}$$

Table 3.1: Transition point $k_{c,\Gamma}$, exponents y_Γ and y_h of the linearized renormalization-group transformations in Eqs. (3.38) and (3.48), and critical exponents for the transverse-field Ising chain.

	$k_{c,\Gamma}$	y_Γ	y_h	α	β	γ	δ	ν	η
exact solution	1	1	1.875	0	1.125	1.75	15	1	0.25
our result	1	1	1.543	0	0.457	1.086	3.377	1	0.914

where a longitudinal field is applied only to the same spin with a transverse field applied. Through our transformations, the Hamiltonian is renormalized as

$$PHP = \sum_{i=1}^{N/2} \frac{\varepsilon^{(1)} + \varepsilon^{(2)}}{2} 1_i - \tilde{J} \sum_{i=1}^{N/2} \tilde{\sigma}_i^z \tilde{\sigma}_{i+1}^z - \tilde{\Gamma} \sum_{i=1}^{N/2} \tilde{\sigma}_i^x - \tilde{h} \sum_{i=1}^{N/2} \tilde{\sigma}_i^z, \tag{3.42}$$

where parameters are modified as

$$\varepsilon^{(1)} = -\sqrt{(J+h)^2 + \Gamma^2}, \quad \varepsilon^{(2)} = -\sqrt{(J-h)^2 + \Gamma^2}, \tag{3.43}$$

$$\tilde{J} = \frac{J}{2} \left(a_{1,1}^2 + a_{1,-1}^2 - a_{-1,1}^2 - a_{-1,-1}^2 \right), \tag{3.44}$$

$$\tilde{\Gamma} = \Gamma \left(a_{1,1} a_{-1,-1} + a_{1,-1} a_{-1,1} \right), \tag{3.45}$$

$$\tilde{h} = -\frac{1}{2} \left(\varepsilon^{(1)} - \varepsilon^{(2)} \right) + \frac{J}{2} \left(a_{1,1}^2 - a_{1,-1}^2 - a_{-1,1}^2 + a_{-1,-1}^2 \right) + h_z, \tag{3.46}$$

with

$$a_{x,y} = \sqrt{\frac{1}{2} \left(1 + x \frac{J + y\,h}{\sqrt{(J + y\,h)^2 + \Gamma^2}} \right)}. \tag{3.47}$$

This is the generalization of the result without the longitudinal field. Of course, the previous result is reproduced by the condition $h = 0$. The form of the Hamiltonian is preserved through the transformation also with the longitudinal field.

A renormalization-group flow is described by the change of parameters $k_\Gamma = \Gamma/J$ and $k_h = h/J$ following Eqs. (3.43)–(3.47). The flow has stable fixed points $(k_\Gamma, k_h) = (0,0), (\infty, 0)$, and $(k_\Gamma, \pm\infty)$, and the critical fixed point discussed above $(k_\Gamma, k_h) = (1, 0)$. Linearizing $\tilde{k}_h (= \tilde{h}/\tilde{J})$ around the critical fixed point $(k_\Gamma, k_h) = (1, 0)$, we obtain

$$\tilde{k}_h = \left(\frac{3}{2} + \sqrt{2} \right) k_h + O[k_h^2, (k_\Gamma - 1) k_h]. \tag{3.48}$$

This equation yields an eigenvalue 2^{y_h} with $y_h = \log_2(\frac{3}{2} + \sqrt{2}) \simeq 1.543$. Consequently, critical exponents are estimated as listed in Table 3.1, with the relations explained in Secs. 2.1.2 and 2.2.2.

It is remarkable that the critical point and critical exponents α and ν are exact, since real-space renormalization group calculations seldom yield exact results. Other

exponents related to the longitudinal field, however, are not exact. The longitudinal field does disturb the symmetry of the block Hamiltonian which seems essential to obtain the exact values. This point will be discussed in Sec. 3.1.4.

3.1.3 Other block partitions

We examine other block partitions than a partition in Eqs. (3.2) and (3.3). The block partition in the previous section seems natural for the transverse-field Ising model, since both of the block Hamiltonians [Eqs. (3.2) and (3.3)] have an interaction term and a transverse-field term. We consider another partition,

$$H_i^{\rm intra} = -J\sigma_{2i-1}^z\sigma_{2i}^z - \Gamma\sigma_{2i-1}^x - \Gamma\sigma_{2i}^x, \quad H_{i,i+1}^{\rm inter} = -J\sigma_{2i}^z\sigma_{2i+1}^z. \tag{3.49}$$

The eigenvalues of $H_i^{\rm intra}$ are

$$\varepsilon^{(1)} = -\sqrt{J+4\Gamma^2}, \quad \varepsilon^{(2)} = -J, \quad \varepsilon^{(3)} = J, \quad \varepsilon^{(4)} = \sqrt{J+4\Gamma^2}. \tag{3.50}$$

The corresponding eigenvectors are

$$|1\rangle = b_+|\uparrow\uparrow\rangle + b_-|\uparrow\downarrow\rangle + b_-|\downarrow\uparrow\rangle + b_+|\downarrow\downarrow\rangle, \quad |2\rangle = \frac{1}{\sqrt{2}}|\uparrow\uparrow\rangle - \frac{1}{\sqrt{2}}|\downarrow\downarrow\rangle, \tag{3.51}$$

$$|3\rangle = \frac{1}{\sqrt{2}}|\uparrow\downarrow\rangle - \frac{1}{\sqrt{2}}|\downarrow\uparrow\rangle, \quad |4\rangle = b_-|\uparrow\uparrow\rangle + b_+|\uparrow\downarrow\rangle + b_+|\downarrow\uparrow\rangle + b_-|\downarrow\downarrow\rangle \tag{3.52}$$

with

$$b_\pm = \frac{1}{2}\sqrt{1 \pm \frac{J}{\sqrt{J^2+4\Gamma^2}}}. \tag{3.53}$$

Eigenvalues are not degenerate in this case. This fact causes a problem. When we renormalize the system with a projector $P = \bigotimes_i P_i = \bigotimes_i (|1\rangle\langle 1| + |2\rangle\langle 2|)_i$ composed of the two lowest-lying eigenstates, the intrablock Hamiltonian produces a longitudinal-field term, that is,

$$P_i H_i^{\rm intra} P_i = \varepsilon^{(1)}|1\rangle\langle 1| + \varepsilon^{(2)}|2\rangle\langle 2| \tag{3.54}$$

$$= \frac{\varepsilon^{(1)}+\varepsilon^{(2)}}{2} 1_i + \frac{\varepsilon^{(1)}-\varepsilon^{(2)}}{2}\tilde{\sigma}_i^z. \tag{3.55}$$

The renormalized terms from the interblock Hamiltonian do not compensate this longitudinal-field term. Hence, the transformation for the whole system produces the longitudinal field, even if no longitudinal field is applied to the original system. This consequence is contrary to the truth that the system without a longitudinal field does not flow to the system with finite longitudinal field in a renormalization-group picture.

To resolve this problem, we redefine a projector as

$$P_i' = |1'\rangle\langle 1'| + |2'\rangle\langle 2'| \tag{3.56}$$

with

$$|1'\rangle = \frac{1}{\sqrt{2}}|1\rangle + \frac{1}{\sqrt{2}}|2\rangle, \tag{3.57}$$

$$|2'\rangle = \frac{1}{\sqrt{2}}|1\rangle - \frac{1}{\sqrt{2}}|2\rangle. \tag{3.58}$$

The intrablock Hamiltonian is projected by the new projector as

$$P_i' H_i^{\rm intra} P_i' = \frac{\varepsilon^{(1)} + \varepsilon^{(2)}}{2} 1_i + \frac{\varepsilon^{(1)} - \varepsilon^{(2)}}{2} \tilde{\sigma}_i^x. \tag{3.59}$$

This projector does not produce a longitudinal-field term. A transverse-field term is produced instead, that is a consequence of the rotation of states in the space spanned by $|1\rangle$ and $|2\rangle$. The interblock Hamiltonian is projected as

$$(P_i' \otimes P'_{i+1}) H_{i,i+1}^{\rm inter} (P_i' \otimes P'_{i+1}) = \frac{J}{2}\left(\frac{J}{\sqrt{J+4\Gamma^2}} + 1\right)\tilde{\sigma}_i^z \tilde{\sigma}_{i+1}^z. \tag{3.60}$$

Consequently, the whole Hamiltonian is renormalized as

$$P'HP' = \sum_{i=1}^{N/2} \frac{\varepsilon^{(1)} + \varepsilon^{(2)}}{2} 1_i - \tilde{J} \sum_{i=1}^{N/2} \tilde{\sigma}_i^z \tilde{\sigma}_{i+1}^z - \tilde{\Gamma} \sum_{i=1}^{N/2} \tilde{\sigma}_i^x \tag{3.61}$$

with

$$\tilde{J} = \frac{J}{2}\left(\frac{J}{\sqrt{J^2+4\Gamma^2}} + 1\right), \tag{3.62}$$

$$\tilde{\Gamma} = \frac{\sqrt{J^2+4\Gamma^2} - J}{2}. \tag{3.63}$$

The form of the Hamiltonian is preserved also in the block partition written in Eq. (3.49).

We next consider fixed points of $k_\Gamma = \Gamma/J$. The renormalization-group equation for this case is

$$\tilde{k}_\Gamma = \frac{\sqrt{1+4k_\Gamma^2}\left(\sqrt{1+4k_\Gamma^2} - 1\right)}{\sqrt{1+4k_\Gamma^2} + 1}. \tag{3.64}$$

This equation has two trivial fixed points $k_\Gamma = 0, \infty$ and a non-trivial fixed point $k_\Gamma \simeq 1.27674$. The non-trivial fixed point deviates from the true critical point $k_{c,\Gamma} = 1$, which is reproduced by the previous block partition. The linearized renormalization-group equation around the non-trivial fixed point yields a critical exponent $\nu \simeq 1.482$. This value also has a difference from the true solution $\nu = 1$.

With the modification of the projector, the block partition in Eq. (3.49) preserves the form of the Hamiltonian through the renormalization-group transformation, but the method does not yield the exact transition point and the exact critical exponent ν, which is obtained with the previous block partition defined as Eqs. (3.2) and (3.3).

Let us consider another natural block partition,

$$H_i^{\rm intra} = -J\sigma_{2i-1}^z\sigma_{2i}^z - \frac{\Gamma}{2}\sigma_{2i-1}^x - \frac{\Gamma}{2}\sigma_{2i}^x, \quad H_{i,i+1}^{\rm inter} = -J\sigma_{2i}^z\sigma_{2i+1}^z - \frac{\Gamma}{2}\sigma_{2i}^x - \frac{\Gamma}{2}\sigma_{2i+1}^x. \tag{3.65}$$

This partition also does not yield a good result. Indeed, the renormalization-group equation for this case is

$$\tilde{k}_\Gamma = \frac{\sqrt{1+k_\Gamma^2}-1}{\sqrt{1+k_\Gamma^2}+1}, \tag{3.66}$$

which has only a trivial fixed point $k_\Gamma = 0$.

These examples show that our block partition defined as Eqs. (3.2) and (3.3) is an exceptional one. We move to discussion on our block partition.

3.1.4 Our block partition

The reason why the block partition in Eqs. (3.2) and (3.3) gives the exact transition point is intuitively understood as follows. One of the key points is the preservation of the form of the Hamiltonian under our renormalization-group transformation. Due to this property, we have no need of extra approximations. Another key point is the self-duality in the block Hamiltonians without the longitudinal field, which preserves the form of the Hamiltonian apart from the interchange of magnitude of the coupling constant and transverse field under the transformation on spin variables from σ to new Pauli matrices τ: $\tau_i^x = \sigma_i^z\sigma_{i+1}^z$ and $\tau_i^z = \prod_{j\le i}\sigma_i^x$. Although the transformation changes the site which the transverse field is applied to, this change does not affect the subsequent results. The self-duality is an intrinsic property of the transverse-field Ising chain as explained in Sec. 1.3.1. The block Hamiltonians in Eqs. (3.2) and (3.3) inherit this nature. We consider below influence of the self-duality on the results of our renormalization-group calculations.

Under our renormalization-group scheme, the block Hamiltonians determine the resulting Hamiltonian. Thus, by using the dual block Hamiltonians substantially generated by the interchange of J and Γ in the original block Hamiltonians, we obtain the renormalized Hamiltonian with the role of J's and Γ's in renormalized parameters, Eqs. (3.36) and (3.37), interchanged. Note that the interchange of J and Γ in Eqs. (3.36) and (3.37) bring the interchange of $\tilde{J}$ and $\tilde{\Gamma}$ themselves. In other words, the duality transformation in the original Hamiltonian is equivalent to that in the renormalized Hamiltonian. Accordingly, when we derive the renormalized dual Hamiltonian or the dual renormalized Hamiltonian, the resulting Hamiltonian is independent of the order of the duality transformation and our coarse-graining procedure in the derivation. This is a nontrivial and outstanding feature of the block partition defined as Eqs. (3.2) and (3.3). We found a counter-example, Eqs. (3.62) and (3.63), resulted from another block partition defined as Eq. (3.49).

This feature leads to the exact correspondence between the fixed points of the duality transformations in the original and renormalized systems. The fixed point of the duality transformation in the transverse-field Ising chain is the phase-transition

point. Hence, the original system on the transition point is mapped onto the renormalized system on its transition point through the coarse-graining procedure. Consequently, the transition point of the original system agrees with the fixed point of our renormalization-group transformation. Our renormalization-group scheme thus yields the exact transition point of the transverse-field Ising chain.

To summarize, our success in the calculation of the transition point is a consequence of the two exceptional features of the transformation: the preservation of the form of the Hamiltonian and the commutativity of the coarse-graining procedure and the duality transformation. On the other hand, the above argument gives no reason why our scheme yields the exact values of critical exponents α and ν. It might be a clue to clarify the reason that the resulting values of the other critical exponents associated with the exponent y_h for the longitudinal field deviate from the exact solutions, for instance, β and γ. Our scheme thus yields the exact critical exponents only when the system has no longitudinal field. Similarly, the self-duality is found in the transverse-field Ising chain only when no longitudinal field is applied. Hence, it is natural to expect the self-duality to be a key also for the calculation of the exact critical exponents.

However, we will find in the next section that our method yields accurate values of critical exponents α and ν also in two and three dimensions, where the system has no self-duality. This result shows that the self-duality is not essential to obtain accurate critical exponents with our method at least in higher dimensions. Hence, additional factors should contribute to the success, and they should lead to the self-duality only in one dimension. We can still expect the importance of the self-duality in the one-dimensional case.

3.2 Generalization to higher-dimensional models

We generalize the renormalization-group method discussed in the previous section to the higher-dimensional transverse-field Ising models. Section 3.2.1 explains a strategy of the generalization, and applies the method to the two-dimensional model. The three-dimensional model is examined in Sec. 3.2.2.

3.2.1 Two dimensions

We consider the two-dimensional transverse-field Ising model on a square lattice. The Hamiltonian is

$$H = -J \sum_{\langle i,j \rangle} \sigma_i^z \sigma_j^z - \Gamma \sum_i \sigma_i^x, \tag{3.67}$$

where spins interact with their nearest neighbors $\langle i, j \rangle$. We assume the couplings are positive as in the one-dimensional case. For simplicity, we do not consider a longitudinal field at first. The key idea consists of performing renormalization-group transformations that preserve the form of the Hamiltonian by a projective isometry that preserves the bond algebra (i.e. the algebra realized by the operators $\sigma_i^z \sigma_j^z$ and σ_i^x). Exploiting our experience in one dimension, we divide the lattice into blocks just as in one dimension (Fig. 3.2). The two-spin blocks enable us to analytically perform the renormalization-group calculations. We combine the one-dimensional block method in

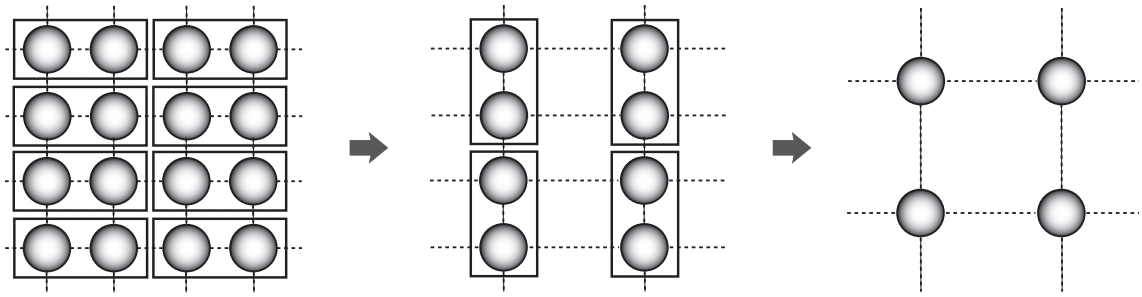

Figure 3.2: Construction of one-dimensional blocks and two steps of the single renormalization-group transformation for a two-dimensional model on a square lattice.

horizontal and vertical directions to restore the symmetry of the lattice. Specifically, we iterate the renormalization in two directions: first in the horizontal direction and then in the vertical direction (Fig. 3.2). We redefine the coupling constants for the horizontal direction J_h and the vertical direction J_v to distinguish these two quantities in this scheme.

In the first step of the renormalization (in the horizontal direction) we can replace each block with a single spin using the same procedure as in the one-dimensional case. The equations corresponding to Eqs. (3.21), (3.27) and (3.33) are

$$P_i \left(1_{2i-1} \otimes \sigma_{2i}^z\right) P_i = \sigma_i^z, \tag{3.68}$$

$$P_{i+1} \left(\sigma_{2i+1}^z \otimes 1_{2i+2}\right) P_{i+1} = \frac{J_h}{\sqrt{J_h^2 + \Gamma^2}} \sigma_{i+1}^z, \tag{3.69}$$

$$P_i \left(1_{2i-1} \otimes \sigma_{2i}^x\right) P_i = \frac{\Gamma}{\sqrt{J_h^2 + \Gamma^2}} \sigma_i^x. \tag{3.70}$$

The renormalized coupling constants and transverse field are written as,

$$\tilde{J}_h = \frac{J_h^2}{\sqrt{J_h^2 + \Gamma^2}}, \tag{3.71}$$

$$\tilde{J}_v = J_v \left(\frac{J_h^2}{J_h^2 + \Gamma^2} + 1\right), \tag{3.72}$$

$$\tilde{\Gamma} = \frac{\Gamma^2}{\sqrt{J_h^2 + \Gamma^2}}. \tag{3.73}$$

In Eq. (3.72), $J_v J_h^2/(J_h^2 + \Gamma^2)$ is derived from the coupling of two spins on the left spot in each block, and the rest is derived from the one on the right spot in the blocks. This coarse-graining process for the horizontal direction is illustrated in Fig. 3.3

Next the system is renormalized in the vertical direction in the same way as the horizontal direction to retrieve the symmetry. The coupling constants and the transverse field are now

$$\tilde{\tilde{J}}_h = \tilde{J}_h \left(\frac{\tilde{J}_v^2}{\tilde{J}_v^2 + \tilde{\Gamma}^2} + 1\right), \tag{3.74}$$

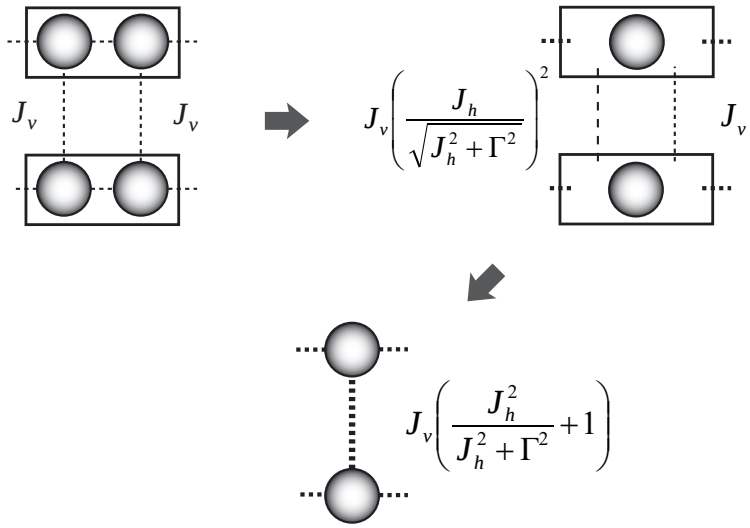

Figure 3.3: Coarse-graining process for the horizontal direction in the transverse-field Ising model on a square lattice.

$$\tilde{\tilde{J}}_v = \frac{\tilde{J}_v^2}{\sqrt{\tilde{J}_v^2 + \tilde{\Gamma}^2}}, \tag{3.75}$$

$$\tilde{\tilde{\Gamma}} = \frac{\tilde{\Gamma}^2}{\sqrt{\tilde{J}_v^2 + \tilde{\Gamma}^2}}. \tag{3.76}$$

From these equations, the following renormalization-group equations are generated,

$$\tilde{\tilde{k}}_h = \frac{k_h^3 k_v \sqrt{\left(1+k_h^2\right)\left\{\left(2+k_h^2\right)^2 + k_h^2 k_v^2\left(1+k_h^2\right)\right\}}}{2\left(2+k_h^2\right)^2 + k_h^2 k_v^2\left(1+k_h^2\right)}, \tag{3.77}$$

$$\tilde{\tilde{k}}_v = \frac{k_h^2 k_v^2\left(1+k_h^2\right)}{\left(2+k_h^2\right)^2}, \tag{3.78}$$

where $k_h = \Gamma/J_h$, $k_v = \Gamma/J_v$. These equations can be represented as

$$\tilde{\tilde{k}}_h^2 = f\left(k_h^2, \tilde{\tilde{k}}_v\right), \tag{3.79}$$

$$\tilde{\tilde{k}}_v = f\left(k_v, k_h^2\right), \tag{3.80}$$

$$f(x,y) = x^2 \frac{y(1+y)}{(2+y)^2}. \tag{3.81}$$

These renormalization-group equations are still asymmetric in k_h and k_v. To render the renormalization symmetric we renormalize the system in the reverse order, vertical and then horizontal. We define the order of the renormalization in the horizontal direction and then in the vertical direction as the order A, and the reverse order as B (Fig. 3.4). Hence, the new step is represented as AB. The renormalization-group

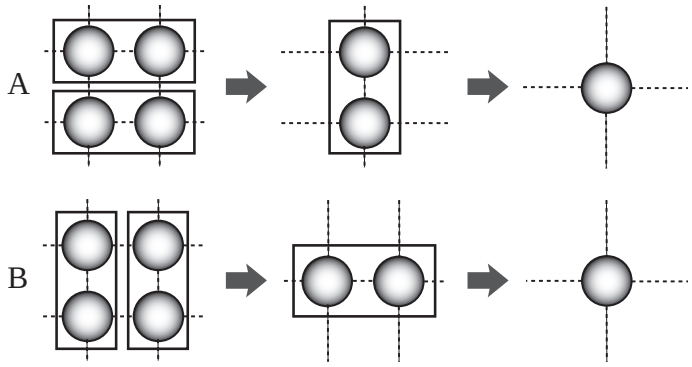

Figure 3.4: The order of the renormalization in the horizontal and vertical directions. With A, we renormalize the system in the horizontal direction and then in the vertical direction. The reverse order is denoted by B.

transformation with order A is established by Eqs. (3.79) and (3.80) while with order B is

$$\tilde{\tilde{k}}_v^2 = f\left(k_v^2, \tilde{\tilde{k}}_h\right), \tag{3.82}$$

$$\tilde{\tilde{k}}_h = f\left(k_h, k_v^2\right). \tag{3.83}$$

The transformation with order AB is obtained from the substitution of $\tilde{\tilde{k}}_h$, Eq. (3.79), for k_h in Eq. (3.83) and $\tilde{\tilde{k}}_v$, Eq. (3.80), for k_v in Eqs. (3.82) and (3.83). Although B relaxes the asymmetry in A, the renormalization group equations with AB is still asymmetric. The symmetrization procedure is thus repeated as ABBA and ABBABAAB.

If we regard the renormalization map in the order ABBABAAB of scaling factor 2^8 as a single transformation, the eigenvalues of the linearized renormalization group transformation are 7731.18 ($= (2^8)^{1.61456}$) and 8.477 ($= (2^8)^{0.385441}$). One of the eigenvalues is much larger than the other, and hence we may be justified to ignore the smaller eigenvalue. The value of the critical exponent ν derived from the larger eigenvalue is 0.61936, which is very close to the reliable numerical result 0.6301 [100].

The effectiveness of the symmetrization scheme is clearly seen in Table 3.2. With only A, $k_{c,h}$ and $k_{c,v}$ are very different, and both eigenvalues of the linearized renormalization-group transformation are relevant. The introduction of reverse order relaxes the asymmetry of the fixed point. In addition, in the space of k_h and k_v, the slope of the dominant flow approaches 1, and the other flow becomes perpendicular to the dominant one (Fig. 3.5). These changes suggest that the larger eigenvalue is the reliable one and we may ignore the other. The latter seems to be an artifact of the approximation.

We can also study the case with a longitudinal field, $h \neq 0$. With the same scheme as for $h = 0$, we obtain the eigenvalues of the linearized renormalization-group transformation and critical exponents as listed in Table 3.3. The exponent y_h, or the critical exponent η, is not very close to the numerical result of the classical Ising model in three dimensions [100], a situation similar to the one-dimensional case. Moreover, this value is not improved by the symmetrization process. This property may give an important clue for the study of the relation between the symmetry of a model and the symmetry of a method.

Table 3.2: The critical point k_c, eigenvalues of the renormalization-group transformation λ, critical exponent ν, the slope of the dominant eigenvector $\boldsymbol{\phi_1}$, and the scalar product of two eigenvectors $\boldsymbol{\phi_1} \cdot \boldsymbol{\phi_2}$ from real-space renormalization group with symmetrization on the square lattice.

	A	AB	ABBA	ABBABAAB	three-dimensional classical
$k_{c,h}$	1.544	1.793	1.828	1.835	3.4351 [101]
$k_{c,v}$	2.383	1.897	1.855	1.848	
λ_1	3.083	9.377	87.901	7731.18	
λ_2	1.297	1.706	2.912	8.477	
ν_1	0.61555	0.61935	0.61941	0.61936	0.6301(4) [100]
ν_2	2.66356	2.59466	2.59372	2.59443	
slope of $\boldsymbol{\phi_1}$	1.758	1.059	1.026	1.002	
$\boldsymbol{\phi_1} \cdot \boldsymbol{\phi_2}$	0.644	0.140	0.071	0.050	

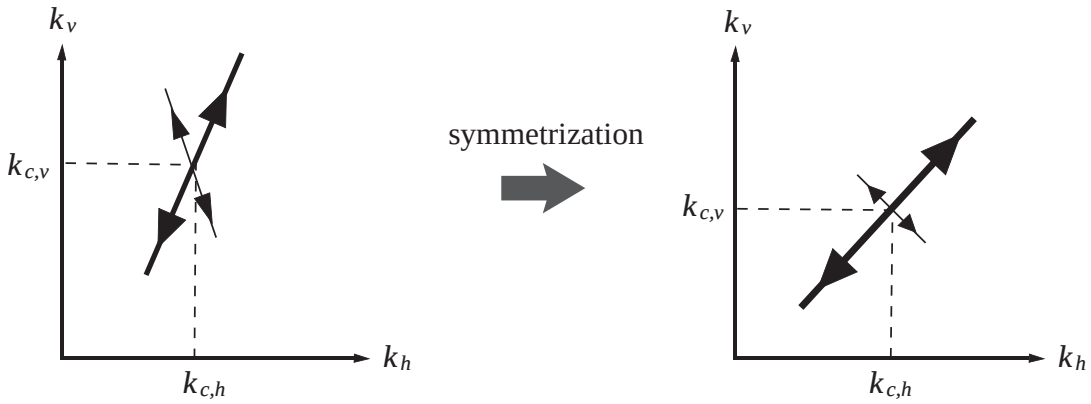

Figure 3.5: The schematic renormalization-group flow near the fixed point in the space of k_h and k_v. With the symmetrization procedure $k_{c,h}$ and $k_{c,v}$ become close to each other, and the slope of the dominant flow (the thicker line) approaches 1, and the subdominant direction becomes perpendicular.

Table 3.3: The exponents y_Γ and y_h for the linearized renormalization group transformation and the critical exponents ν and η for the square lattice, derived from symmetrization.

	A	AB	ABBA	ABBABAAB	three-dimensional classical [100]
y_x	1.62456	1.61459	1.61445	1.61456	
y_z	2.39774	2.38895	-	-	
ν	0.61555	0.61935	0.61941	0.61936	0.6301(4)
η	0.20452	0.22209	-	-	0.0364(5)

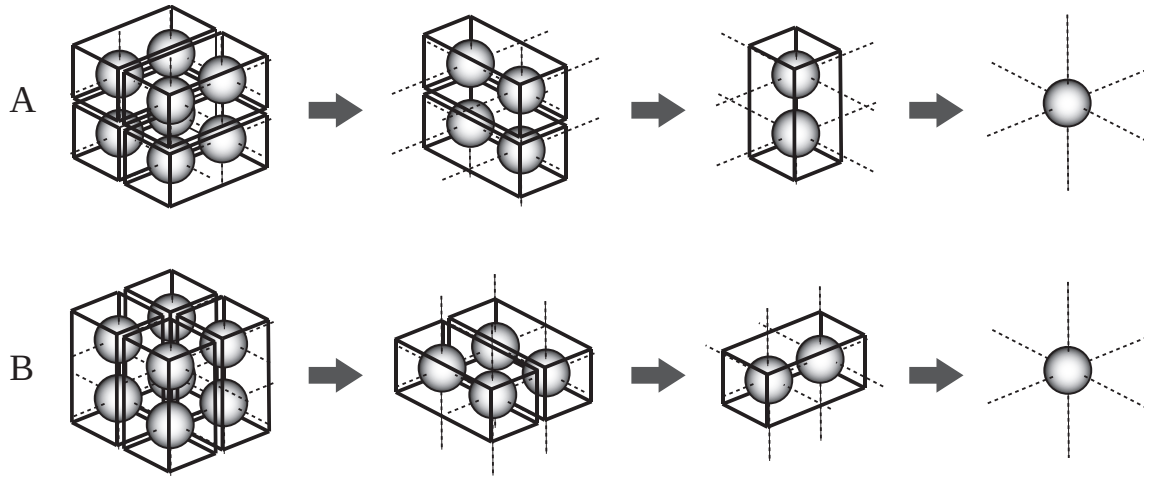

Figure 3.6: The order of renormalization in three dimensions. With A, we renormalize the system in the horizontal, then vertical, and finally in the third direction. The order B is the reverse of A.

3.2.2 Three dimensions

Next, we generalize the scheme to a cubic lattice in three dimensions. Let us again restrict ourselves to the system without longitudinal field for simplicity. We have to renormalize the three-dimensional system in three directions. The order A is defined as horizontal, then vertical and finally along the third direction. The order B is the reverse of A (Fig. 3.6). We now define the coupling constant for the third direction as J_t in addition to J_h and J_v for the horizontal and vertical directions.

In the first step of order A, which is the renormalization in the horizontal direction, the parameters change as

$$\tilde{J}_h = \frac{J_h^2}{\sqrt{J_h^2 + \Gamma^2}}, \tag{3.84}$$

$$\tilde{J}_v = J_v \left(\frac{J_h^2}{J_h^2 + \Gamma^2} + 1 \right), \tag{3.85}$$

$$\tilde{J}_t = J_t \left(\frac{J_h^2}{J_h^2 + \Gamma^2} + 1 \right), \tag{3.86}$$

$$\tilde{\Gamma} = \frac{\Gamma^2}{\sqrt{J_h^2 + \Gamma^2}}. \tag{3.87}$$

Note that the coupling constants of vertical and third directions are changed under the same rule. In general, when the system is renormalized in the direction α and another direction is represented as β, the parameters are transformed as

$$\tilde{J}_\alpha = \frac{J_\alpha^2}{\sqrt{J_\alpha^2 + \Gamma^2}}, \tag{3.88}$$

$$\tilde{J}_\beta = J_\beta \left(\frac{J_\alpha^2}{J_\alpha^2 + \Gamma^2} + 1 \right), \tag{3.89}$$

Table 3.4: The exponents y_Γ and y_h for the linearized renormalization-group transformation and the critical exponents ν and η for the cubic lattice, derived from symmetrization.

	A	AB	classical mean-field
y_Γ	2.0213	2.0092	2
y_h	3.1507	3.1428	3
ν	0.49474	0.49772	1/2
η	−0.30145	−0.28553	0

$$\tilde{\Gamma} = \frac{\Gamma^2}{\sqrt{J_\alpha^2 + \Gamma^2}}. \tag{3.90}$$

Carrying out the three steps of the scheme with these relations, we can obtain the parameters of the system renormalized in the three directions.

The symmetrization with the combinations of A and B as in the two-dimensional system improves the result (Table 3.4). The value of ν with A is 0.49474 and with AB is 0.49772. In the classical mean-field Ising model, which corresponds to the three-dimensional transverse-field Ising model, the value of ν is 1/2. Our procedure yields almost the exact value of ν, and the symmetrization is an effective way to improve the results just as in the two-dimensional case.

The result of the exponent related to a longitudinal field in three dimensions is also shown in Table 3.4. The value of η is not as good as the result for ν, a situation similar to the one- and two-dimensional cases.

3.3 Summary

In this chapter, we have performed our renormalization-group scheme in the transverse-field Ising models. Our method is a kind of block-spin transformations. We divide systems into blocks and define block Hamiltonians. Dropping the highest-lying energy eigenstates of the block Hamiltonians, the system is projected onto the coarse-grained system. The changes of parameters through the transformation draw a renormalization-group flow. This scheme is intuitively reasonable, since the lower-lying energy states, which we exploit in the scheme, seem to strongly influence properties of the ground state.

Our method is appropriate to analyze a phase transition and critical phenomena in the transverse-field Ising model in finite dimensions. Our scheme preserves the form of the Hamiltonian under the transformation. In addition, the block Hamiltonian adopted in our analysis has an outstanding property associated with the self-duality. These are expected to be essential to successfully extract the critical point and the critical exponents. A remarkable feature of the method is that it yields exact results in one dimension.

We have generalized this idea to higher dimensions. The one-dimensional block method is also effective in higher dimensions, and we have combined the method in

horizontal, vertical and the third directions to restore the symmetry of the lattice. Our results demonstrate the utility of the block Hamiltonian we have adopted. Although the results fall short of the exact solutions as in the one-dimensional case, they still represent important steps because the real-space renormalization group rarely gives accurate estimates of critical exponents in two and three dimensions. Since the critical exponent ν has been estimated to good accuracy in two and three dimensions where there is no self-duality, additional factors should have contributed such as the preservation of the bond algebra embedded in our construction of the block Hamiltonian.

Chapter 4

Real-space renormalization-group analysis of the random transverse-field Ising models

This chapter studies the nature of critical phenomena in the random transverse-field Ising models, more specifically, the random ferromagnetic Ising models and the Ising spin glasses in transverse fields in one, two, and three dimensions, with the real-space renormalization-group method explained in Chaps. 2 and 3. The one-dimensional model with randomness was studied with the same strategy as our scheme [102]. The present study covers higher-dimensional cases, spin-glass models in particular. A special emphasis is placed to resolve the problem of whether or not the infinite-randomness fixed point exists in these models. The critical exponent ν for the correlation length will be calculated. It is to be noted that ν is a representative exponent of infinite-randomness fixed points.

We do not calculate critical exponents other than ν in this chapter, since our method has not yielded accurate values of the other exponents, for example η, in non-random systems [85] in Chap. 3. Accordingly, we do not consider a longitudinal field. Also, there are exponents peculiar to the random systems, for example ψ [12], for which we have not established a method to calculate in our framework. We thus concentrate ourselves on the presence of infinite-randomness fixed points and the exponent ν.

In Sec. 4.1, we generalize the real-space renormalization-group scheme to the random transverse-field Ising chain after a short review of the model. Some previous results are correctly reproduced under the scheme. In particular, the presence of the infinite-randomness fixed point is verified. Our method is generalized to higher spatial dimensions in Secs. 4.2 and 4.3, where the random ferromagnetic Ising models in transverse fields and Ising spin glasses in transverse fields are investigated. We devote Sec. 4.4 to summarize the study in this chapter. This chapter is built on author's original work, which has been published in [86].

4.1 One dimension

This section investigates the one-dimensional random transverse-field Ising model,

$$H = -\sum_{i=1}^{N} J_i \sigma_i^z \sigma_{i+1}^z - \sum_{i=1}^{N} \Gamma_i \sigma_i^x, \tag{4.1}$$

where σ_i^α denotes the α-component of the Pauli matrix on site i. The boundary condition is periodic $\sigma_i = \sigma_{i+N}$, where N is the number of spins assumed to be even. The couplings J_i and transverse fields Γ_i are random variables independently distributed. Without loss of generality, we restrict random variables to be positive since the system is a chain with even sites as in Sec. 3.1. For simplicity, we do not consider a longitudinal field. As seen in

This model has already been analyzed in detail [19,20,28], and then peculiar features have been revealed as reviewed in Chap. 1. In Sec. 4.1.1, we review the model again, in particular the transition point and critical exponents related to our study in this chapter. Our renormalization-group analysis is performed in Sec. 4.1.2.

4.1.1 Random transverse-field Ising chain

Let us recall a few previous results [19, 20, 28] related to the random transverse-field Ising chain, Eq. (4.1).

When the average of transverse fields is much larger than that of couplings, the system lies in the paramagnetic phase, that is, the expectation value of σ^z is zero. A phase transition to the ferromagnetic phase takes place at some point as we reduce the average value of fields. The system, as a result, obtains a finite expectation value of σ^z. The para-ferro transition point has been analytically obtained [28],

$$\sum_{i=1}^{N} \log J_i = \sum_{i=1}^{N} \log \Gamma_i, \tag{4.2}$$

which includes the non-random case [23–25].

The model has an infinite-randomness fixed point [12,19,20]. One of the characteristic features appears in the behavior of correlation length near the fixed point. There are two kinds of critical exponent ν about the divergence of correlation length, and the two critical exponents take different values in the random transverse-field Ising chain, $\nu = 2$ [19, 20] and $\nu_{\rm typ} = 1$ [41]. The first one ν is for the (average) correlation length ξ, and it correctly takes into account the effects of randomness. The other exponent $\nu_{\rm typ}$ is for the typical correlation length $\xi_{\rm typ}$, which describes the typical behavior of the system and does not reflect the influence of rare events on macroscopic properties. The correlation length ξ properly describing the effect of rare events in the random system is defined as the largest length L, where the probability that all the spins in the block of length L are correlated, exceeds some finite value [19, 20, 103, 104].

In the random transverse-field Ising model, average and variance of $(\log \Gamma - \log J)$ plays an important role in the determination of the correlation-length exponent [19,20].

We now express the average as Δ,

$$\Delta = \frac{1}{N}\sum_{i=1}^{N} \log \frac{\Gamma_i}{J_i}. \tag{4.3}$$

According to Eq. (4.2), the phase transition in one dimension occurs when this average is equal to zero. The system lies in the paramagnetic phase if $\Delta > 0$, and the system in the ferromagnetic phase has a negative Δ. The average per block having a length of L is $L\Delta$. Roughly speaking, in the Gaussian distribution for example, the variance of $(\log \Gamma - \log J)$ per block is LV, where V expresses the variance per spin,

$$V = \frac{1}{N}\sum_{i=1}^{N} \left(\log \frac{\Gamma_i}{J_i} - \Delta \right)^2. \tag{4.4}$$

If $L\Delta > \sqrt{LV}$, most blocks show paramagnetic behavior, and there are few blocks containing perfectly correlated spins. Otherwise, there is a significant probability that all spins are correlated in a block. The relation $\xi\Delta \sim \sqrt{\xi V}$ is thus a good estimate for the correlation length. Hence, we have

$$\xi \sim \left(\frac{\Delta}{\sqrt{V}} \right)^{-2}. \tag{4.5}$$

The correlation length diverges around the transition point $\Delta = 0$, and we find $\Delta/\sqrt{V}$ to be a proper parameter measuring the "distance" from the critical point. In general, including the case $\Delta_c \neq 0$, we expect the relation between the correlation length ξ and the critical exponent ν to be represented as

$$\xi \sim \left(\frac{\Delta - \Delta_c}{\sqrt{V}} \right)^{-\nu}. \tag{4.6}$$

The above-mentioned crude estimate suggests $\nu = 2$.

If we measure the distance without variance, which reflects the effect of rare events, we can associate the typical correlation length $\xi_{\rm typ}$ with the critical exponent $\nu_{\rm typ}$,

$$\xi_{\rm typ} \sim (\Delta - \Delta_c)^{-\nu_{\rm typ}}. \tag{4.7}$$

This expression of the exponent $\nu_{\rm typ}$ is due to [19, 20], a leading study on the one-dimensional model. Nevertheless, this is not a common definition of $\nu_{\rm typ}$. Usually, $\nu_{\rm typ}$ is expressed as $\nu(1-\psi)$ with another exponent ψ describing the relationship between the length scale and the energy scale [12]. Since we do not have a method to estimate ψ, we do not calculate in the present study $\nu_{\rm typ}$ other than the simple one-dimensional model. In higher-dimensional cases, we mention only whether the two exponents defined in Eqs. (4.6) and (4.7) may have differences.

4.1.2 Real-space renormalization group in one dimension

We develop a real-space renormalization-group procedure for the random transverse-field Ising model in one dimension of Eq. (4.1) at zero temperature [86, 102]. This

is a natural generalization of our previous method for the pure transverse-field Ising model [85, 99] in Sec. 3.1.

We start by dividing the chain into blocks of two spins as in the pure case in Chap. 3. The Hamiltonian is also split into intra-block and inter-block parts,

$$H_i^{\text{intra}} = -J_{2i-1}\sigma_{2i-1}^z\sigma_{2i}^z - \Gamma_{2i-1}\sigma_{2i-1}^x, \tag{4.8}$$

$$H_{i,i+1}^{\text{inter}} = -J_{2i}\sigma_{2i}^z\sigma_{2i+1}^z - \Gamma_{2i}\sigma_{2i}^x, \tag{4.9}$$

where spins $2i-1$ and $2i$ belong to block i, and spin $2i+1$ belongs to block $i+1$. The label of block i runs from 1 to $N/2$. Most importantly, this particular block partition is suited to preserve the form of the Hamiltonian under the renormalization-group transformations [85] and is the key for the success of our calculations.

The eigenvalues of H_i^{intra} are degenerate,

$$\varepsilon_i^{(1)} = \varepsilon_i^{(2)} = -\sqrt{(J_{2i-1})^2 + (\Gamma_{2i-1})^2}, \tag{4.10}$$

$$\varepsilon_i^{(3)} = \varepsilon_i^{(4)} = \sqrt{(J_{2i-1})^2 + (\Gamma_{2i-1})^2}. \tag{4.11}$$

The corresponding eigenvectors are

$$|1\rangle_i = a_i^+|\uparrow\uparrow\rangle + a_i^-|\downarrow\uparrow\rangle, \quad |2\rangle_i = a_i^+|\downarrow\downarrow\rangle + a_i^-|\uparrow\downarrow\rangle, \tag{4.12}$$

$$|3\rangle_i = a_i^-|\downarrow\downarrow\rangle - a_i^+|\uparrow\downarrow\rangle, \quad |4\rangle_i = a_i^-|\uparrow\uparrow\rangle - a_i^+|\downarrow\uparrow\rangle, \tag{4.13}$$

where

$$a_i^\pm = \sqrt{\frac{1}{2}\left(1 \pm \frac{J_{2i-1}}{\sqrt{(J_{2i-1})^2 + (\Gamma_{2i-1})^2}}\right)}, \tag{4.14}$$

and $\{|\uparrow\uparrow\rangle, |\uparrow\downarrow\rangle, |\downarrow\uparrow\rangle, |\downarrow\downarrow\rangle\}$ is the orthonormal basis in the σ^z-basis, i.e. $\sigma^z|\uparrow\rangle = |\uparrow\rangle$, $\sigma^z|\downarrow\rangle = -|\downarrow\rangle$.

We next keep the two lowest lying energy eigenstates $|1\rangle$ and $|2\rangle$, and drop the others, $|3\rangle$ and $|4\rangle$, to perform a coarse-graining. We then replace each block with a single spin representing the $|1\rangle$ and $|2\rangle$ states as in Sec. 3.1.1. Using the projector defined as Eqs. (3.10) and (3.11) with $|1\rangle_i$ and $|2\rangle_i$ in Eq. (4.12), the coarse-grained Hamiltonian is written as PHP. The renormalized intra-block Hamiltonian is trivially represented with the identity operator 1_i on block i as

$$P_i H_i^{\text{intra}} P_i = \varepsilon_i^{(1)} 1_i. \tag{4.15}$$

Terms in the inter-block Hamiltonian are projected as

$$P_i\left(1_{2i-1} \otimes \sigma_{2i}^z\right) P_i = \tilde{\sigma}_i^z, \tag{4.16}$$

$$P_{i+1}\left(\sigma_{2i+1}^z \otimes 1_{2i+2}\right) P_{i+1} = \frac{J_{2i+1}}{\sqrt{(J_{2i+1})^2 + (\Gamma_{2i+1})^2}}\tilde{\sigma}_{i+1}^z, \tag{4.17}$$

$$P_i\left(1_{2i-1} \otimes \sigma_{2i}^x\right) P_i = \frac{\Gamma_{2i-1}}{\sqrt{(J_{2i-1})^2 + (\Gamma_{2i-1})^2}}\tilde{\sigma}_i^x, \tag{4.18}$$

where $\tilde{\sigma}_i^\alpha$ is the α-component of the Pauli matrix on block i, or new site i in the coarse-grained system.

The renormalized Hamiltonian is consequently expressed as

$$PHP = \sum_{i=1}^{N/2} \varepsilon_i^{(1)} 1_i - \sum_{i=1}^{N/2} \tilde{J}_i \tilde{\sigma}_i^z \tilde{\sigma}_{i+1}^z - \sum_{i=1}^{N/2} \tilde{\Gamma}_i \tilde{\sigma}_i^x \tag{4.19}$$

with renormalized couplings

$$\tilde{J}_i = \frac{J_{2i} J_{2i+1}}{\sqrt{(J_{2i+1})^2 + (\Gamma_{2i+1})^2}}, \tag{4.20}$$

$$\tilde{\Gamma}_i = \frac{\Gamma_{2i-1} \Gamma_{2i}}{\sqrt{(J_{2i-1})^2 + (\Gamma_{2i-1})^2}}. \tag{4.21}$$

Note that our transformation preserves the form of the Hamiltonian. In other words, our method does not generate additional couplings under renormalization. Other choices of the intra- and inter-block Hamiltonians lead to more inconvenient transformations as discussed in Sec. 3.1.3.

Let us calculate renormalized Δ to generate the renormalization-group equation,

$$\begin{aligned} \tilde{\Delta} &= \frac{1}{N/2} \sum_{i=1}^{N/2} \log \frac{\tilde{\Gamma}_i}{\tilde{J}_i} \\ &= 2\Delta, \end{aligned} \tag{4.22}$$

where we have used a property of the periodic boundary condition $\tilde{\Gamma}_{N/2+1} = \tilde{\Gamma}_1$. The renormalization-group equation $\tilde{\Delta} = 2\Delta$ has a fixed point

$$\Delta_c = 0. \tag{4.23}$$

This agrees with the exact transition point [28]. Combining the change of Δ with that of the typical correlation length $\tilde{\xi}_{\rm typ} = \xi_{\rm typ}/2$ through the scale transformation with the scaling factor 2, we obtain the critical exponent

$$\nu_{\rm typ} = 1 \tag{4.24}$$

under Eq. (4.7). This is also the exact value [41].

To take atypical effects into account, we have to explore the change of variance of $(\log \Gamma - \log J)$ through renormalization. However, it is difficult to analytically investigate it. We hence study the change of variance by numerical methods.

In numerical calculations, we first prepare a pool containing N couplings and N transverse fields to construct a chain having N sites, where N has been chosen to be 10^6. The parameters obey the uniform distributions

$$P_J(J_i) = \theta(J_i)\theta(1 - J_i), \tag{4.25}$$

$$P_\Gamma(\Gamma_i) = \frac{1}{\Gamma_u} \theta(\Gamma_i)\theta(\Gamma_u - \Gamma_i), \tag{4.26}$$

where if $x > 0$, $\theta(x) = 1$, and $\theta(x) = 0$ otherwise. If the upper bound Γ_u of the values of transverse fields is equal to 1, the distributions of J and Γ coincide, and the system lies at the critical point.

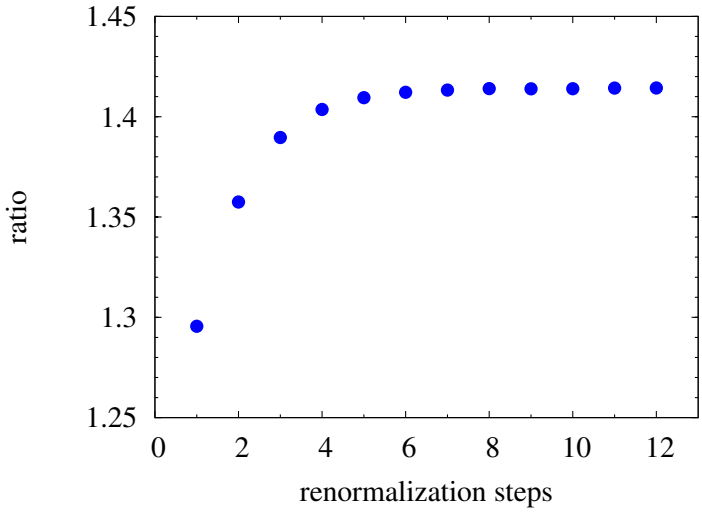

Figure 4.1: Ratio of the square root of the variance of $(\log\Gamma - \log J)$ after a renormalization to that before the renormalization in the random transverse-field Ising model in one dimension.

We next perform the renormalization according to Eqs. (4.20) and (4.21) with the periodic boundary condition, and the pool is renewed by generating the renormalized couplings and fields. Then the size of the system becomes a half of that of the original system. To repeat the renormalization on a large system, we add a copy of all couplings and fields in the renormalized system to the pool. Consequently, the number of couplings and fields in the pool is recovered, and the couplings and fields obey the identical distribution with that of the pool before the copies are added. We then reconstruct a chain with the renormalized parameters in the pool. In other words, we relabel the parameters to mix originals and copies. It is noted that, since $\tilde{J}_i$ and $\tilde{\Gamma}_{i+1}$ in the renormalized system share J_{2i+1} and Γ_{2i+1} [Eqs. (4.20) and (4.21)], if $\tilde{J}_i$ is relabeled as $\tilde{J}_j$, $\tilde{\Gamma}_{i+1}$ has to be relabeled as $\tilde{\Gamma}_{j+1}$.

Repeating this scheme, we observe the change of the variance of $(\log\Gamma - \log J)$. To reduce statistical errors, we run up to 100 samples. We set the system very close to the critical point $\Delta_c = 0$ when the calculation is carried out. More precisely, the upper bound of fields Γ_u in the initial condition is set to be 1, where the distributions of couplings and fields coincide. Nevertheless these distributions in practice have a small difference owing to the finiteness of the number of couplings and fields.

A result of the numerical estimate is shown in Fig. 4.1, where the ratio of the square root of the variance of $(\log\Gamma - \log J)$ after a renormalization to that before the renormalization is plotted. The ratio is always larger than 1, that is, the distributions of the logarithms of parameters keep broadening. This fact demonstrates the existence of an infinite-randomness fixed point in the random transverse-field Ising spin chain. Furthermore, the ratio reaches a stationary state after several steps of renormalization. The value of critical exponent ν calculated from Eq. (4.6) also becomes stable accordingly, because the ratio of Δ after a renormalization to that before the renormalization is constant, 2. Since randomness is strong when the stationary behavior appears, we

expect to extract the nature of the system near the infinite-randomness fixed point from this stationary behavior. We therefore estimate the critical exponent ν with the values in the stationary region as

$$\nu = 2.00(7), \tag{4.27}$$

where we have assumed that a renormalized correlation length is a half of the original correlation length through the renormalization of scaling factor 2. This value is in good agreement with the exact one $\nu = 2$ [19, 20].

Although our real-space renormalization group procedure includes approximations, it reproduces the exact critical point, and the exact values of the critical exponents $\nu_{\rm typ}$ and ν. Our simple scheme correctly reflects the physics of the infinite-randomness behavior, which is one of the most peculiar features in the random transverse-field Ising spin chain.

4.2 Two dimensions

We generalize the renormalization-group method to the two-dimensional transverse-field Ising model with randomness on the square lattice. This is also a generalization of the previous study on the pure model in two dimensions discussed in Sec. 3.2 [85] to the random model. The Hamiltonian of the two-dimensional model is

$$H = -\sum_{\langle i,j \rangle} J_{ij}\sigma_i^z\sigma_j^z - \Gamma\sum_i \sigma_i^x, \tag{4.28}$$

where spins interact with their nearest neighbors $\langle i, j\rangle$. Couplings J_{ij} are random variables and are independently identically distributed. In Sec. 4.2.2, the couplings are uniformly distributed as $P_J(J_{ij}) = \theta(J_{ij})\theta(1 - J_{ij})$, whereas Sec. 4.2.3 examines the spin-glass case with the Gaussian distribution, $P_J(J_{ij}) = \exp[-(J_{ij} - J_0)^2/2]/\sqrt{2\pi}$.

4.2.1 Generalization to the two-dimensional models

We generalize our method in two dimensions. As in the pure case, we iterate the renormalization in two directions: first in the horizontal direction and then in the vertical direction (Fig. 3.2). Now, we redefine the coupling constants for the horizontal direction and the vertical direction to distinguish these two quantities in this scheme. The coupling constants between the spin at (i, j) and the neighboring spin to the right side is $J_{h(i,j)}$ and that between the spin at (i, j) and the neighboring spin to the upper side is $J_{v(i,j)}$, where (i, j) denotes the location of a single site on the two dimensional lattice.

In the first step of the renormalization (in the horizontal direction) we replace each block with a single spin using the same procedure as in the one-dimensional case. We have the relation corresponding to Eqs. (4.16)–(4.18),

$$\tilde{P}_{(i,j)}\left(1_{(2i-1,j)} \otimes \sigma^z_{(2i,j)}\right)\tilde{P}_{(i,j)} = \tilde{\sigma}^z_{(i,j)}, \tag{4.29}$$

$$\tilde{P}_{(i+1,j)}\left(\sigma^z_{(2i+1,j)}\otimes 1_{(2i+2,j)}\right)\tilde{P}_{(i+1,j)}=\frac{J_{h(2i+1,j)}}{\sqrt{J^2_{h(2i+1,j)}+\Gamma^2_{(2i+1,j)}}}\tilde{\sigma}^z_{(i+1,j)}, \tag{4.30}$$

$$\tilde{P}_{(i,j)}\left(1_{(2i-1,j)}\otimes \sigma^x_{(2i,j)}\right)\tilde{P}_{(i,j)}=\frac{\Gamma_{(2i-1,j)}}{\sqrt{J^2_{h(2i-1,j)}+\Gamma^2_{(2i-1,j)}}}\tilde{\sigma}^x_{(i,j)}, \tag{4.31}$$

where $\tilde{P}_{(i,j)}$ denotes the projector onto the state space of the block spin, namely the spin at (i,j) in the renormalized system. We find that the z-component of the spin on the right spot in a block becomes the z-component of the block spin, but the z-component of the spin on the left spot in a block becomes the z-component of the block spin multiplied by $J_h/\sqrt{J_h^2+\Gamma^2}$. The renormalized couplings and fields are then written as,

$$\tilde{J}_{h(i,j)}=\frac{J_{h(2i,j)}J_{h(2i+1,j)}}{\sqrt{J^2_{h(2i+1,j)}+\Gamma^2_{(2i+1,j)}}}, \tag{4.32}$$

$$\tilde{J}_{v(i,j)}=\frac{J_{h(2i-1,j)}}{\sqrt{J^2_{h(2i-1,j)}+\Gamma^2_{(2i-1,j)}}}\frac{J_{h(2i-1,j+1)}}{\sqrt{J^2_{h(2i-1,j+1)}+\Gamma^2_{(2i-1,j+1)}}}J_{v(2i-1,j)}+J_{v(2i,j)}, \tag{4.33}$$

$$\tilde{\Gamma}_{(i,j)}=\frac{\Gamma_{(2i-1,j)}\Gamma_{(2i,j)}}{\sqrt{J^2_{h(2i-1,j)}+\Gamma^2_{(2i-1,j)}}}. \tag{4.34}$$

In Eq. (4.33), $J_{v(2i,j)}$ is derived from the coupling of two spins on the right spot in each block, and the rest is derived from the one on the left spot in the blocks.

Next the system is renormalized in the vertical direction in the same way as the horizontal direction. The coupling constants and the transverse fields are now

$$\tilde{\tilde{J}}_{h(i,j)}=\frac{\tilde{J}_{v(i,2j-1)}}{\sqrt{\tilde{J}^2_{v(i,2j-1)}+\tilde{\Gamma}^2_{(i,2j-1)}}}\frac{\tilde{J}_{v(i+1,2j-1)}}{\sqrt{\tilde{J}^2_{v(i+1,2j-1)}+\tilde{\Gamma}^2_{(i+1,2j-1)}}}\tilde{J}_{h(i,2j-1)}+\tilde{J}_{h(i,2j)}, \tag{4.35}$$

$$\tilde{\tilde{J}}_{v(i,j)}=\frac{\tilde{J}_{v(i,2j)}\tilde{J}_{v(i,2j+1)}}{\sqrt{\tilde{J}^2_{v(i,2j+1)}+\tilde{\Gamma}^2_{(i,2j+1)}}}, \tag{4.36}$$

$$\tilde{\tilde{\Gamma}}_{(i,j)}=\frac{\tilde{\Gamma}_{(i,2j-1)}\tilde{\Gamma}_{(i,2j)}}{\sqrt{\tilde{J}^2_{v(i,2j-1)}+\tilde{\Gamma}^2_{(i,2j-1)}}}. \tag{4.37}$$

It is important that our transformations in two dimensions also do not generate extra terms as the one-dimensional case, and the form of the Hamiltonian is preserved. In addition, the lattice structure is preserved.

Note that our transformations are not local. After the first step of the renormalization, $\tilde{J}_{h(i,j)}$, $\tilde{J}_{v(i+1,j)}$, and $\tilde{\Gamma}_{(i+1,j)}$ share $J_{h(2i+1,j)}$ and $\Gamma_{(2i+1,j)}$. Hence, $\tilde{J}_{h(i,j)}$, $\tilde{J}_{v(i+1,j)}$, and $\tilde{\Gamma}_{(i+1,j)}$ are correlated with each other. Similarly, $\tilde{J}_{h(i,j+1)}$, $\tilde{J}_{v(i+1,j)}$, and $\tilde{\Gamma}_{(i+1,j+1)}$ share $J_{h(2i+1,j+1)}$ and $\Gamma_{(2i+1,j+1)}$. Thus, $\tilde{J}_{h(i,j)}$, $\tilde{J}_{h(i,j+1)}$, $\tilde{J}_{v(i+1,j)}$, $\tilde{\Gamma}_{(i+1,j)}$, and $\tilde{\Gamma}_{(i+1,j+1)}$ are correlated with each other. In a column, couplings in the vertical direction, couplings to the left-hand spin, and fields are mutually correlated after the horizontal renormalization. The vertical renormalization accordingly makes couplings in the horizontal direction, couplings to the lower-side spin, and fields in a row mutually correlate.

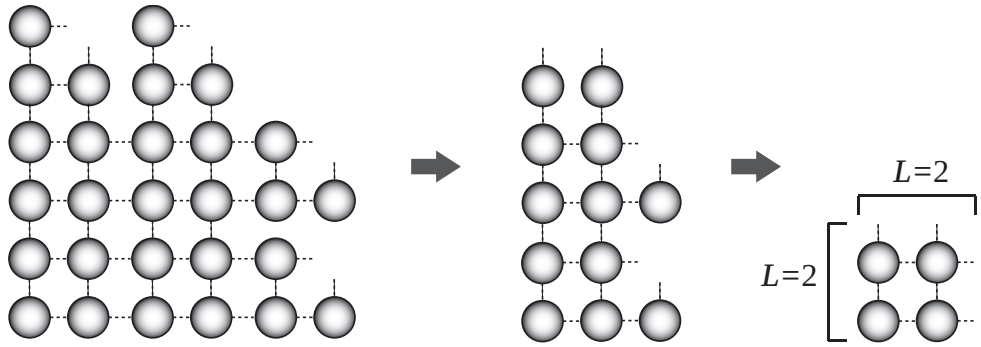

Figure 4.2: Construction of a cluster (left) for the renormalized cluster of size $L = 2$ (right) in two dimensions and two steps of renormalization of the cluster in the horizontal and vertical directions.

After two steps of the procedure, no set of couplings and fields are independent from others, consequently.

The renormalization-group transformations are numerically performed as follows. We prepare a pool of couplings J and fields Γ. The pool contains N couplings in the horizontal and vertical directions, respectively, as well as N fields. In our calculation N is 10^6. We build a two-dimensional partial lattice, which we call a "cluster" hereafter, of couplings and fields randomly taken from the pool. The cluster is renormalized according to Eqs. (4.32)–(4.37), and we put the renormalized cluster in a new pool. We prepare the shape of the cluster before renormalization to obtain a renormalized square cluster of size $L \times L$. For example, a renormalization process for a cluster in the case of $L = 2$ is depicted in Fig. 4.2. The scheme, from building a cluster to putting the renormalized cluster in the new pool, for a square cluster of size $L \times L$ is executed $N/(L \times L)$ times. The new pool is filled by $N/(L \times L)$ renormalized clusters of size $L \times L$ as a result, and a single renormalization-group transformation for the whole system is completed. In the next renormalization step, we construct new clusters of the clusters in the pool and repeat the process. In our calculation L is set equal to 20. The renormalization for the whole system is repeated 15 times, and we run up to 100 samples. The procedure is partially based on the calculation method by Nobre [105] in which one randomly takes couplings and fields from the pool as often as one makes a cluster.

The reason why we use the clusters in our calculation lies on the nonlocal property of our renormalization-group transformations. Although in one dimension we have rearranged the labels of couplings and fields to repeat the renormalization calculations on the large system, we cannot freely do so in two dimensions because the renormalized parameters are mutually correlated. It is difficult to fully keep the correlation in the calculation, but the cluster procedure takes it into account to a certain extent. We correctly deal with the correlation in clusters. Although this procedure still ignores the correlation between the clusters on interfaces, the effect of the surfaces is expected to be small if L is large.

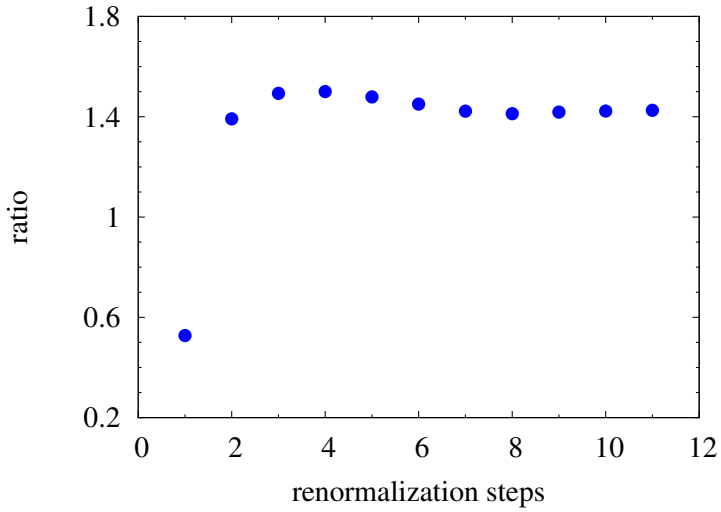

Figure 4.3: Ratio of the square root of the variance of $(\log\Gamma - \log J)$ after a renormalization to that before the renormalization in the random ferromagnetic Ising model in a transverse field in two dimensions. The initial transverse field is set equal to 0.920.

4.2.2 Random ferromagnet in two dimensions

We apply the renormalization-group method to the random ferromagnetic Ising model in a transverse field in two dimensions. The couplings J in the pool are uniformly distributed:

$$P(J) = \theta(J)\theta(1-J), \tag{4.38}$$

and the initial value of the field Γ is fixed to a constant at all sites.

We determine the critical point in terms of the parameter $(\log\Gamma - \log J)$ as in the one-dimensional case. If the average of $(\log\Gamma - \log J)$, which is denoted by Δ, after 15 times of the renormalization-group transformation is larger than the initial value of Δ, we conclude the system to be in the paramagnetic phase. Otherwise, the system is regarded to be in the ferromagnetic phase. We obtain the critical value of the transverse field $\Gamma_c = 0.9115(5)$ as a result. This value is to be compared with another estimate 0.84338(2) [67], which is fairly close to our result in consideration of the simplicity of our idea. Note that the two-dimensional system does not have the duality which plays an important role in producing the exact transition point via our method in one dimension as discussed in Sec. 3.1.4.

We next observe the change of the variance V of $(\log\Gamma - \log J)$. The ratio of $\sqrt{V}$ after a renormalization to that before the renormalization is plotted in Fig. 4.3. Although the result shows a difference form the result in one dimension in that the ratio in the first renormalization is smaller than 1, the ratio is always larger than 1 after that. We conclude that the two-dimensional random ferromagnetic Ising model in transverse fields has an infinite-randomness fixed point. This result is the same as in the strong-disorder renormalization group [5] and Monte Carlo simulation [63].

To estimate the critical exponent ν for the average correlation length, we use the

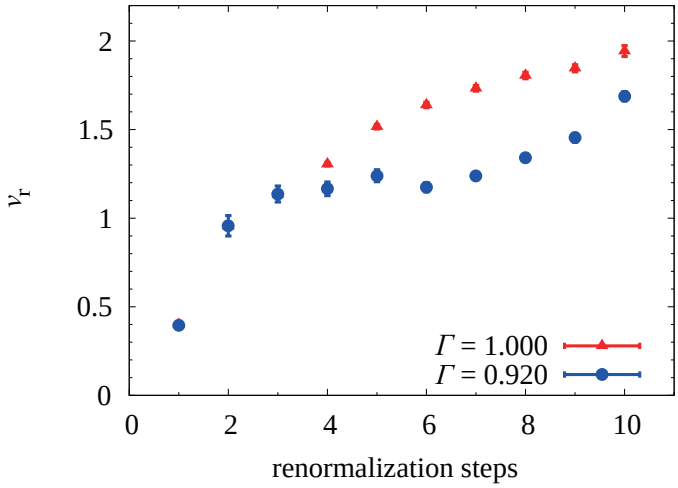

Figure 4.4: Running exponent ν_r calculated with Eq. (4.39) in the random ferromagnet Ising model in transverse fields in two dimensions. The result in the case $\Gamma = 0.920$, where the system is close to the critical point, has a plateau.

relation

$$\frac{\Delta^{i+1} - \Delta_c^{i+1}}{\sqrt{V^{i+1}}} = 2^{1/\nu_r} \frac{\Delta^i - \Delta_c^i}{\sqrt{V^i}}. \tag{4.39}$$

We call ν_r the running exponent, which is expected to correspond to the critical exponent ν if the system is sufficiently close to the infinite-randomness fixed point. We have assumed that the renormalized correlation length ought to be a half of the original correlation length through the renormalization with scaling factor 2. The symbols Δ^i and V^i denote Δ and V renormalized i times, respectively, and Δ_c^i means Δ at the transition point after i times of the renormalization-group transformation. We regard the average of the values of Δ^i for the initial transverse fields $\Gamma = 0.911$ and 0.912 as Δ_c^i owing to the uncertainty of our estimation of the transition point.

The value of Δ at the transition point depends on the distribution of couplings J. In general the distribution changes through the renormalization-group transformations even if the system lies just on the transition point. Hence, the value of Δ at the transition point after i times of transformations can be different from the one in the initial distribution. Moreover, note that the running exponent ν_r calculated with Eq. (4.39) can vary with the number i of transformations.

Since we estimate the critical exponent ν from the running exponent ν_r near an infinite-randomness fixed point, ν_r should be calculated near the transition point. However, instabilities occur if we try to evaluate it by starting too closely to the transition point due to statistical uncertainties. We thus evaluate ν_r with the initial transverse field $\Gamma = 0.920$. The results are shown in Fig. 4.4. For comparison, the result of the case of the initial transverse field $\Gamma = 1.000$ is also plotted there.

We can find a plateau around 4 to 7 for the result of $\Gamma = 0.920$, whereas it does not exist in the case of $\Gamma = 1.000$. This plateau is comparable with the stable behavior in the one dimensional case. We interpret it as a sign of the appearance of a critical phenomenon in our renormalization-group scheme. The stable behavior in two

dimensions does not continue long owing to the difficulty to keep the system close to the critical point due to randomness, whereas we can easily do so in one dimension because the fixed point in one dimension is fortunately determined only by the average of $(\log\Gamma - \log J)$ and is independent of the distribution of J. This means that in one dimension we have to control only the initial value of the average to prevent the system from migrating away from the fixed point. Estimating ν from values of $\nu_{\rm r}$ on the plateau (from 4 to 7 in the horizontal axis), we obtain

$$\nu = 1.20(6), \tag{4.40}$$

which is consistent with a previous study from a different approach, namely strong-disorder renormalization group, $\nu = 1.24(2)$ [67].

Although we do not explicitly estimate the value of $\nu_{\rm typ}$ defined in Eq. (4.7), which is slightly different from the conventional definition for the reason mentioned in Sec. 4.1.1, we recognize a difference between the values of ν and $\nu_{\rm typ}$. Since the variance V of $(\log\Gamma - \log J)$ keeps growing through the renormalization-group transformations, the change of $(\Delta - \Delta_c)/\sqrt{V}$ disagrees with that of $\Delta - \Delta_c$. This fact, which is one of the characteristics of the infinite-randomness fixed point, leads to a difference between the two exponents.

4.2.3 Spin glass in two dimensions

We next investigate the Ising spin glass in a transverse field, where the sign of couplings J_{ij} can take both positive and negative values. In our calculations, J_{ij} is independently governed by the Gaussian distribution

$$P(J_{ij}) = \frac{1}{\sqrt{2\pi}} \exp\left[- \frac{(J_{ij} - J_0)^2}{2} \right], \tag{4.41}$$

where the variance is set equl to 1. We control the average J_0 of the distribution and a uniform transverse field Γ.

Let us draw the phase boundaries. Which phase the system lies on is determined as follows. The paramagnetic phase and the ordered phases, namely the ferromagnetic phase and the spin-glass phase, are distinguished as in the case of the random ferromagnet. Specifically, if the average of $(\log\Gamma - \log J)$ after 15 times of renormalization-group transformations is larger than its initial value, the system is regarded to be in the paramagnetic phase. Otherwise, the ferromagnetic or spin-glass phase is realized. The boundary between the ferromagnetic phase and the spin-glass phase is drawn by the following rule concerning the value of $[J]^2/V_J$, where $[J]$ denotes the average of J_{ij} and V_J expresses the variance of J_{ij}. We determine that the system is in the ferromagnetic phase if $[J]^2/V_J$ is larger than 1 after 15 times of renormalization-group transformations. Otherwise, it is in the spin-glass phase. We take 30 samples in this calculation.

The resulting phase boundaries are depicted in Fig. 4.5. The result is not quantitatively in precise agreement with a previous study [83] on the transition point along the line $J_0 = 0$, or more specifically, $\Gamma_c = 1.183(3)$ in our result and $\Gamma_c = 0.608(4)$ in [83]. It is nevertheless important that a definite phase diagram has been obtained,

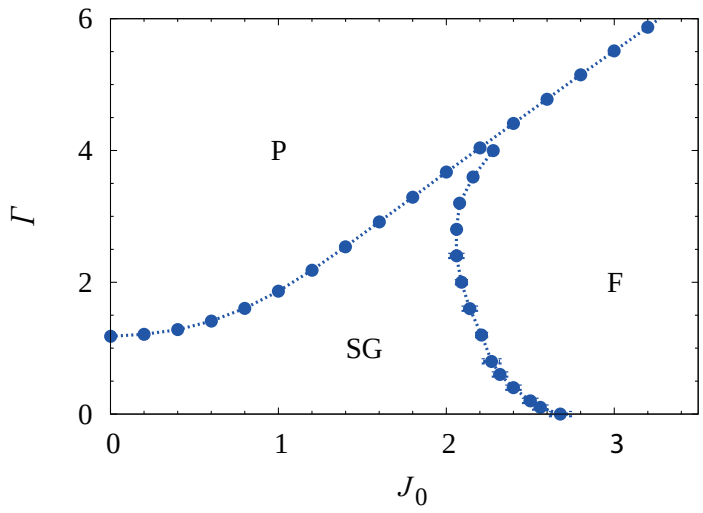

Figure 4.5: Phase diagram of the two-dimensional spin glass in transverse fields. The horizontal axis J_0 expresses the average of the Gaussian distribution of couplings J_{ij}, and the vertical axis is for the magnitude of the transverse field Γ. The symbols, P, SG, and F, denote the paramagnetic, spin glass, and ferromagnetic phases, respectively.

especially with a spin-glass phase, by the present simple renormalization group with block-spin transformations. This result implies that our method properly reflects the effect of frustration, which is one of the most essential features of spin glasses.

The ratio of $\sqrt{V}$ after a renormalization to that before the renormalization is observed also in this spin-glass model in the vicinity of the transition point for $J_0 = 0$ and is plotted in Fig. 4.6, which shows the existence of an infinite-randomness fixed point in the present system. This result supports a conjecture on the possible existence of an infinite-randomness fixed point in spin glasses inferred indirectly (i.e. without explicit calculations) from the strong-disorder renormalization-group approach to the random ferromagnetic system [5]. Moreover, our result leads to a difference between the two exponents ν and $\nu_{\rm typ}$ in the definition [Eq. (4.7)], as in the random ferromagnetic case.

We next calculate the critical exponent ν for the average correlation length. We focus ourselves on the transition point for $J_0 = 0$. As in the case of random ferromagnet, the estimation is executed slightly away from the actual transition point $\Gamma = 1.183(3)$ to avoid instabilities. Specifically, the initial transverse field is set to be $\Gamma = 1.195$. The running exponent $\nu_{\rm r}$ calculated in the same way as in the random ferromagnet is shown in Fig. 4.7. To compare the critical region with another case away from criticality, results with the initial transverse field $\Gamma = 1.300$ is also plotted there. We find a difference between the two cases that the value of $\nu_{\rm r}$ for $\Gamma = 1.195$ reaches a plateau after four times of transformations, and the value increases again after ten times of transformations. Since this behavior corresponds to the plateau in the random ferromagnet, we accordingly evaluate ν with values in this region (from 4 to 9 in the horizontal axis),

$$\nu = 1.21(9). \tag{4.42}$$

For comparison, if we use the values in the same region as in the case of the random

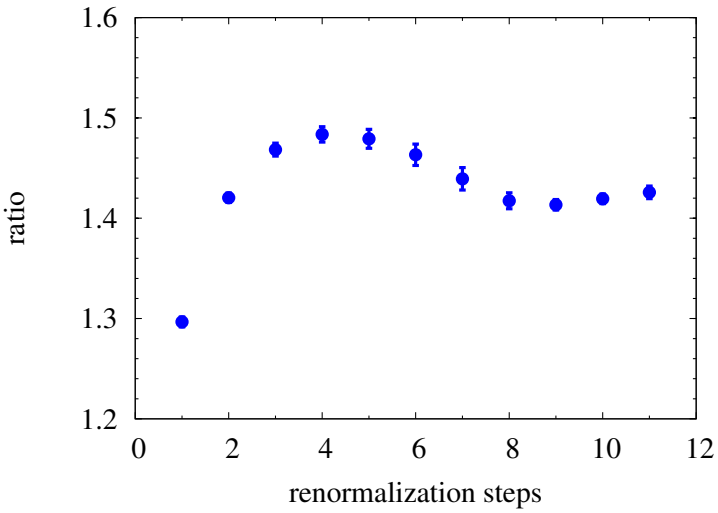

Figure 4.6: Ratio of the square root of variance of $(\log\Gamma - \log J)$ after a renormalization to that before the renormalization in the two-dimensional spin glass in the transverse field $\Gamma = 1.195$.

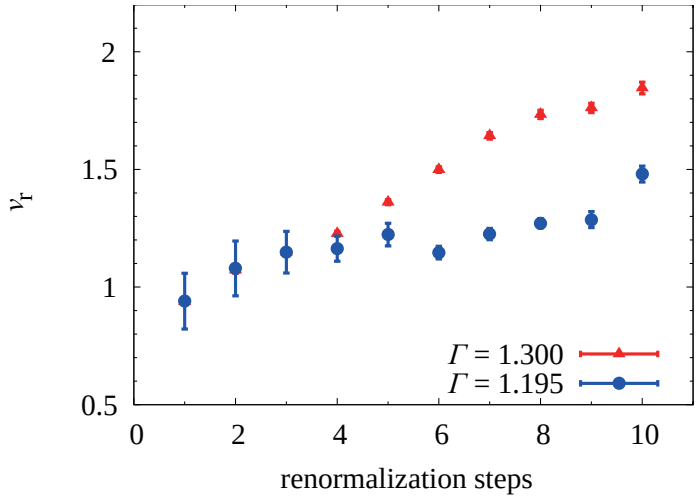

Figure 4.7: Running exponent ν_r calculated from Eq. (4.39) in the two-dimensional spin glass in transverse fields. The result in the case of $\Gamma = 1.195$, where the system is close to the critical point, has a plateau.

ferromagnet (from 4 to 7 in the horizontal axis), we have $\nu = 1.19(8)$.

In addition to having an infinite-randomness fixed point, the value of ν estimated by our method for the spin glass is in good agreement with that for the random ferromagnet [Eq. (4.40)]. Although the quantitative reliability of our method in spin glasses may not be perfect as suggested in the determination of phase boundaries, the above-mentioned agreement may possibly suggest that the random ferromagnetic Ising model in a transverse field and the Ising spin glass in a transverse field would belong to the same universality class. This is a surprising suggestion, since we have observed different phase transitions in the two cases, namely the transitions between the paramagnetic and ferromagnetic phases in the ferromagnet and between the paramagnetic and the spin-glass phases in the spin glass.

4.3 Three dimensions

This section investigates the random transverse-field Ising models on the three-dimensional cubic lattice. After the generalization of our renormalization-group method to three dimensions in Sec. 4.3.1, we apply the method to the random-ferromagnet model in Sec. 4.3.2 and to the spin-glass model in Sec. 4.3.3.

4.3.1 Generalization to the three-dimensional models

Let us generalize our renormalization-group scheme to three dimensions. The transformations are iterated in the horizontal, vertical, and third directions consecutively (Fig. 3.6). We define the coupling constants between spin (i, j, k) and the neighboring spin along the third direction $(i, j, k+1)$ as $J_{t(i,j,k)}$, and similarly for $J_{h(i,j,k)}$ and $J_{v(i,j,k)}$ for the horizontal and vertical directions, respectively.

In the first step of renormalization (in the horizontal direction) the parameters change as

$$\tilde{J}_{h(i,j,k)} = \frac{J_{h(2i+1,j,k)} J_{h(2i+2,j,k)}}{\sqrt{J^2_{h(2i+2,j,k)} + \Gamma^2_{(2i+2,j,k)}}}, \tag{4.43}$$

$$\tilde{J}_{v(i,j,k)} = \frac{J_{h(2i,j,k)}}{\sqrt{J^2_{h(2i,j,k)} + \Gamma^2_{(2i,j,k)}}} \frac{J_{h(2i,j+1,k)}}{\sqrt{J^2_{h(2i,j+1,k)} + \Gamma^2_{(2i,j+1,k)}}} J_{v(2i,j,k)} + J_{v(2i+1,j,k)}, \tag{4.44}$$

$$\tilde{J}_{t(i,j,k)} = \frac{J_{h(2i,j,k)}}{\sqrt{J^2_{h(2i,j,k)} + \Gamma^2_{(2i,j,k)}}} \frac{J_{h(2i,j,k+1)}}{\sqrt{J^2_{h(2i,j,k+1)} + \Gamma^2_{(2i,j,k+1)}}} J_{t(2i,j,k)} + J_{t(2i+1,j,k)}, \tag{4.45}$$

$$\tilde{\Gamma}_{(i,j,k)} = \frac{\Gamma_{(2i,j,k)} \Gamma_{(2i+1,j,k)}}{\sqrt{J^2_{h(2i,j,k)} + \Gamma^2_{(2i,j,k)}}}. \tag{4.46}$$

Note that the coupling constants of the vertical and third directions are changed under the same rule. Carrying out analogous transformations in the vertical direction and then in the third direction after this first step, we obtain the parameters of the system renormalized in the three directions.

This scheme, however, yields anomalous results due to the imbalanced treatment of three directions. As the transformations for three directions are iterated, the magnitude of coupling constants of the third direction J_t rapidly becomes small in comparison with those of the other two directions despite the fact that the original system has no anisotropy. The scheme thus needs some corrections.

To resolve the anisotropy problem, we further renormalize the system in the reverse order, along the third, vertical, and then horizontal directions after the regular order described above (Fig. 3.6). This set of the six steps, the regular order and then the reverse order, is regarded as a single transformation of scaling factor 4. This modified procedure succeeds in rendering virtually isotropic results. This is the same process as introduced in the previous study for the non-random system [85] in Sec. 3.2.2.

Numerical calculations are implemented in the same way as in the two-dimensional case. We generate a pool containing N couplings in the horizontal, vertical, and third directions, respectively, and N fields, where N is 10^6. The cluster method is used also in three dimensions with the cluster of size $L \times L \times L$, and L is set equal to 5. We repeat the (six-step) renormalization-group transformations 5 times, and 100 samples have been run.

4.3.2 Random ferromagnet in three dimensions

We first examine the random ferromagnetic Ising model in transverse fields on a cubic lattice. The initial distribution of couplings J in the pool is

$$P(J) = \theta(J)\theta(1-J) \tag{4.47}$$

identical to the two-dimensional case. We control the magnitude of the uniform field Γ as the initial condition.

We estimate the transition point by comparison of the initial value of Δ and the final value of Δ after 5 times of transformations. The result is $\Gamma = 1.266(2)$.

The ratio of the square root of the variance V of $(\log\Gamma - \log J)$ after a renormalization to that before the renormalization is plotted in Fig. 4.8. The stability of the ratio through renormalization is not obvious, but at least the result demonstrates the existence of an infinite-randomness fixed point.

The critical exponent ν for the average correlation length is also estimated from the values of the running exponent $\nu_{\rm r}$ computed from the relation

$$\frac{\Delta^{i+1} - \Delta_c^{i+1}}{\sqrt{V^{i+1}}} = 4^{1/\nu_{\rm r}} \frac{\Delta^i - \Delta_c^i}{\sqrt{V^i}}, \tag{4.48}$$

where we regard the average of Δ^i for the initial transverse fields $\Gamma = 1.266$ and 1.267 as Δ_c^i. We can find a plateau in the result of $\Gamma = 1.269$ most clearly near the critical point (Fig. 4.9). Evaluating ν from the values of $\nu_{\rm r}$ on the plateau (from 2 to 4 in the horizontal axis), we have

$$\nu = 0.92(4), \tag{4.49}$$

which is rather close to 0.97(5) of the corresponding result by the strong-disorder renormalization group [68, 69].

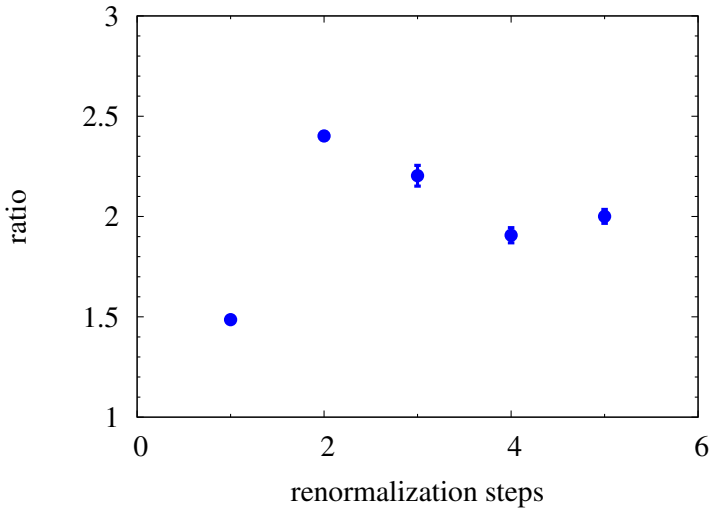

Figure 4.8: Ratio of the square root of variance of $(\log \Gamma - \log J)$ after a renormalization to that before the renormalization in the random ferromagnetic Ising model in a transverse field in three dimensions. The initial transverse field is 1.269.

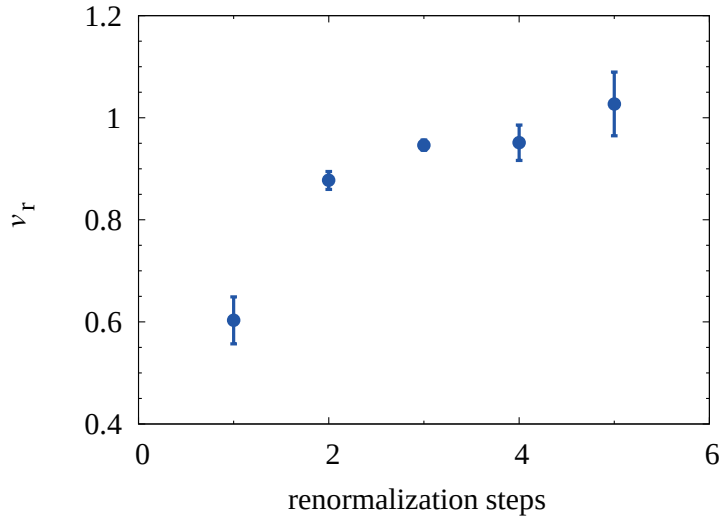

Figure 4.9: Running exponent ν_r calculated by Eq. (4.48) in the random ferromagnetic Ising model in a transverse field in three dimensions.

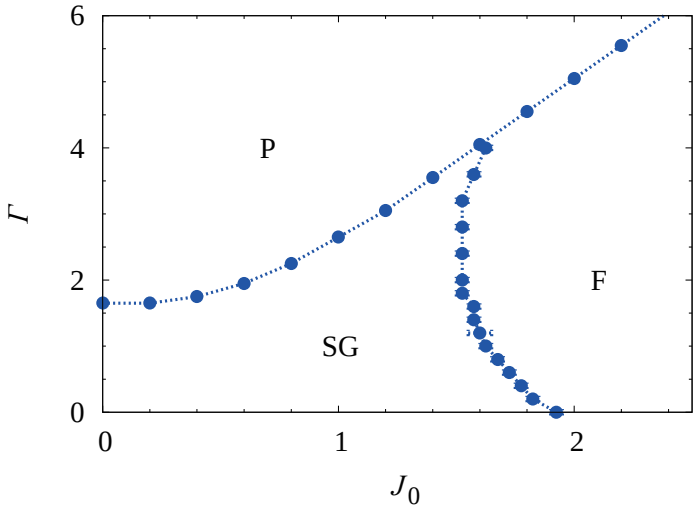

Figure 4.10: Phase diagram of the three-dimensional spin glass in a transverse field. The horizontal axis J_0 expresses the average of the Gaussian distribution of couplings J_{ij}, and the vertical axis expresses the magnitude of the transverse field Γ. The symbols, P, SG, and F, denote the paramagnetic, spin glass, and ferromagnetic phases, respectively.

4.3.3 Spin glass in three dimensions

Let us apply our renormalization-group scheme to the Ising spin glass in a transverse field on a cubic lattice. As in the case of the square lattice, we use the Gaussian distribution

$$P(J_{ij}) = \frac{1}{\sqrt{2\pi}} \exp\left[-\frac{(J_{ij} - J_0)^2}{2} \right], \tag{4.50}$$

and control the average J_0 of the distribution and the uniform transverse field Γ.

We first draw phase boundaries under the same rule as in two dimensions, but phases are determined after five transformations in three dimensions. The resulting boundaries are depicted in Fig. 4.10. It is remarkable that our simple renormalization-group method verifies the existence of the spin glass phase.

Next, critical properties are investigated. Specifically, we treat the critical point for $J_0 = 0$. The existence of an infinite-randomness fixed point is confirmed by the observation of the change of $\sqrt{V}$ through the renormalization-group transformations (Fig. 4.11). The running exponent $\nu_{\rm r}$ is also calculated to obtain the critical exponent ν. We use the average of Δ^i for the initial transverse fields $\Gamma = 1.613$ and 1.612 as Δ_c^i. A plateau is clearly recognized in the result of $\Gamma = 1.619$ (Fig. 4.12), and we determine ν by the values of $\nu_{\rm r}$ on the plateau (from 2 to 4 in the horizontal axis),

$$\nu = 0.94(3). \tag{4.51}$$

This value is close to that of the random ferromagnetic model in three dimensions [Eq. (4.49)].

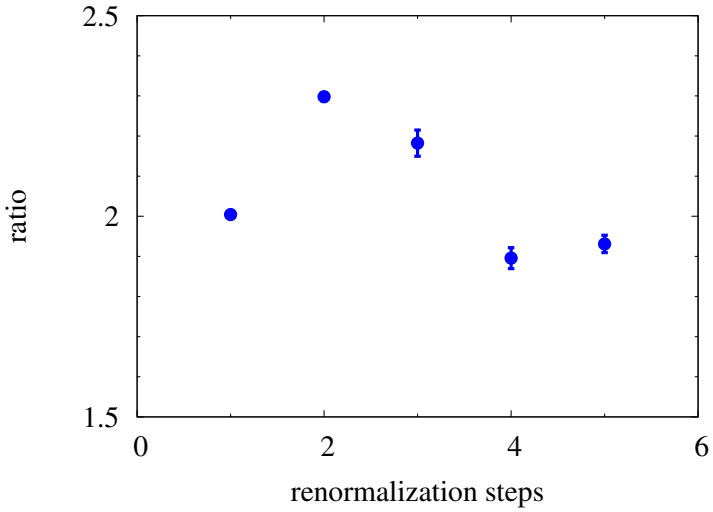

Figure 4.11: Ratio of the square root of variance of $(\log\Gamma - \log J)$ after a renormalization to that before the renormalization in the three-dimensional spin glass in a transverse field with $\Gamma = 1.619$.

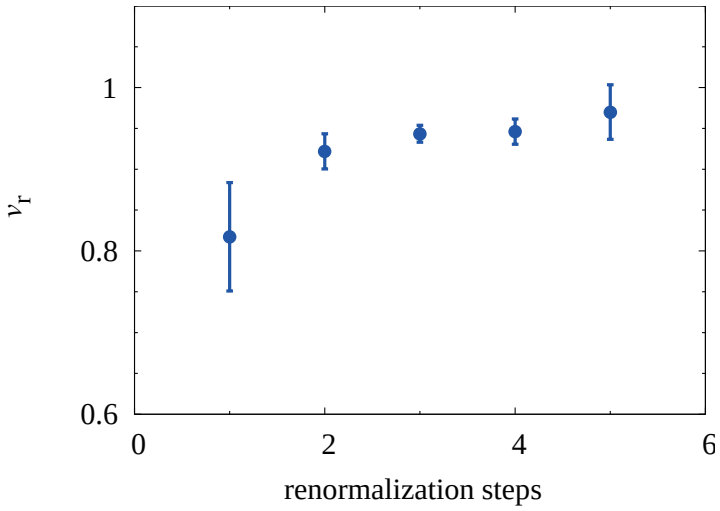

Figure 4.12: Running exponent ν_r calculated from Eq. (4.48) in the three-dimensional spin glass in a transverse field with $\Gamma = 1.619$.

4.4 Summary

We have studied the random transverse-field Ising models in finite dimensions by the real-space renormalization-group method introduced in Chaps. 2 and 3. Our method reproduces exact results for the transition point and critical exponent ν in one dimension in spite of the existence of randomness. Moreover, our generalization of the method to higher dimensions has been shown to be effective not only in the pure model but also in the random model. In fact, we have obtained the values of the critical exponent ν in the two- and three-dimensional random ferromagnetic Ising models in a transverse field close to those from the strong-disorder renormalization-group approach [67–69].

Most remarkable results in our study concern two- and three-dimensional spin glasses in transverse fields. It should be emphasized that this is the first study, to the best of our knowledge, the phase diagrams have been drawn, if qualitatively, for the finite-dimensional spin glasses in transverse fields by analytical methods. In particular, the existence of a spin-glass phase has been confirmed. Also, we have established the existence of infinite-randomness fixed points from indefinite amplifications of the distribution of parameters in a logarithmic scale. This observation supports the conjecture inferred from the case of random ferromagnet under strong-disorder renormalization group [5] but is in conflict with a relatively old numerical study [83]. Furthermore, the estimated exponent ν in spin glasses in transverse fields is very close to that of the corresponding random ferromagnet. Thus, one may expect that these models belong to the same universality class. This is also a highly non-trivial result, since the two investigations in the random ferromagnet and the spin glass have been done on the different phase transitions, namely the transitions between the paramagnetic and ferromagnetic phase in the random ferromagnet and between the paramagnetic and spin-glass phases in the spin glass. However, further investigations are needed to settle this issue because we have to establish the quantitative reliability of the method developed here.

Chapter 5

Real-space renormalization-group analysis of the transverse-field Ising model with the hierarchical interaction

This chapter studies the transverse-field Ising chains with hierarchical interactions. This study is intended to research the systems with interactions showing the power-law decay, that is, $J_{ij} \propto r_{ij}^{-\alpha}$ with distance of an interacting pair r_{ij}. The power-law interaction is found in a compound $LiHo_xY_{1-x}F_4$ [33–36], which is related to the transverse-field Ising model [29–32]. In addition to this fact, the study in this chapter is motivated by the conjecture [84] that Ising spin glass in a transverse field with the power-law interaction has an infinite-randomness fixed point.

The relationship between the power-law interaction and hierarchical interaction is explained in Sec. 5.1. This section surveys previously known results [84, 88] of the transverse-field Ising models with the power-law interaction, after giving motivation to tackle this topic. In Sec. 5.2 we analyze the transverse-field Ising chain with the hierarchical interaction by means of the real-space renormalization-group method developed in previous chapters. The corresponding hierarchical spin-glass model is analyzed in Sec. 5.3. We summarize our findings in Sec. 5.4. The two sections 5.2 and 5.3 are built on the author's original works, which have not been published yet.

5.1 Power-law interactions and hierarchical interactions

This section outlines the background of the subsequent studies. Section 5.1.1 discusses the relation between the power-law interaction and our interest. This subsection also remarks on the range of interaction where we study. Section 5.1.2 reviews the transverse-field Ising model with the power-law interaction. The corresponding spin-glass model is reviewed in Sec. 5.1.3, and we mention the conjecture which is one of the goals in this chapter. Section 5.1.4 introduces the hierarchical interaction.

5.1.1 Power-law interactions

Power-law interactions, which behave like $r^{-\alpha}$ for spatial distance r of an interacting pair, are ubiquitous: gravitational systems, charged systems, dipolar systems, two-dimensional elasticity, etc. For our interest, it is quite significant that electrons are governed by a power-law interaction. Since the exchange interaction of spins, one of the origins of magnetism, is derived from Coulomb's law (and the antisymmetry in fermions) [106], it is natural to include the power-law interaction in our subject. However, usually, only the nearest-neighbor interactions are considered. We have studied them in the previous chapters accordingly. Screening effects by other electrons give the validity of this rough treatment. We nevertheless cannot ignore the power-law interaction, since it is especially related to our studies. As mentioned in Sec. 1.3.2, the random transverse-field Ising model is realized in $LiHo_xY_{1-x}F_4$ to a good approximation [29–32], where the dipolar interaction written in Eq. (1.17) dominates [33–36]. In addition, the Ruderman-Kittel-Kasuya-Yosida (RKKY) interaction [78–80], which is one of the representative mechanisms in spin glasses [76,77], is a kind of the power-law interaction as seen in Eq. (1.33). Consideration of the power-law interaction is thus an essential issue in the field of random quantum spin systems.

We would remark on the term *long range*. One of the definitions of this term is used for the case $\alpha \leq d$ [107] with the exponent of the power law α and the spatial dimensionality d. The exponent α should not be confused with the critical exponent α for specific heat. The reason for the definition is that the system is not extensive in the region. Imagine a particle interacting with other particles homogeneously distributed. If interactions are given via a potential $V(r) = r^{-\alpha}$, the contribution to the energy ε of this particle from other particles in radius R is

$$\varepsilon = \int_{\delta}^{R} d^d r \frac{1}{r^\alpha} \propto \begin{cases} R^{d-\alpha} - \delta^{d-\alpha}, & \text{if } \alpha \neq d, \\ \log \frac{R}{\delta}, & \text{if } \alpha = d, \end{cases} \tag{5.1}$$

where the contribution from neighborhoods of radius δ is excluded, since it is not concerned with the long-range nature. If $\alpha \leq d$, the energy of one particle diverges in the infinite-volume limit, which implies the violation of extensivity. A lot of interesting (or pathological) problems in long-range interacting systems have been extensively discussed [107]. For example, negative specific heat [108] and ensemble inequivalence [109] have been found. We do not go into this region hereafter. We use the term *long range* not in the context explained above.

5.1.2 Transverse-field Ising model with the power-law interaction

We have investigated the transverse-field Ising models in the previous chapters. Let us accordingly consider the transverse-field Ising models with the power-law interaction. First, we look at the pure model,

$$H = -\sum_{i,j} \frac{J}{r_{ij}^\alpha} \sigma_i^z \sigma_j^z - \Gamma \sum_i \sigma_i^x. \tag{5.2}$$

This model has been studied by using the ϕ^4 model [88]. In particular, the mean-field theory, which is yielded by the Gaussian model, has been developed. The Gaussian model is obtained by ignoring the terms ϕ^4 in the ϕ^4 model. In the manner in Sec. 2.2, where we reviewed the Gaussian model derived from the transverse-field Ising model, only the terms bilinear in $\hat{s}_{\omega,\boldsymbol{q}}$ in effective Hamiltonian are kept in the Gaussian model. We review some previously known results [88] below.

As reviewed in Sec.2.2, critical exponents of the mean-field theory are extracted from the coefficients of the bilinear terms, namely $u_2(\omega, \boldsymbol{q})$ written in Eq. (2.60) in the case of the transverse-field Ising model. If the system has the power-law interaction represented as $J(R) = R^{-d-\alpha'}$, where $\boldsymbol{R}$ denotes a spatial vector in d dimensions and $\alpha' = \alpha - d$, we have

$$\hat{J}(\boldsymbol{q}) = \hat{J}(0) - jq^2 + Aq^{\alpha'} + O(q^4). \tag{5.3}$$

and

$$u_2(\omega, \boldsymbol{q}) = \frac{1}{4\Gamma j}\omega^2 + \frac{1}{j}[\Gamma - \hat{J}(0)] + q^2 + Aq^{\alpha'} + O(q^4) \tag{5.4}$$

at zero temperature. These equations show $\hat{J}_{\text{n.a.}}(\boldsymbol{q}) = Aq^{\alpha'}$ with some coefficient A, whereas the term $\hat{J}_{\text{n.a.}}(\boldsymbol{q})$ vanishes in the case of the short-range interaction. The rescaling performed in Sec. 2.2 leads to

$$A' = b^{-d'-2x_s-\alpha'}A, \tag{5.5}$$

Where $d' = d + z$ with $\omega' = b^z\omega$. If we normalize the coefficient of q^2 to be unity, we have $x_s = -(d'+2)/2$ given by Eq. (2.64), and then,

$$A' = b^{2-\alpha'}A. \tag{5.6}$$

Hence, in the mean-field picture, the long-range interaction is relevant in the sense of renormalization group only in $\alpha' < 2$. This statement means that if $\alpha' < 2$, we can find the characteristic behavior of the power-law interaction in critical phenomena. If $\alpha' > 2$, critical phenomena appear in the standard short-range fashion. The boundary $\alpha' = 2$ is a special point, where the Kosterlitz-Thouless (KT) transition [110] occurs. We do not further mention the KT type behavior.

If we normalize the coefficient of $q^{\alpha'}$ to be unity instead of q^2, we have $x_s = -(d' + \alpha')/2$, and then, in the rescaling process, the coefficient of q^2 becomes $b^{\alpha'-2}$, which shows that the short-range interaction is irrelevant if $\alpha' < 2$. Hence, the normalization of the coefficient of $q^{\alpha'}$ is appropriate for the case $\alpha' < 2$. We then have

$$r' = b^{\alpha'}r, \quad h' = b^{(\alpha'+d')/2}h, \tag{5.7}$$

where r here denotes a transverse field and h is a longitudinal field. These relations lead to $y_\Gamma = \alpha'$ and $y_h = (\alpha' + d')/2$. Thus, the mean-field values of critical exponents in the long-range regime ($\alpha' < 2$) are given as

$$\gamma = 1, \quad \nu = \frac{1}{\alpha'}, \quad \eta = 2 - \alpha', \quad z = \frac{\alpha'}{2}, \tag{5.8}$$

where z is determined by the normalization of the coefficient of ω'^2 to be unity as in Sec. 2.2.2. These exponents depend on α'. The limit $\alpha' \to 2$ yields the mean-field values in the short-range regime.

The upper critical dimension d_u has also been deduced. The mean-field values (calculated with the Gaussian model) of critical exponents are valid in larger-dimensional systems than d_u. At or below d_u the hyperscaling relation $2 - \alpha = \nu d'$ is found. With the mean-field values, the relation is expressed as

$$2 - \alpha = \frac{1}{\alpha'}\left(d + \frac{\alpha'}{2}\right), \tag{5.9}$$

where we should not confuse the critical exponent α with the exponent of the power-law α'. Demanding $\alpha = 0$ at d_u, we obtain

$$d_u = \frac{3\alpha'}{2}, \tag{5.10}$$

which is rewritten for the upper critical range of interaction α'_u in a given dimension as

$$\alpha'_u = \frac{2d}{3}. \tag{5.11}$$

The schematic diagram of the critical behavior in the α'–d plane is shown in Fig. 5.1 (a). The boundary of short-range behavior $\alpha' = 2$ provides $d_u = 3$. This value reproduces the well known upper critical dimension of the classical Ising system [1] with the fact that the d dimensional transverse-field Ising system is mapped onto the $d + 1$ dimensional classical Ising system.

The mean-field values of critical exponents in the long-range regime ($\alpha' < 2$) are valid in the spatial dimension $d > d_u = 3\alpha'/2$. The nontrivial exponents below d_u have been evaluated with a perturbative expansion. For example, the exponent for the correlation length is

$$\nu = \frac{1}{\alpha'} + \frac{\epsilon}{3} = \frac{1}{\alpha'} + \frac{\Delta\alpha'}{2}, \tag{5.12}$$

where $\epsilon = d_u - d$ for fixed α' and $\Delta\alpha' = \alpha' - \alpha'_u$ for fixed d are perturbative parameters. We will also evaluate the exponent ν later with our real-space renormalization-group method.

5.1.3 Ising spin glass in a transverse field with the power-law interaction

We next review Ising spin glass in a transverse field with the power-law interaction [84] written as

$$H = -\sum_{i,j} \frac{J_{ij}}{r_{ij}^{\alpha/2}} \sigma_i^z \sigma_j^z - \Gamma \sum_i \sigma_i^x, \tag{5.13}$$

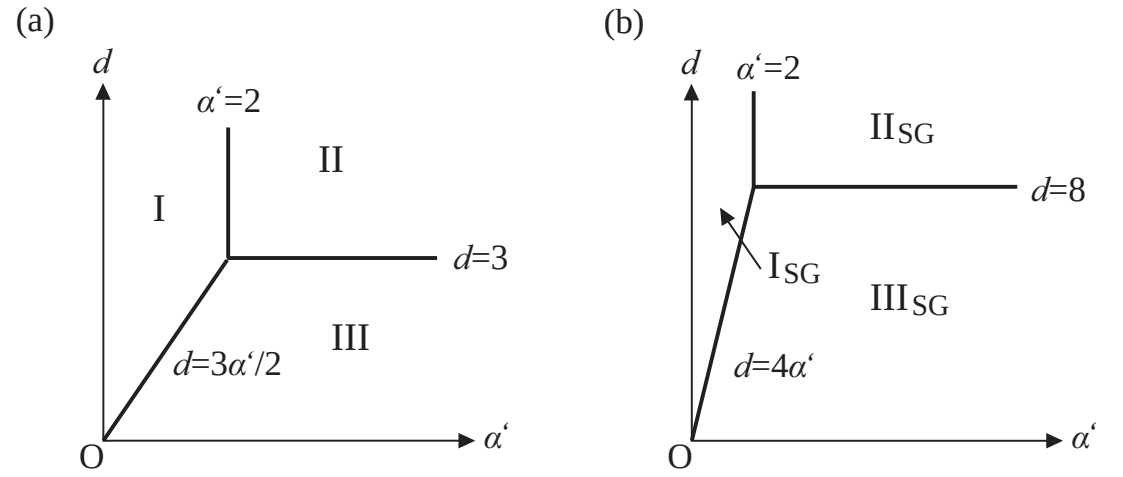

Figure 5.1: Schematic diagram of the critical behavior in the α'–d plane of (a) the transverse-field Ising model with the power-law interaction and (b) the Ising spin glass in a transverse field with the power-law interaction. (a) Critical phenomena in the pure model exhibit the long-range mean-field fashion in the region I, and the short-range mean-field fashion in the region II. The term "mean-field" implies the fixed point of the Gaussian model. Nontrivial critical phenomena occur in the region III. (b) Similarly, in the spin-glass model, $\mathrm{I_{SG}}$ and $\mathrm{II_{SG}}$ denote the regions for the long-range mean-field fashion and the short-range mean-field fashion, respectively. Critical phenomena in the region $\mathrm{III_{SG}}$ are considered to be governed by an infinite-randomness fixed point [84].

where random variables J_{ij} are assumed to be taken from the Gaussian distribution $P(J_{ij}) = \exp(-J_{ij}^2/2)/\sqrt{2\pi}$ with zero mean and standard deviation unity. The model without the transverse field has also received wide attention [111–114].

The power of interaction is defined as $\alpha/2$ instead of α, which makes the variance of interaction $\int dJ_{ij} P(J_{ij})[J_{ij}/r^{-\alpha/2}]^2$ fall off as $r^{-\alpha}$. The extensivity of the system is kept in $\alpha > d$. This fact is explicitly seen in the free energy via the replica method [115], which is one of the standard analytical tools in spin glasses. The main goal of investigations of spin glasses is to calculate the average of free energy with the random interactions J_{ij}. Since the form of the free energy $\log Z$ with the partition function Z is awkward to estimate its average, we deal with Z^n instead. The two functions $\log Z$ and Z^n are connected by a simple formula,

$$\log Z = \lim_{n\to 0} \frac{Z^n - 1}{n}. \tag{5.14}$$

This strategy is called the replica method [77], where we deal with the n replicated systems. With inverse temperature β, we have

$$[Z(\beta)]^n = \left[\mathrm{Tr} \exp\left(\beta \sum_{i,j} \frac{J_{ij}}{r_{ij}^{\alpha/2}} \sigma_i^z \sigma_j^z + \beta\Gamma \sum_i \sigma_i^x \right) \right]^n \tag{5.15}$$

$$= \mathrm{Tr} \exp\left(\beta \sum_{i,j} \frac{J_{ij}}{r_{ij}^{\alpha/2}} \sum_{a=1}^{n} \sigma_i^{a,z} \sigma_j^{a,z} + \beta\Gamma \sum_i \sum_{a=1}^{n} \sigma_i^{a,x} \right), \tag{5.16}$$

where $\sigma_i^{a,z}$ denotes the z component of a spin on site i in a replica system a. The average of $[Z(\beta)]^n$ is calculated as

$$\int \prod_{i,j} dJ_{ij} P(J_{ij}) [Z(\beta)]^n$$

$$= \int \prod_{i,j} dJ_{ij} \frac{1}{\sqrt{2\pi}} \exp\left(-\frac{J_{ij}^2}{2} \right) \mathrm{Tr} \exp\left(\beta \sum_{i,j} \frac{J_{ij}}{r_{ij}^{\alpha/2}} \sum_{a=1}^{n} \sigma_i^{a,z} \sigma_j^{a,z} + \beta\Gamma \sum_i \sum_{a=1}^{n} \sigma_i^{a,x} \right) \tag{5.17}$$

$$= \mathrm{Tr} \int \prod_{i,j} dJ_{ij} \frac{1}{\sqrt{2\pi}} \exp\left\{ \sum_{i,j} \left[-\frac{1}{2} \left(J_{ij} - \frac{\beta}{r^{\alpha/2}} \sum_{a=1}^{n} \sigma_i^{a,z} \sigma_j^{a,z} \right)^2 + \frac{1}{2} \left(\frac{\beta}{r^{\alpha/2}} \sum_{a=1}^{n} \sigma_i^{a,z} \sigma_j^{a,z} \right)^2 \right] + \beta\Gamma \sum_i \sum_{a=1}^{n} \sigma_i^{a,x} \right\} \tag{5.18}$$

$$= \mathrm{Tr} \exp\left(\frac{\beta^2}{2r^\alpha} \sum_{i,j,a,b} \sigma_i^{a,z} \sigma_j^{a,z} \sigma_i^{b,z} \sigma_j^{b,z} + \beta\Gamma \sum_{i,a} \sigma_i^{a,x} \right). \tag{5.19}$$

The original spin-glass model thus corresponds to the above nonrandom system with the power-law interactions proportional to $r^{-\alpha}$, the extensivity of which is kept in $\alpha > d$.

The boundary of the range of interaction in the model in Eq. (5.13) locates on the same point as in the pure case, α' $(= \alpha - d)$ $= 2$. More specifically, the power-law interaction is relevant only for $\alpha' < 2$. However, the upper critical dimension d_u^{SG} shows a difference,

$$d_u^{\mathrm{SG}} = 4\alpha'. \tag{5.20}$$

The upper critical range of interaction $\alpha_u'^{\mathrm{SG}}$ is equivalently written as

$$\alpha_u'^{\mathrm{SG}} = \frac{d}{4}. \tag{5.21}$$

The mean-field values of critical exponents, which are derived from the Gaussian model, of the long-range regime ($\alpha' < 2$) are

$$\nu = \frac{1}{2\alpha'}, \quad \eta = 2 - \alpha', \quad z = \alpha'. \tag{5.22}$$

These relations have been derived in the same spirit as in the pure case, with more complicated calculations [84].

Below the upper critical dimension ($d < d_u^{\mathrm{SG}}$ or $\alpha' > \alpha_u'^{\mathrm{SG}}$), no stable fixed point has been found with a perturbative analysis. The simplest conjecture [84] has been stated that the critical fixed point in this region is an infinite-randomness fixed point. We find the schematic diagram of the critical behavior including the conjecture in Fig. 5.1 (b). Although the statement is only a guess, it appears reasonable because of the actual result that the presence of the infinite-randomness fixed point has been reported in several low-dimensional random quantum spin systems with short-range (the nearest-neighbor) interactions [5, 19, 20, 38, 39, 47–52, 54–56, 60–62, 64–69]. Our study in this chapter is intended to examine this conjecture.

5.1.4 Dyson's hierarchical model

Let us focus on a study on magnetism with the power-law interaction done by Dyson [116], where the hierarchical interaction was introduced. He has studied a one-dimensional Ising ferromagnet with a Hamiltonian $H = -\sum_{i>j} J(i-j)S_iS_j$, where $J(i-j)$ denotes a coupling constant between spins i and j. Concerning the case $J(r) = r^{-\alpha}$, he has rigorously proved that the model has a phase transition at a finite temperature if $1 < \alpha < 2$. This is one of the examples that shows a difference in macroscopic properties, generated by long-range interactions. The model only with the nearest-neighbor interaction has no phase transition at any finite temperature [1].

To prove the occurrence of a phase transition, he has introduced a model with hierarchical interactions represented as

$$\begin{aligned} H =& -J(\sigma_1^z\sigma_2^z + \sigma_3^z\sigma_4^z + \cdots + \sigma_{2^N-1}^z\sigma_{2^N}^z) \\ & - J\delta[(\sigma_1^z+\sigma_2^z)(\sigma_3^z+\sigma_4^z) + (\sigma_5^z+\sigma_6^z)(\sigma_7^z+\sigma_8^z) + \cdots] \\ & - J\delta^2[(\sigma_1^z+\sigma_2^z+\sigma_3^z+\sigma_4^z)(\sigma_5^z+\sigma_6^z+\sigma_7^z+\sigma_8^z) + \cdots] \\ & \cdots \end{aligned} \tag{5.23}$$

$$= -J\sum_{n=1}^{N}\delta^{n-1}\sum_{m=1}^{2^{N-n}} S_{n,2m-1}S_{n,2m}, \tag{5.24}$$

$$S_{n,m} = \sum_{i=(m-1)2^{n-1}+1}^{m2^{n-1}} \sigma_i^z, \tag{5.25}$$

where σ_i^z is the Ising variable on site i. To be precise, the definition of the hierarchical model in Eq. (5.24) is not exactly the same as Dyson's model [116]. However, the same hierarchical structure in couplings, which is the main feature of this model, is correctly shared. The hierarchical structure is depicted in Fig. 5.2. As written in Eq. (5.25), $S_{n,m}$ is a set of 2^{n-1} consecutive spins. Index n indicates the size of a block and m is for the label of a block. Interactions between these blocks constitute the model. Ferromagnetic interactions $J > 0$ are assumed and the number of spins is 2^N.

The parameter δ is introduced so that the strength of a coupling $J\delta^{n-1}$ decays as the size of interacting blocks 2^{n-1} grows. The value of δ is smaller than 1 accordingly. Roughly speaking, the decay corresponds to the power-law dependence of the strength on the distance of an interacting pair, as depicted in Fig. 5.2. Let us consider a spin, say, spin 1, on the left end in Fig. 5.2, which is a spin on the left end of a block $S_{4,m}$ in general. We assume the distance between this spin and a spin on a right site to be r, where the unit of the distance is defined by the neighboring site. When the strength of couplings of the two spins is denoted by $J(r)$, we have $J(r) = J\delta^{n-1}$ with integer n satisfying $2^{n-1} \le r < 2^n$, that is,

$$J(r) = J\delta^{[\log_2 r]}, \tag{5.26}$$

where $[x]$ is the largest integer less than or equal to x. This equation leads to a relation

$$\delta^{-1}Jr^{\log_2\delta} < J(r) \le Jr^{\log_2\delta}. \tag{5.27}$$

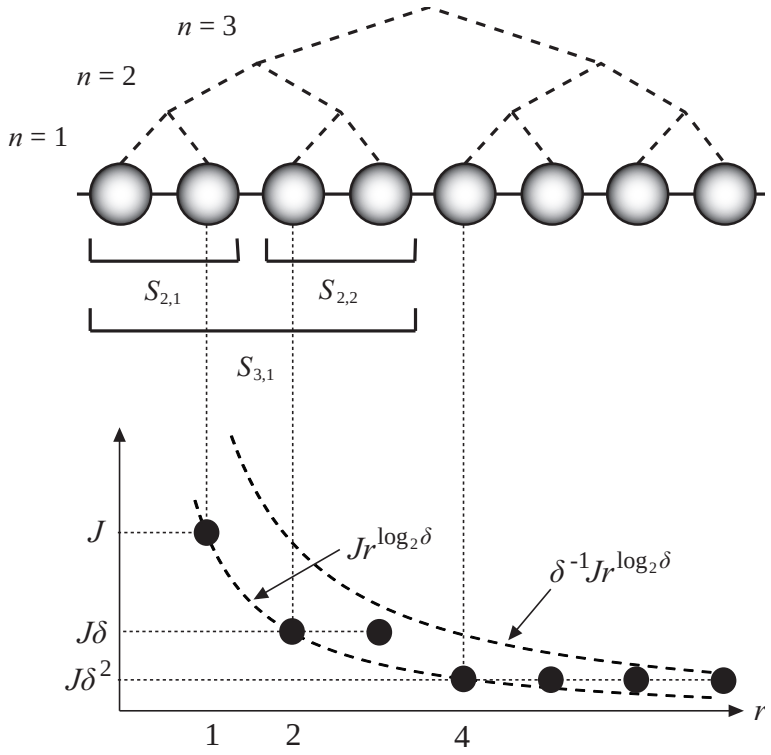

Figure 5.2: Dyson's hierarchical interaction. The dashed lines which links spins (spheres) together express the hierarchical structure, while the solid lines are drawn to emphasize the spatial structure of the model. This example has three layers, that is, $N = 3$. The graph below the spins shows the decay of strength of the interactions. A dot denotes the strengh of interaction between the spin on the left end in the illustration and a spin placed above the dot. The dots are limited to two curves $Jr^{\log_2 \delta}$ and $\delta^{-1} Jr^{\log_2 \delta}$.

With $\alpha = -\log_2 \delta$, we have

$$\delta^{-1} Jr^{-\alpha} < J(r) \leq Jr^{-\alpha}. \tag{5.28}$$

Recall $\delta < 1$, then $\alpha > 0$. Equation (5.28) clearly shows that the interactions in the hierarchical model is close to the power-law interaction.

It is natural to expect the resemblance in interactions leads to similarities in macroscopic properties. Indeed, a phase transition occurs in the hierarchical model if and only if $1 < \alpha < 2$ [116] and the power-law model also exhibits a phase transition if $1 < \alpha < 2$ [116]. This has resulted from the analysis of the hierarchical model and the fact that in any Ising ferromagnet the spontaneous magnetization can only decrease when any coupling is decreased [117]. Moreover, similar critical behavior has been confirmed in the power-law system [118, 119] and the hierarchical system, which shows the close similarity between them especially in the vicinity of a critical point.

Descendants of Dyson's hierarchical model have been utilized also in the analyses of random systems [120–128]. The hierarchical structure is suitable to perform iterative calculations based on renormalization group, which is one of the reasons of the high utility. In subsequent sections, we will use Dyson's hierarchical model in a transverse

field to inspect the conjecture [84] on Ising spin glass in a transverse field with the power-law interaction, that is, the presence of an infinite-randomness fixed point.

5.2 Transverse-field Ising chain with the hierarchical interaction

We consider one-dimensional Dyson's hierarchical models [116] in a transverse field. Our target is the spin glass model, but we first explore the pure model to gain intuition and check the validity of the scheme in the hierarchical structure of interactions. The Hamiltonian of the pure model is written as

$$H = -J \sum_{n=1}^{N} \delta^{n-1} \sum_{m=1}^{2^{N-n}} S_{n,2m-1} S_{n,2m} - \Gamma \sum_{i=1}^{2^N} \sigma_i^x, \tag{5.29}$$

where $S_{n,m}$ is defined as Eq. (5.25), and σ_i is the Pauli matrix on site i. A transverse field Γ is applied. This hierarchical model parallels the power-law interacting model written in Eq. (5.2) with $\alpha = -\log_2 \delta$. We investigate this model only for $\delta < 1/2$, namely $\alpha' \ (= \alpha - 1) > 0$, since we do not study the region in which the system violates the extensivity as discussed in Sec. 5.1.1. Renormalization-group equations are generated in Sec. 5.2.1. A transition point and the critical exponent ν are then obtained as a function of δ. Section 5.2.2 discusses the relation between our method and the extensivity of the system.

5.2.1 Renormalization-group analysis

We apply the renormalization-group scheme [85, 99] developed in previous chapters to the model at zero temperature. We start by dividing the lattice into blocks of two spins as shown in Fig. 5.3. The same intrablock Hamiltonian as in the previous cases is adopted

$$H_i^{\text{intra}} = -J \sigma_{2i-1}^z \sigma_{2i}^z - \Gamma \sigma_{2i-1}^x. \tag{5.30}$$

With this Hamiltonian, we can express the original Hamiltonian as

$$H = \sum_{i=1}^{2^{N-1}} H_i^{\text{intra}} + H^{\text{inter}}, \tag{5.31}$$

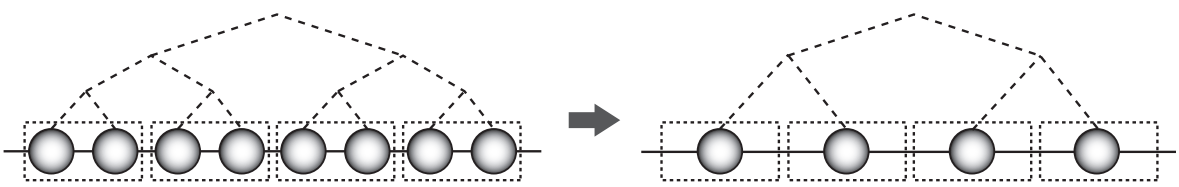

Figure 5.3: Construction of block spins and coarse-grining process in our renormalization-group transformation in the hierarchical model.

$$H^{\rm inter} = -J\sum_{n=2}^{N}\delta^{n-1}\sum_{m=1}^{2^{N-n}} S_{n,2m-1}S_{n,2m} - \Gamma\sum_{i=1}^{2^{N-1}}\sigma_{2i}^{x}. \tag{5.32}$$

Most importantly, this particular block partition, which was also used in the analysis of the transverse-field Ising model with short-range interactions in previous chapters [85, 86, 99], is suited to preserve the form of the Hamiltonian under the renormalization-group transformations.

Since we have adopted the same intrablock Hamiltonian as in the previous cases, the same projector $P = \bigotimes_{i=1}^{2^{N-1}} P_i$ onto the coarse-grained system is generated. Accordingly, renormalized spin operators result in the same form as Eqs. (3.21), (3.27), and (3.33), that is,

$$P_i\left(1_{2i-1}\otimes\sigma_{2i}^{z}\right)P_i = \tilde{\sigma}_i^{z}, \tag{5.33}$$

$$P_i\left(\sigma_{2i-1}^{z}\otimes 1_{2i}\right)P_i = \frac{J}{\sqrt{J^2+\Gamma^2}}\tilde{\sigma}_i^{z}, \tag{5.34}$$

$$P_i\left(1_{2i-1}\otimes\sigma_{2i}^{x}\right)P_i = \frac{\Gamma}{\sqrt{J^2+\Gamma^2}}\tilde{\sigma}_i^{x}, \tag{5.35}$$

where $\tilde{\sigma}_i^{\alpha}$ is the α-component of the Pauli matrix on block i, or new site i in the coarse-grained system. With these relations, $S_{n,m}$ in Eq. (5.32) becomes

$$PS_{n,m}P = P\left[\sum_{i=(m-1)2^{n-2}+1}^{m2^{n-2}}(\sigma_{2i-1}^{z}+\sigma_{2i}^{z})\right]P \tag{5.36}$$

$$= \sum_{i=(m-1)2^{n-2}+1}^{m2^{n-2}}\left(\frac{J}{\sqrt{J^2+\Gamma^2}}+1\right)\tilde{\sigma}_i^{z} \tag{5.37}$$

$$= \left(\frac{J}{\sqrt{J^2+\Gamma^2}}+1\right)\tilde{S}_{n-1,m}. \tag{5.38}$$

Note that the change of $S_{n,m}$ depends on neither n nor m. As a consequence, $H^{\rm inter}$ is renormalized as,

$$PH^{\rm inter}P = -J\sum_{n=2}^{N}\delta^{n-1}\sum_{m=1}^{2^{N-n}}\left(\frac{J}{\sqrt{J^2+\Gamma^2}}+1\right)^2\tilde{S}_{n-1,2m-1}\tilde{S}_{n-1,2m} - \Gamma\sum_{i=1}^{2^{N-1}}\frac{\Gamma}{\sqrt{J^2+\Gamma^2}}\tilde{\sigma}_i^{x} \tag{5.39}$$

$$= -J\sum_{n=1}^{N-1}\delta^{n}\sum_{m=1}^{2^{N-1-n}}\left(\frac{J}{\sqrt{J^2+\Gamma^2}}+1\right)^2\tilde{S}_{n,2m-1}\tilde{S}_{n,2m} - \frac{\Gamma^2}{\sqrt{J^2+\Gamma^2}}\sum_{i=1}^{2^{N-1}}\tilde{\sigma}_i^{x} \tag{5.40}$$

$$= -\tilde{J}\sum_{n=1}^{N-1}\delta^{n-1}\sum_{m=1}^{2^{N-1-n}}\tilde{S}_{n,2m-1}\tilde{S}_{n,2m} - \tilde{\Gamma}\sum_{i=1}^{2^{N-1}}\tilde{\sigma}_i^{x} \tag{5.41}$$

with

$$\tilde{J} = J\delta\left(\frac{J}{\sqrt{J^2+\Gamma^2}}+1\right)^2, \tag{5.42}$$

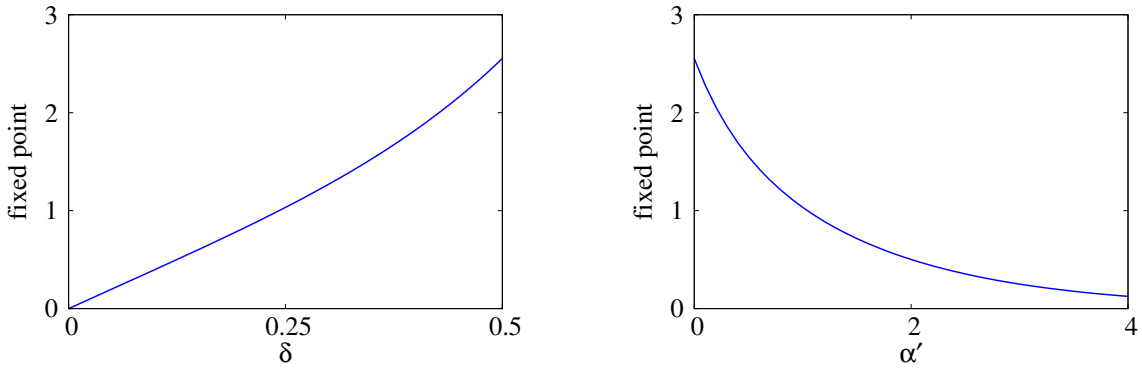

Figure 5.4: Non-trivial fixed point k_c of the renormalization-group equation [Eq. (5.46)]. Note that $\alpha' = -\log_2 \delta - 1$.

$$\tilde{\Gamma} = \frac{\Gamma^2}{\sqrt{J^2 + \Gamma^2}}. \tag{5.43}$$

Hence, the renormalized Hamiltonian is

$$PHP = \sum_{i=1}^{2^{N-1}} \varepsilon^{(1)} 1_i - \tilde{J} \sum_{n=1}^{N-1} \delta^{n-1} \sum_{m=1}^{2^{N-1-n}} \tilde{S}_{n,2m-1} \tilde{S}_{n,2m} - \tilde{\Gamma} \sum_{i=1}^{2^{N-1}} \tilde{\sigma}_i^x, \tag{5.44}$$

with the lowest eigenvalue of the intrablock Hamiltonian

$$\varepsilon^{(1)} = -\sqrt{J^2 + \Gamma^2}. \tag{5.45}$$

Our transformation keeps the form of the Hamiltonian. In particular, it is remarkable that the hierarchical structure in interactions is preserved as depicted in Fig. 5.3.

The renormalization-group equation for a parameter $k = \Gamma/J$ is generated from Eqs. (5.42) and (5.43) as

$$\tilde{k} = \frac{k^2 \sqrt{1 + k^2}}{\delta \left(1 + \sqrt{1 + k^2}\right)^2}. \tag{5.46}$$

This equation has non-trivial fixed points, which correspond to the solutions of a cubic equation,

$$(1 - \delta^2)k^3 - 4\delta k^2 + k - 4\delta = 0. \tag{5.47}$$

Two solutions can be real. When one of the solutions is real, the other is not real. The real solution k_c exists for all values of δ in the range $0 < \delta < 1/2$, shown in Fig. 5.4. The value of k_c grows as δ increases, that is, as the range of interaction extends. This result is reasonable since the longer-range interactions strongly link spins together, and the stronger transverse field (quantum fluctuation) is needed to destroy the order. In addition, our scheme correctly produces a natural consequence that the transition vanishes in the limit $\delta \to 0$, where the whole system consists of isolate two-spin systems.

An eigenvalue y of a linearized renormalization-group transformation close to the non-trivial fixed point k_c is obtained from

$$\tilde{k} - k_c = 2^{y_\Gamma}(k - k_c) + O\left((k - k_c)^2\right), \tag{5.48}$$

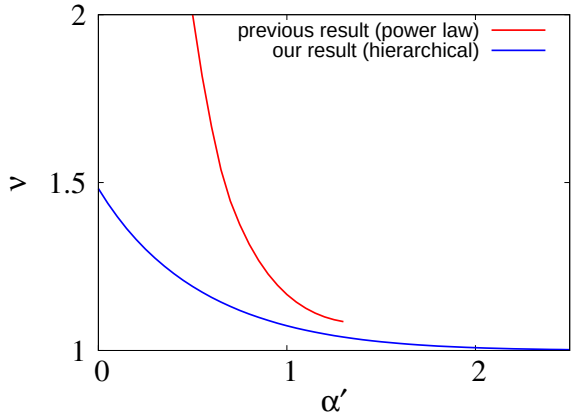

Figure 5.5: Critical exponent ν of the transverse-field Ising chain with the hierarchical interaction (blue) and the power-law interaction (red) [88]. The blue line is derived from Eq. (5.48). The red line expresses $\nu = 1/\alpha'$ if $\alpha' > 2/3$ and $\nu = 1/\alpha' + \Delta\alpha'/2$ with $\Delta\alpha' = \alpha' - 2/3$ if $\alpha' < 2/3$. The red line is drawn in $\alpha' < 4/3$, since the simple expression $\nu = 1/\alpha' + \Delta\alpha'/2$ is reliable only if $\Delta\alpha'$ is small.

where 2 is the scaling factor of this renormalization. This eigenvalue determines the critical exponent $\nu = 1/y_\Gamma$. Resulting values are shown in Fig. 5.5. When α' is small, our values of ν have a large difference from values derived from another approach [88], where the mean-field values of critical exponents in systems with power-law interactions (not Dyson's hierarchical interactions) are obtained by using the Gaussian model. This is an unavoidable deviation because our renormalization-group procedure does not perfectly treat interactions between blocks and hence it is natural that the accuracy of our result deteriorates as long-range interactions become stronger, that is, α' becomes smaller. Our result is expected to produce accurate values when α' is not small. Indeed, for $\alpha' > 2$, our value of ν approaches unity, which is the exact value in the transverse-field Ising chain with the nearest-neighbor interactions.

5.2.2 Constraint on the exponent of power-law

We now estimate the ground-state energy with our renormalization-group procedure. Since the procedure ignores some states of the block Hamiltonians, it cannot exactly calculate the ground-state energy. However, even our rough estimation is useful to the constraint on the range of δ. Our calculation necessarily yields a higher value E_{RG} than the true ground-state energy E, and the values are negative. Hence, when the absolute value of our estimation of the energy per spin diverges, the true energy also diverges, and the range of δ which causes this situation is not suited for a physical situation.

Let us calculate the ground-state energy with our renormalization-group procedure. We first define $J^{(m)}$ and $\Gamma^{(m)}$ as J and Γ renormalized m times, and then

$$J^{(m)} = J^{(m-1)}\delta\left(\frac{J^{(m-1)}}{\sqrt{(J^{(m-1)})^2 + (\Gamma^{(m-1)})^2}} + 1\right)^2, \tag{5.49}$$

$$\Gamma^{(m)} = \frac{(\Gamma^{(m-1)})^2}{\sqrt{(J^{(m-1)})^2 + (\Gamma^{(m-1)})^2}}. \tag{5.50}$$

The energy calculated at the first step of renormalization is the terms of identity operators on the right hand side of Eq. (5.44). iterating the renormalization, we obtain the ground-state energy per spin E_{RG},

$$E_{RG} = -\frac{1}{2^N}\sum_{n=1}^{N} 2^{N-n}\sqrt{(J^{(n-1)})^2 + (\Gamma^{(n-1)})^2}. \tag{5.51}$$

For any value of Γ, E_{RG} should not diverge. Let us consider a case easy to analyze, $\Gamma = 0$. Then $J^{(n-1)}$ is

$$J^{(n-1)} = J^{(n-2)}\delta\ 2^2 \tag{5.52}$$

$$= J\delta^{n-1}2^{2(n-1)}. \tag{5.53}$$

Accordingly, E_{RG} becomes

$$E_{RG} = -\frac{1}{2^N}\sum_{n=1}^{N} 2^{N-n} J\delta^{n-1}\ 2^{2(n-1)} \tag{5.54}$$

$$= -\frac{J}{4\delta}\sum_{n=1}^{N}(2\delta)^n. \tag{5.55}$$

To prevent E_{RG} from diverging, we need a condition

$$\delta < \frac{1}{2}. \tag{5.56}$$

This constraint already has been imposed to keep the extensivity of the system.

5.3 Random transverse-field Ising model with the hierarchical interaction

We dope randomness into interactions in Dyson's hierarchical model in a transverse field represented in Eq. (5.29). We then have a Hamiltonian

$$H = -\sum_{n=1}^{N}\delta^{n-1}\sum_{m=1}^{2^{N-n}}\sum_{i=(2m-2)2^{n-1}+1}^{(2m-1)2^{n-1}}\sum_{j=(2m-1)2^{n-1}+1}^{2m2^{n-1}} J_{ij}\sigma_i^z\sigma_j^z - \Gamma\sum_{i=1}^{2^N}\sigma_i^x. \tag{5.57}$$

This Hamiltonian is complicated, but is simply generated by substituting random variables J_{ij} of couplings between spins i and j for J in the Hamiltonian of the pure model. This hierarchical model parallels the power-law interacting model written in Eq. (5.13) with $\alpha/2 = -\log_2\delta$. We investigate this model only for $\delta < 1/\sqrt{2} \simeq 0.707$, namely $\alpha'\ (= \alpha - 1) > 0$, where the system keeps extensivity. We deduce renormalization-group equations in Sec. 5.3.1 and numerically iterate the transformations in Sec. 5.3.2. Section 5.3.3 discusses results of the spin glass model.

5.3.1 Renormalization-group equations

We apply the renormalization-group method [85, 86] to the random transverse-field Ising model with the hierarchical interactions. We employ the same block partition as for the pure model, and the intrablock and interblock Hamiltonians are thus

$$H_i^{\rm intra} = -J_{2i-1,2i}\sigma_{2i-1}^z\sigma_{2i}^z - \Gamma_{2i-1}\sigma_{2i-1}^x, \tag{5.58}$$

$$H^{\rm inter} = -\sum_{n=2}^{N}\delta^{n-1}\sum_{m=1}^{2^{N-n}}\sum_{i=(2m-2)2^{n-1}+1}^{(2m-1)2^{n-1}}\sum_{j=(2m-1)2^{n-1}+1}^{2m2^{n-1}} J_{ij}\sigma_i^z\sigma_j^z - \sum_{i=1}^{2^{N-1}}\Gamma_{2i}\sigma_{2i}^x. \tag{5.59}$$

The transverse fields are labeled, because their changes through the renormalization-group transformations depend on $J_{2i-1,2i}$. Since the intrablock Hamiltonian is the same one as in the random model only with the nearest-neighbor interactions studied in Chap. 4, we obtain the same renormalized spins with the same projector onto the coarse-grained system,

$$P_i\left(1_{2i-1}\otimes\sigma_{2i}^z\right)P_i = \tilde{\sigma}_i^z, \tag{5.60}$$

$$P_i\left(\sigma_{2i-1}^z\otimes 1_{2i}\right)P_i = \frac{J_{2i-1,2i}}{\sqrt{(J_{2i-1,2i})^2+(\Gamma_{2i-1})^2}}\tilde{\sigma}_i^z, \tag{5.61}$$

$$P_i\left(1_{2i-1}\otimes\sigma_{2i}^x\right)P_i = \frac{\Gamma_{2i-1}}{\sqrt{(J_{2i-1,2i})^2+(\Gamma_{2i-1})^2}}\tilde{\sigma}_i^x, \tag{5.62}$$

where $\tilde{\sigma}_i^\alpha$ is the α-component of the Pauli matrix on block i, or new site i in the coarse-grained system.

Four couplings $\sigma_{2i-1}^z\sigma_{2j-1}^z$, $\sigma_{2i-1}^z\sigma_{2j}^z$, $\sigma_{2i}^z\sigma_{2j-1}^z$, and $\sigma_{2i}^z\sigma_{2j}^z$ in the original Hamiltonian [Eq. (5.57)] turn into a renormalized coupling $\tilde{\sigma}_i^z\tilde{\sigma}_j^z$. This fact is found also in the pure case, and leads to the simple expression written in Eq. (5.38). However, the random case needs more complicated calculations. We should mind which spot a spin sits on in a block. For example, σ_{2i-1}^z sits on the left spot in a block, and is then renormalized as Eq. (5.61), whereas σ_{2i}^z on the right spot is as Eq. (5.60). Hence, the four couplings are renormalized as

$$P\sigma_{2i-1}^z\sigma_{2j-1}^z P = \frac{J_{2i-1,2i}}{\sqrt{(J_{2i-1,2i})^2+(\Gamma_{2i-1})^2}}\frac{J_{2j-1,2j}}{\sqrt{(J_{2j-1,2j})^2+(\Gamma_{2j-1})^2}}\tilde{\sigma}_i^z\tilde{\sigma}_j^z, \tag{5.63}$$

$$P\sigma_{2i-1}^z\sigma_{2j}^z P = \frac{J_{2i-1,2i}}{\sqrt{(J_{2i-1,2i})^2+(\Gamma_{2i-1})^2}}\tilde{\sigma}_i^z\tilde{\sigma}_j^z, \tag{5.64}$$

$$P\sigma_{2i}^z\sigma_{2j-1}^z P = \frac{J_{2j-1,2j}}{\sqrt{(J_{2j-1,2j})^2+(\Gamma_{2j-1})^2}}\tilde{\sigma}_i^z\tilde{\sigma}_j^z, \tag{5.65}$$

$$P\sigma_{2i}^z\sigma_{2j}^z P = \tilde{\sigma}_i^z\tilde{\sigma}_j^z. \tag{5.66}$$

Consequently, we have

$$
\begin{aligned}
&P(J_{2i-1,2j-1}\sigma^z_{2i-1}\sigma^z_{2j-1}+J_{2i-1,2j}\sigma^z_{2i-1}\sigma^z_{2j}+J_{2i,2j-1}\sigma^z_{2i}\sigma^z_{2j-1}+J_{2i,2j}\sigma^z_{2i}\sigma^z_{2j})P\\
&\quad=\Bigg[J_{2i-1,2j-1}\frac{J_{2i-1,2i}}{\sqrt{(J_{2i-1,2i})^2+(\Gamma_{2i-1})^2}}\frac{J_{2j-1,2j}}{\sqrt{(J_{2j-1,2j})^2+(\Gamma_{2j-1})^2}}\\
&\qquad+J_{2i-1,2j}\frac{J_{2i-1,2i}}{\sqrt{(J_{2i-1,2i})^2+(\Gamma_{2i-1})^2}}+J_{2i,2j-1}\frac{J_{2j-1,2j}}{\sqrt{(J_{2j-1,2j})^2+(\Gamma_{2j-1})^2}}+J_{2i,2j}\Bigg]\tilde{\sigma}^z_i\tilde{\sigma}^z_j. \qquad (5.67)\\
&\quad=:\delta^{-1}\tilde{J}_{ij}\tilde{\sigma}^z_i\tilde{\sigma}^z_j. \qquad (5.68)
\end{aligned}
$$

We have defined $\tilde{J}_{ij}$ here, and δ^{-1} has been multiplied for convenience in the next calculation.

Hence, the renormalized interblock Hamiltonian is calculated as

$$
\begin{aligned}
&PH^{\text{inter}}P\\
&\quad=-\sum_{n=2}^{N}\delta^{n-1}\sum_{m=1}^{2^{N-n}}\sum_{i=(2m-2)2^{n-1}+1}^{(2m-1)2^{n-1}}\sum_{j=(2m-1)2^{n-1}+1}^{2m2^{n-1}}PJ_{ij}\sigma^z_i\sigma^z_jP-\sum_{i=1}^{2^{N-1}}\Gamma_{2i}P\sigma^x_{2i}P \qquad (5.69)\\
&\quad=-\sum_{n=2}^{N}\delta^{n-1}\sum_{m=1}^{2^{N-n}}\sum_{i=(2m-2)2^{n-2}+1}^{(2m-1)2^{n-2}}\sum_{j=(2m-1)2^{n-2}+1}^{2m2^{n-2}}P(J_{2i-1,2j-1}\sigma^z_{2i-1}\sigma^z_{2j-1}\\
&\qquad\qquad+J_{2i-1,2j}\sigma^z_{2i-1}\sigma^z_{2j}+J_{2i,2j-1}\sigma^z_{2i}\sigma^z_{2j-1}+J_{2i,2j}\sigma^z_{2i}\sigma^z_{2j})P \qquad (5.70)\\
&\qquad-\sum_{i=1}^{2^{N-1}}\Gamma_{2i}P\sigma^x_{2i}P\\
&\quad=-\sum_{n=2}^{N}\delta^{n-1}\sum_{m=1}^{2^{N-n}}\sum_{i=(2m-2)2^{n-2}+1}^{(2m-1)2^{n-2}}\sum_{j=(2m-1)2^{n-2}+1}^{2m2^{n-2}}\delta^{-1}\tilde{J}_{ij}\tilde{\sigma}^z_i\tilde{\sigma}^z_j-\sum_{i=1}^{2^{N-1}}\tilde{\Gamma}_i\tilde{\sigma}^x_i \qquad (5.71)\\
&\quad=-\sum_{n=1}^{N-1}\delta^{n-1}\sum_{m=1}^{2^{N-n}}\sum_{i=(2m-2)2^{n-1}+1}^{(2m-1)2^{n-1}}\sum_{j=(2m-1)2^{n-1}+1}^{2m2^{n-1}}\tilde{J}_{ij}\tilde{\sigma}^z_i\tilde{\sigma}^z_j-\sum_{i=1}^{2^{N-1}}\tilde{\Gamma}_i\tilde{\sigma}^x_i, \qquad (5.72)
\end{aligned}
$$

where

$$
\begin{aligned}
\tilde{J}_{ij}=\delta\Bigg[&J_{2i-1,2j-1}\frac{J_{2i-1,2i}}{\sqrt{(J_{2i-1,2i})^2+(\Gamma_{2i-1})^2}}\frac{J_{2j-1,2j}}{\sqrt{(J_{2j-1,2j})^2+(\Gamma_{2j-1})^2}}\\
&+J_{2i-1,2j}\frac{J_{2i-1,2i}}{\sqrt{(J_{2i-1,2i})^2+(\Gamma_{2i-1})^2}}+J_{2i,2j-1}\frac{J_{2j-1,2j}}{\sqrt{(J_{2j-1,2j})^2+(\Gamma_{2j-1})^2}}+J_{2i,2j}\Bigg], \qquad (5.73)
\end{aligned}
$$

$$
\tilde{\Gamma}_i=\frac{\Gamma_{2i-1}\Gamma_{2i}}{\sqrt{(J_{2i-1,2i})^2+(\Gamma_{2i-1})^2}}. \qquad (5.74)
$$

Since the renormalization process changes the intrablock Hamiltonian into an identity operator, the resulting interblock Hamiltonian in Eq. (5.72) shows that the form of the

whole Hamiltonian is preserved through our renormalization-group transformations as in previous cases. Equations (5.73) and (5.74) form renormalization-group equations. When interactions and fields take constant values J and Γ, the above relations reproduce the results in the pure case [Eqs. (5.41)–(5.43)].

5.3.2 Numerical implementation

We extract the nature of phase transitions and critical phenomena in the model from Eqs. (5.73) and (5.74). Since it is too difficult to analytically investigate the two equations, we numerically iterate them. Simply performing the renormalization-group iteration, size of the system becomes smaller and smaller. Thus, after several steps of the process, we cannot obtain statistics of the parameters in the large system. This fact causes a serious problem in our investigation, since to search for an infinite-randomness fixed point, we need to examine the variance of the logarithm of parameters.

To get around the difficulty, let us make use of a similar method to one introduced in Chap. 4. We arrange parameters J_{ij} and Γ_i of a hierarchical system of 2^N spins described as Eq. (5.57). Although Eq. (5.57) indicates a uniform field, we here assume nonuniform fields, which are necessarily generated after the first renormalization. In addition, we prepare J_{ii}, which do not exist in the real system. This imaginary interactions are defined for convenience in subsequent calculations discussed in the next paragraph. Executing the renormalization-group transformation according to Eqs. (5.73) and (5.74), we obtain renormalized interactions and fields. Note that imaginary interactions J_{ii} yield imaginary renormalized interactions $\tilde{J}_{ii}$. This process reduces the system size, or the number of parameters, by half. Specifically, the number of spins is 2^{N-1} at the present. To retain the size, we replenish interactions and fields with the copy of the renormalized parameters.

First, we produce a copy of the renormalized system and combine it with the original renormalized system by connecting the tops of the trees of the hierarchical structure of interactions as depicted in Fig. 5.6. We now label copied spins as $2^{N-1}+1$, $2^{N-2}+2$, $\ldots$, 2^N. The combining procedure generates new couplings between spins separated by the root node. We determine values of the new couplings as $\tilde{J}_{i,2^{N-1}+j} := \tilde{J}_{i,j}$. The imaginary interactions have been defined to determine $\tilde{J}_{i,2^{N-1}+i}$ under this rule. The copy and the new interactions do not disturb distributions of interactions $\tilde{J}_{ij}$ and fields $\tilde{\Gamma}_i$, since they have the same distributions as the original ones.

Next, we shuffle the positions of spins only in the copy, namely spins $2^{N-1}+1$,

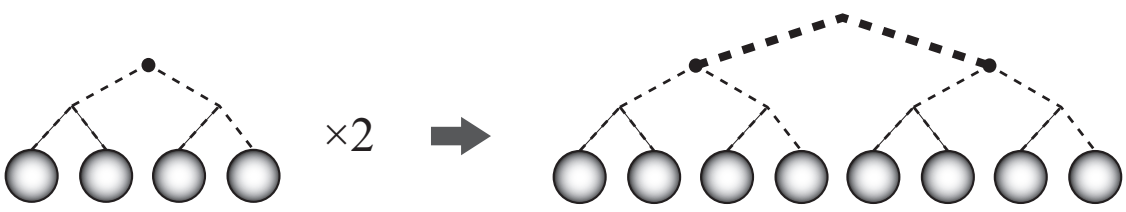

Figure 5.6: Connection of the original renormalized system and its copy. The thick dashed line links the root node (dot) of the original system to that of its copy.

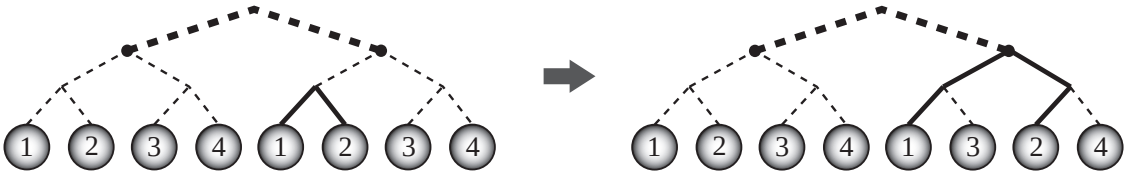

Figure 5.7: Shuffling procedure in the numerical implementation of the renormalization-group transformations in the hierarchical model. For simplicity, we label spins in a copy as 1, 2, ..., while they are redefine $2^{N-1}+1$, $2^{N-1}+2$, ... in the text. This example interchanges spin 2 and spin 3 in a copy. The solid lines denote the interaction between spin 1 and spin 2. The interaction before the shuffling procedure is $\tilde{J}_{1,2}$ and after is $\delta\tilde{J}_{1,2}$.

$2^{N-2}+2, \ldots, 2^N$ illustrated in Fig. 5.7. In the shuffling procedure, we preserve couplings $\tilde{J}_{ij}$ between spins i and j as well as fields Γ_i. Even if spins i and j move onto other sites, their coupling remains $\tilde{J}_{ij}$. This treatment takes into account the following fact. As seen in Eqs. (5.73) and (5.74), renormalized parameters are correlated with other renormalized parameters. Furthermore, the correlations are not local, which results from the all-connected structure of interactions. We preserve the relationship accordingly even in the shuffling procedure. This procedure, however, changes distances between spins. For example, if spin $2^{N-1}+2$ moves onto site $2^{N-1}+3$ whereas spin $2^{N-1}+1$ remains on site $2^{N-1}+1$ after the shuffling, the interaction between the two spins including the spatial dependence changes as $\tilde{J}_{2^{N-1}+1,2^{N-1}+2} \to \delta\tilde{J}_{2^{N-1}+1,2^{N-1}+2}$. One of the merits of the shuffling procedure is that this change does not violate our coarse-graining rule. In other words, the system provided by the shuffling procedure can be created by our renormalization-group transformation with an appropriate setting of original parameters. Concretely speaking, the system provided by the shuffling procedure after the renormalization-group transformation is equivalent to the system provided by the renormalization-group transformation after the corresponding shuffling procedure. This relationship is illustrated in Fig. 5.8. The shuffling procedure builds another possible system without another renormalization-group calculation.

The above two steps restore the system size without disturbing distributions of interactions J_{ij} and fields Γ_i. Although we use just a copy of the original renormalized system, the shuffling procedure provides a different system. This fact affects the next renormalization-group transformation. The shuffled positions of spins in a half of the system lead to different intrablock Hamiltonians and different resulting projectors onto the renormalized system.

5.3.3 Spin glass

We analyze a spin glass in a transverse field with hierarchical couplings by means of the renormalization-group method. We focus on whether the system has an infinite-randomness fixed point. In particular, the system with short-range interactions (small δ) is an important subject, since the system with short-range power-law interactions has been conjectured to have an infinite-randomness fixed point. Thus, we especially

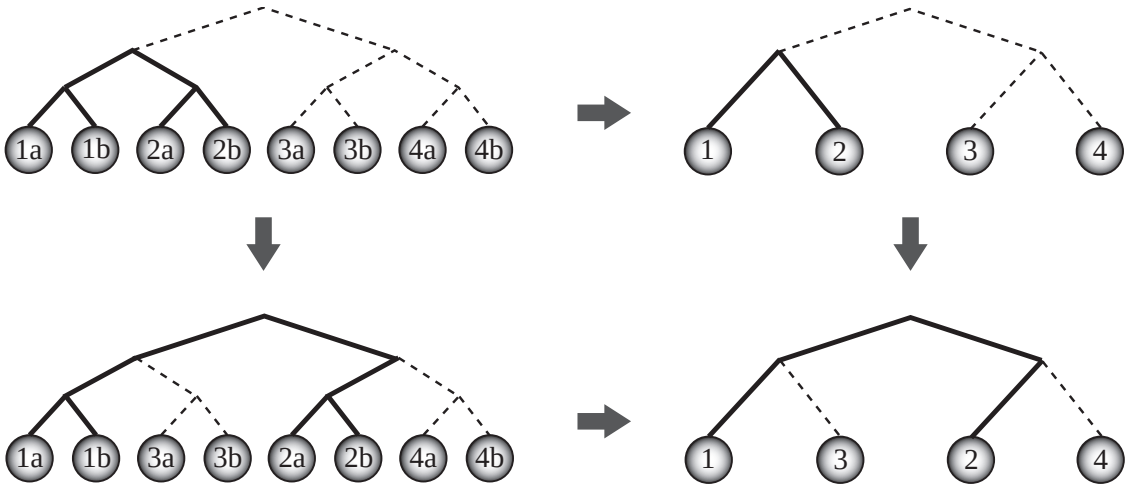

Figure 5.8: Equivalence between two schemes. We leave the system depicted at the upper left for the system at the lower right. Arrows pointing to the right express the renormalization-group transformation, and to the down, the shuffling procedure. We have two routes to the goal. The two schemes can provide the same system accordingly.

pay attention to how the critical phenomenon changes as we control δ.

The original interactions J_{ij} have been taken from the Gaussian distribution

$$P(J_{ij}) = \frac{1}{2\pi} \exp\left(-\frac{J_{ij}^2}{2} \right) \tag{5.75}$$

with zero mean and standard deviation unity. The original field is assumed to be uniform and set to be a constant value Γ. Repeating the scheme developed above, we observe the change of parameters. In our numerical calculations, the original system size has been set equal to 512, or $N = 9$, and 1000 samples are run.

We determine the critical point in terms of the parameter $(\log \Gamma - \log J)$ as in the previous cases. If the average of $(\log \Gamma - \log J)$, which is denoted by Δ, after 20 times of the renormalization-group transformation is larger than the initial value of Δ, we conclude the system to be in the paramagnetic phase. Otherwise, the system is regarded to be in an ordered phase. The ordered phase is expected to be the spin-glass phase, since the initial distribution of couplings has no finite average. We are now interested in the transition and do not further investigate the phase itself. The estimations are implemented in the systems with $\delta = 0.1, 0.2, \ldots, 0.7$ and with $\delta = 0.01$ as infinitesimal-range interactions. The resulting critical values of the transverse field Γ_c are plotted in Fig. 5.9. The figure shows a feature of the result that the system has longer-range interactions, critical transverse field becomes larger. This feature is shared with the pure case [Fig. 5.4].

We next observe the change of the variance V of $(\log \Gamma - \log J)$. The ratio of $\sqrt{V}$ after a renormalization to that before the renormalization is plotted in Fig. 5.10. To show the variation of behavior by changes of δ, the data for some values of δ are contained in the figure. Transverse fields are set to be a little smaller than the critical transverse fields, that is, we have examined the ordered side of the vicinity of the transition point.

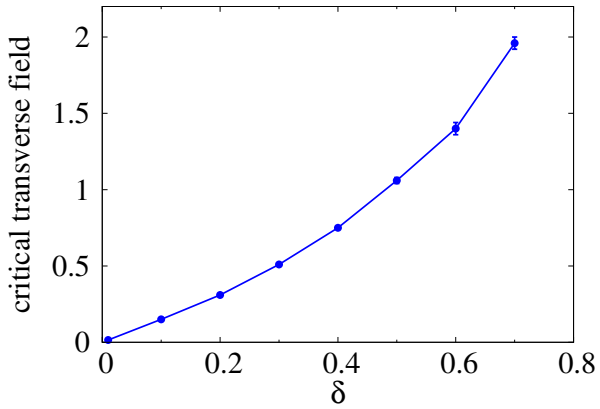

Figure 5.9: Critical transverse fields Γ_c of Ising spin glass in a transverse field with the hierarchical interaction resulting from our renormalization-group calculations.

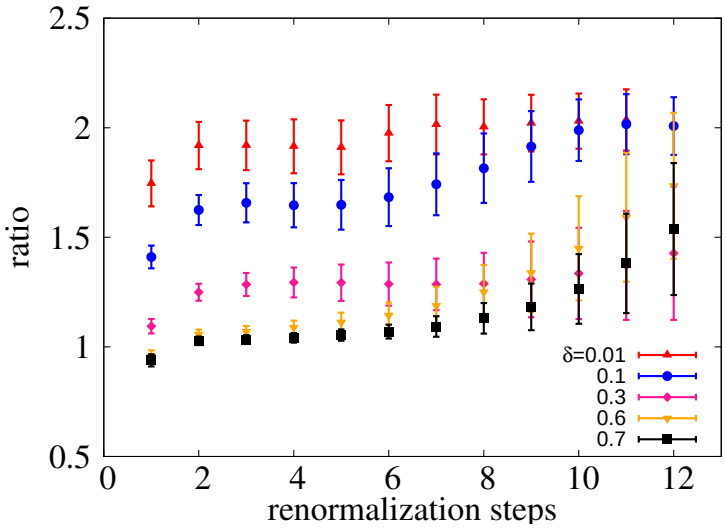

Figure 5.10: Ratio of the square root of the variance of $(\log \Gamma - \log J)$ after a renormalization to that before the renormalization in Ising spin glass in a transverse field with the hierarchical interaction. The data are obtained from the ordered-phase side of the vicinity of the critical point.

In the result of $\delta = 0.01$, the ratio increases at first several steps of the renormalization-group transformation and is always larger than unity, which means that the width of the distribution of parameters keeps growing. This result demonstrates the presence of an infinite-randomness fixed point. After that growth, a stable behavior appears, and the ratio stays around 2. This sequence of behavior has been found also in the result of the system with nearest-neighbor interactions as studied in Chap. 4. Hence, our analysis of the hierarchical model with the short-range limit reproduces the result for the nearest-neighbor interactions. This agreement is reasonable but not self-evident.

As the value of δ rises, the growth of the ratio slows down. In $\delta = 0.7$, the ratio remains almost unity through several times of the renormalization. The ratio, however, grows after 7 steps. This growth is seen also in other δ. The argument mentioned later convinces us that the growth after 7 steps is not concerned with critical phenomena. In the system with $\delta = 0.7$, thus, critical phenomena are not controlled by an infinite-randomness fixed point. This consequence agrees with the previous report [84] that the fixed point for $\alpha' > 1/4$, where $\delta = 2^{-(\alpha'+1)/2} > 0.648$, is not an infinite-randomness fixed point. For $\delta = 0.6$, it is obscure whether the ratio shows a flow to an infinite-randomness fixed point. It is difficult to definitely determine the boundary from our results, since the data have rather large error bars. We can conclude at least that critical phenomena in systems with short-range interactions are governed by infinite-randomness fixed points. This statement has been inferred in the analysis of the mean-field region [84].

It is remarkable that our single scheme yields both the infinite-randomness criticality for small δ and the conventional criticality for large δ. Our analyses of random systems with nearest-neighbor interactions had resulted only in the infinite-randomness criticality, which seems to imply that our method always concludes the presence of an infinite-randomness fixed point regardless of the actual nature. The result of large δ denies this suspicion and supports the validity of our other results in Chap. 4 as well as the result of small δ.

We discuss the growth of the ratio after 7 times of the renormalization. To this end, Fig. 5.11 is provided. The value of δ is 0.7 in this figure. The ratios estimated on both sides of the ordered and disordered phases, of the vicinity of the critical point are plotted in this figure, whereas we have considered the ratio only in the ordered side in Fig. 5.10. Figure 5.11, in addition, includes the plots of $|\Delta - \Delta_c|/\sqrt{V}$. This quantity expresses the distance from a critical point as discussed in Sec. 4.1.1. We interpret a value of $(\Delta - \Delta_c)/\sqrt{V}$ larger than 1 (smaller than -1) as a signal that almost all subsystems exhibit behavior in the disordered (ordered) phase. Further, we can conclude that the system definitely belongs to some phase away from a critical fixed point, when a value of $|\Delta - \Delta_c|/\sqrt{V}$ is larger than 1.

Figure 5.11 shows strange results in the region after 7 times of the renormalization. While the ratio of the ordered side rises, the ratio of the disordered side remains around unity. The difference between the two sides appears around the point where $|\Delta - \Delta_c|/\sqrt{V}$ exceeds unity. Hence, the difference in the ratios may originate from the difference in phases. In particular, the growth of the ratio in the ordered side is derived from the properties of the ordered (spin-glass) phase. The growth therefore is not concerned with critical phenomena. As mentioned earlier, this fact leads to

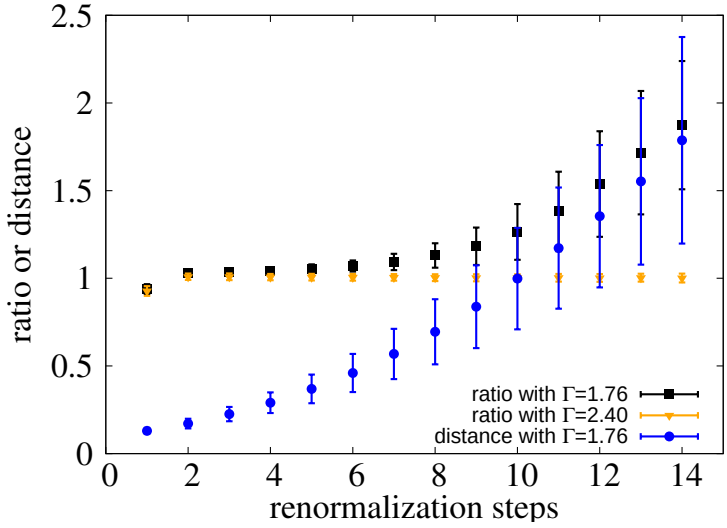

Figure 5.11: Ratio of the square root of the variance of $(\log\Gamma - \log J)$ after a renormalization to that before the renormalization in Ising spin glass in a transverse field with the hierarchical interaction. The parameter δ is set equal to 0.7. Black is data for the ordered-phase side and orange is for the disordered-phase side. Blue is for distance from a transition point.

that the system with $\delta = 0.7$ has no infinite-randomness fixed point. The difference between the two sides in the ratios is unexpected. No similar difference has been found in systems with the nearest-neighbor interactions. The difference in the hierarchical system is thus a special result and might characterize properties of the phases.

The next objective is critical exponents. As in the previous cases, exponent ν for the correlation length is accessible with our method and important to estimate the properties of the fixed point. Reliable values of ν, however, have not been evaluated, since results in this model have unignorable errors as seen in the ratios. This subject is left to future works.

5.4 Summary

We have studied the transverse-field Ising models with the hierarchical interaction, which is similar to the power-law interaction. One of the motivations of this study lies in the fact that the dipolar interaction dominates a compound $LiHo_xY_{1-x}F_4$ [33–36], which is expected to realize the transverse-field Ising model with randomness [29–32]. In addition, a fascinating conjecture has been reported [84] about critical phenomena in the Ising spin glass in a transverse field with the power-law interaction. The conjecture states that critical phenomena for α' $(= a - d)$ $< d/4$ in Eq. (5.13) are governed by an infinite-randomness fixed point. We have tried to examine the conjecture by means of our real-space renormalization group method developed in previous chapters.

We first have applied the method to the transverse-field Ising chain with the hierarchical interaction. The renormalization-group scheme has been analytically performed

and yields transition points and critical exponents. The resulting value of critical exponent ν has a rather large difference from previous results by another approach [88] when α' is small, that is, the long-range region. However, as α' becomes small, the difference decreases, and then the value of ν converges to 1, which is the corresponding value in the nearest-neighbor interacting system. Hence, our method can be qualitatively reliable in the short-range region.

We next have analyzed the Ising spin glass in a transverse field with the hierarchical interaction. The renormalization-group scheme has been numerically iterated. We have evaluated the locations of transition points. In the vicinity of the transition points, we have observed the growth of the variance of $(\log\Gamma - \log J)$ through the renormalization-group transformations. The rapid growth has been found when δ in Eq. (5.57) is small. Our method has concluded as a result that critical phenomena in the short-range region is governed by an infinite-randomness fixed point. As δ becomes large, the growth slows down. For $\delta = 0.7$, the clear growth has not been confirmed, which agrees with a result in a previous study [84]. This agreement supports the validity of our results.

Our method, moreover, has shown a characteristic difference in the variance between the ordered-phase side and the disordered-phase side. This finding might be a clue to a further understanding of the power-law systems with randomness. Critical exponents have not been accurately evaluated yet, since we cannot remove large error bars in the resulting values at the present moment.

Chapter 6

Conclusion

We have investigated the random transverse-field Ising models by means of the real-space renormalization-group method. In particular, we have examined the models to resolve the problem of whether or not the models have infinite-randomness fixed points.

Our renormalization-group procedure has been introduced in Chap. 2 and demonstrated in the transverse-field Ising models in Chap. 3. We divide the system into blocks and define appropriate block Hamiltonians. We keep only the lowest-lying energy eigenstates of the block Hamiltonians and ignore the others. The whole Hamiltonian is reconstructed only with remaining states, and the renormalized Hamiltonian is obtained. We have employed a particular partition which results in preserving the form of the Hamiltonian of the transverse-field Ising chain. The resulting values of the transition point and the critical exponents α and ν agree with the exact solutions. We have generalized this promising method to higher dimensions. In the two-dimensional case, the system is renormalized in two directions: first in the horizontal direction and then in the vertical direction. In the three-dimensional case, the system is renormalized also in the third direction. This generalization also has succeeded in yielding accurate results of the critical exponent ν.

We have approached to one of the main targets in this thesis, the random transverse-field Ising models, in Chap. 4. In the one-dimensional case, the transition point has been analytically calculated under our renormalization-group scheme, and the result agrees with the exact solution. The indefinitely growth is numerically found in the variance of the distributions of $(\log\Gamma - \log J)$, which demonstrates the presence of an infinite-randomness fixed point. This observation also leads to the evaluation of the critical exponent ν. Our analysis in one dimension has reproduced the known exact solutions [19, 20] of the transition point and the critical exponent ν as well as the presence of the fixed point.

In two- and three-dimensional cases, we have investigated the Ising ferromagnet in a transverse field and the Ising spin glass in a transverse field, and have obtained the following results. In the random ferromagnets in a transverse field in two and three dimensions, the presence of infinite-randomness fixed points have been confirmed by observing the unlimited growth of the variance. In addition, the critical exponent ν has been evaluated, and the resulting values are consistent with the previous results [67–69]. Also in the Ising spin glasses in a transverse field in two and three dimensions, we have found evidence of the presence of an infinite-randomness fixed point. We have also

evaluated the critical exponents ν in the spin-glasses, and the resulting values are in good agreement with the corresponding values in the random ferromagnets. This result suggests a nontrivial consequence that the two cases might belong to the same universality class.

Chapter 5 investigates the other of the main targets, the transverse-field Ising chains with the hierarchical interaction. This model is expected to show the similar critical phenomena to the power-law interacting systems. In the analysis of the pure model, we have demonstrated that our method can be qualitatively reliable in the short-range region. Although in the long-range region our result deviates from a previous result of the corresponding power-law interacting system by another approach [84], the difference decreases in the short-range region.

We next have analyzed the Ising spin glass in a transverse field with the hierarchical interaction. The renormalization-group scheme has numerically found the growth of the variance of $(\log\Gamma - \log J)$ in the vicinity of the estimated transition points. The rapid growth has been found if δ in Eq. (5.57) is small. Our method has concluded that critical phenomena in the short-range region is governed by an infinite-randomness fixed point. As δ becomes large, the growth slows down. For $\delta = 0.7$, the clear growth has not been confirmed, which agrees with a result in a previous study of the power-law interacting system [84]. This agreement supports the validity of our results. Our method, moreover, has shown a characteristic difference in the variance between the disordered-phase side and the ordered-phase side. This finding might be a clue to a further understanding of the power-law systems with randomness.

The main result of the present thesis is that we have found evidence of the presence of infinite-randomness fixed points in the two- and three-dimensional Ising spin glasses in a transverse field and in the one-dimensional Ising spin glass with the hierarchical interaction in a transverse field, which have been conjectured by other approaches [5,84]. The result leads to a picture that the presence of the fixed point is not influenced by frustration, which usually produces an essential difference between random ferromagnets and spin glasses.

We can further speculate that Ising spin glasses in a transverse field have the fixed points even if their interactions obey the short-ranged power law, $J_{ij} \propto r^{-\alpha/2}$ with $\alpha \gg 5d/4$, which would include the dipolar interaction, proportional to r^{-3}, with randomness in three dimensions. If that is the case, materials which realize the model should have the nature of the fixed point. This speculation suggests that the reason why the properties of the fixed point have not been found in $LiHo_xY_{1-x}F_4$ [31] is not due to the dipolar interaction in the compound.

Finally, we mention some remaining issues in our study. The validity of our renormalization-group method is not readily obvious because it drops higher-energy eigenstates in the block Hamiltonians. Although the consistencies of our results with previous studies would justify our procedures as a method to extract the essential features of random quantum systems, it is necessary to establish methods to evaluate other critical exponents to reinforce the quantitative reliability of the present method. A method for critical exponents in the hierarchical spin-glass case is especially needed. The correspondence in properties of quantum critical phenomena between the power-law systems and the hierarchical systems remains unclear in our study. To clarify this

point is essential in applying our results to real physical systems. These issues should be resolved in future.

Bibliography

[1] H. Nishimori and G. Ortiz, *Elements of Phase Transitions and Critical Phenomena*, Oxford University Press, 2011.

[2] N. Goldenfeld, *Lectures On Phase Transitions And The Renormalization Group*, Westview Press, 1992.

[3] K. G. Wilson and J. Kogut, Phys. Rep. **12**, 75 (1974).

[4] A. B. Harris, J. Phys. C **7**, 1671 (1974).

[5] O. Motrunich, S.-C. Mau, D. A. Huse, and D. S. Fisher, Phys. Rev. B **61**, 1160 (2000).

[6] T. Vojta, J. Phys. A **39**, R143 (2006).

[7] A. Aharony and A. B. Harris, Phys. Rev. Lett. **77**, 3700 (1996).

[8] S. Wiseman and E. Domany, Phys. Rev. Lett. **81**, 22 (1998).

[9] C. Holm and W. Janke, Phys. Rev. B **48**, 936 (1993).

[10] A. M. Ferrenberg and D. P. Landau, Phys. Rev. B **44**, 5081 (1991).

[11] H. G. Ballesteros et al., Phys. Rev. B **58**, 2740 (1998).

[12] D. S. Fisher, Physica A **263**, 222 (1999).

[13] B. M. McCoy and T. T. Wu, Phys. Rev. **176**, 631 (1968).

[14] B. M. McCoY and T. T. WU, Phys. Rev. **188**, 982 (1969).

[15] B. M. McCoY, Phys. Rev. **188**, 1014 (1969).

[16] B. M. McCoy, Phys. Rev. B **2**, 2795 (1970).

[17] R. B. Griffiths, Phys. Rev. Lett. **23**, 17 (1969).

[18] Y. Imry, Phys. Rev. B **15**, 4448 (1977).

[19] D. S. Fisher, Phys. Rev. Lett. **69**, 534 (1992).

[20] D. S. Fisher, Phys. Rev. B **51**, 6411 (1995).

[21] T. Vojta and J. Schmalian, Phys. Rev. B **72**, 045438 (2005).

[22] M. Suzuki, Prog. Theor. Phys. **56**, 1454 (1976).

[23] P. Pfeuty, Ann. Phys. **57**, 79 (1970).

[24] S. Sachdev, *Quantum Phase Transitions*, Cambridge University Press, 2011.

[25] S. Suzuki, J.-i. Inoue, and B. K. Chakrabarti, *Quantum Ising Phases and Transitions in Transverse Ising Models*, Springer, 2012.

[26] E. Fradkin and L. Susskind, Phys. Rev. D **17**, 2637 (1978).

[27] P. Pfeuty and R. J. Elliott, J. Phys. C **4**, 2370 (1971).

[28] P. Pfeuty, Phys. Lett. A **72**, 245 (1979).

[29] D. H. Reich et al., Phys. Rev. B **42**, 4631 (1990).

[30] W. Wu, B. Ellman, T. F. Rosenbaum, G. Aeppli, and D. H. Reich, Phys. Rev. Lett. **67**, 2076 (1991).

[31] W. Wu, D. Bitko, T. F. Rosenbaum, and G. Aeppli, Phys. Rev. Lett. **71**, 1919 (1993).

[32] D. Bitko, T. F. Rosenbaum, and G. Aeppli, Phys. Rev. Lett. **77**, 940 (1996).

[33] P. E. Hansen, T. Johansson, and R. Nevald, Phys. Rev. B **12**, 5315 (1975).

[34] P. Beauvillain, J. P. Renard, I. Laursen, and P. J. Walker, Phys. Rev. B **18**, 3360 (1978).

[35] A. H. Cooke, D. A. Jones, J. F. A. Silva, and M. R. Wells, J. Phys. C **8**, 4083 (1975).

[36] G. Mennenga, L. de Jongh, and W. Huiskamp, J. Mag. Magn. Mater. **44**, 59 (1984).

[37] S. M. A. Tabei, M. J. P. Gingras, Y.-J. Kao, P. Stasiak, and J.-Y. Fortin, Phys. Rev. Lett. **97**, 237203 (2006).

[38] S.-k. Ma, C. Dasgupta, and C.-k. Hu, Phys. Rev. Lett. **43**, 1434 (1979).

[39] C. Dasgupta and S.-k. Ma, Phys. Rev. B **22**, 1305 (1980).

[40] F. Iglói and C. Monthus, Phys. Rep. **412**, 277 (2005).

[41] R. Shankar and G. Murthy, Phys. Rev. B **36**, 536 (1987).

[42] A. P. Young and H. Rieger, Phys. Rev. B **53**, 8486 (1996).

[43] F. Iglói and H. Rieger, Phys. Rev. Lett. **78**, 2473 (1997).

[44] F. Iglói and H. Rieger, Phys. Rev. B **57**, 11404 (1998).

[45] D. S. Fisher and A. P. Young, Phys. Rev. B **58**, 9131 (1998).

[46] F. Y. Wu, Rev. Mod. Phys. **54**, 235 (1982).

[47] T. Senthil and S. N. Majumdar, Phys. Rev. Lett. **76**, 3001 (1996).

[48] E. Carlon, P. Lajkó, and F. Iglói, Phys. Rev. Lett. **87**, 277201 (2001).

[49] E. Carlon, C. Chatelain, and B. Berche, Phys. Rev. B **60**, 12974 (1999).

[50] D. S. Fisher, Phys. Rev. B **50**, 3799 (1994).

[51] K. Damle, O. Motrunich, and D. A. Huse, Phys. Rev. Lett. **84**, 3434 (2000).

[52] O. Motrunich, K. Damle, and D. A. Huse, Phys. Rev. B **63**, 134424 (2001).

[53] F. D. M. Haldane, Phys. Lett. A **93**, 464 (1983).

[54] R. A. Hyman and K. Yang, Phys. Rev. Lett. **78**, 1783 (1997).

[55] C. Monthus, O. Golinelli, and T. Jolicœur, Phys. Rev. Lett. **79**, 3254 (1997).

[56] A. Saguia, B. Boechat, and M. A. Continentino, Phys. Rev. Lett. **89**, 117202 (2002).

[57] Y. Nishiyama, Physica A: Statistical Mechanics and its Applications **252**, 35 (1998).

[58] Y. Nishiyama, Eur. Phys. J. B **6**, 335 (1998).

[59] K. Hida, Phys. Rev. Lett. **83**, 3297 (1999).

[60] S. Bergkvist, P. Henelius, and A. Rosengren, Phys. Rev. B **66**, 134407 (2002).

[61] G. Refael, S. Kehrein, and D. S. Fisher, Phys. Rev. B **66**, 060402 (2002).

[62] K. Damle and D. A. Huse, Phys. Rev. Lett. **89**, 277203 (2002).

[63] C. Pich, A. P. Young, H. Rieger, and N. Kawashima, Phys. Rev. Lett. **81**, 5916 (1998).

[64] Y.-C. Lin, N. Kawashima, F. Iglói, and H. Rieger, Prog. Theor. Phys. Suppl. **138**, 479 (2000).

[65] D. Karevski, Y.-C. Lin, H. Rieger, N. Kawashima, and F. Iglói, Euro. Phys. J. B **20**, 267 (2001).

[66] I. A. Kovács and F. Iglói, Phys. Rev. B **80**, 214416 (2009).

[67] I. A. Kovács and F. Iglói, Phys. Rev. B **82**, 054437 (2010).

[68] I. A. Kovács and F. Iglói, Phys. Rev. B **83**, 174207 (2011).

[69] I. A. Kovács and F. Iglói, J. Phys.: Condens. Matter **23**, 404204 (2011).

[70] O. Dimitrova and M. Mzard, J. Stat. Mech. **2011**, P01020 (2011).

[71] C. Monthus and T. Garel, J. Phys. A **45**, 095002 (2012).

[72] C. Monthus and T. Garel, J. Stat. Mech. **2012**, P01008 (2012).

[73] C. Monthus and T. Garel, J. Stat. Mech. **2012**, P05002 (2012).

[74] C. Monthus and T. Garel, J. Stat. Mech. **2012**, P09016 (2012).

[75] C. Monthus and T. Garel, J. Stat. Mech. **2012**, P10010 (2012).

[76] K. Binder and A. P. Young, Rev. Mod. Phys. **58**, 801 (1986).

[77] K. H. Fischer and J. A. Hertz, *Spin Glasses*, Cambridge University Press, 1993.

[78] M. A. Ruderman and C. Kittel, Phys. Rev. **96**, 99 (1954).

[79] T. Kasuya, Prog. Theor. Phys. **16**, 58 (1956).

[80] K. Yosida, Phys. Rev. **106**, 893 (1957).

[81] S. F. Edwards and P. W. Anderson, J. Phys. F **5**, 965 (1975).

[82] M. Guo, R. N. Bhatt, and D. A. Huse, Phys. Rev. Lett. **72**, 4137 (1994).

[83] H. Rieger and A. P. Young, Phys. Rev. Lett. **72**, 4141 (1994).

[84] A. Dutta, Phys. Rev. B **65**, 224427 (2002).

[85] R. Miyazaki, H. Nishimori, and G. Ortiz, Phys. Rev. E **83**, 051103 (2011).

[86] R. Miyazaki and H. Nishimori, Phys. Rev. E **87**, 032154 (2013).

[87] A. Aharony, Dependence of universal critical behaviour on symmetry and range of interaction, in *Phase Transitions and Critical Phenomena*, edited by C. Domb and M. S. Green, volume 6, chapter 6, Academic Press, 1976.

[88] A. Dutta and J. K. Bhattacharjee, Phys. Rev. B **64**, 184106 (2001).

[89] A. P. Young, J. Phys C **8**, L309 (1975).

[90] P. R. Gerber and H. Beck, J. Phys. C **10**, 4013 (1977).

[91] F. Iglói, Phys. Rev. B **65**, 064416 (2002).

[92] L. P. Kadanoff, Physics **2**, 263 (1966).

[93] S. D. Drell, M. Weinstein, and S. Yankielowicz, Phys. Rev. D **16**, 1769 (1977).

[94] R. Jullien, P. Pfeuty, J. N. Fields, and S. Doniach, Phys. Rev. B **18**, 3568 (1978).

[95] G. Um, Phys. Rev. B **15**, 2736 (1977).

[96] J. E. Hirsch and G. F. Mazenko, Phys. Rev. B **19**, 2656 (1979).

[97] B. Hu, Phys. Lett. A **71**, 83 (1979).

[98] E. Fradkin and S. Raby, Phys. Rev. D **20**, 2566 (1979).

[99] A. Fernandez-Pacheco, Phys. Rev. D **19**, 3173 (1979).

[100] A. Pelissetto and E. Vicari, Phys. Rep. **368**, 549 (2002).

[101] H. W. J. Blote, E. Luijten, and J. R. Heringa, J. Phys. A **28**, 6289 (1995).

[102] K. Uzelac, R. Jullien, and P. Pfeuty, J. Phys. A **13**, 3735 (1980).

[103] J. T. Chayes, L. Chayes, D. S. Fisher, and T. Spencer, Phys. Rev. Lett. **57**, 2999 (1986).

[104] J. Chayes, L. Chayes, D. Fisher, and T. Spencer, Commun. Math. Phys. **120**, 501 (1989).

[105] F. D. Nobre, Phys. Rev. E **64**, 046108 (2001).

[106] A. Auerbach, *Interacting Electrons and Quantum Magnetism*, Springer, 1998.

[107] A. Campa, T. Dauxois, and S. Ruffo, Physics Reports **480**, 57 (2009).

[108] W. Thirring, Z. Phys. **235**, 339 (1970).

[109] J. Barré, D. Mukamel, and S. Ruffo, Phys. Rev. Lett. **87**, 030601 (2001).

[110] J. M. Kosterlitz and D. J. Thouless, J. Phys. C **5**, L124 (1972).

[111] G. Kotliar, P. W. Anderson, and D. L. Stein, Phys. Rev. B **27**, 602 (1983).

[112] H. G. Katzgraber and A. P. Young, Phys. Rev. B **72**, 184416 (2005).

[113] L. Leuzzi, G. Parisi, F. Ricci-Tersenghi, and J. J. Ruiz-Lorenzo, Phys. Rev. Lett. **103**, 267201 (2009).

[114] M. A. Moore, Phys. Rev. B **82**, 014417 (2010).

[115] T. Mori, Phys. Rev. E **84**, 031128 (2011).

[116] F. Dyson, Commun. Math. Phys. **12**, 91 (1969).

[117] R. B. Griffiths, J. Math. Phys. **8** (1967).

[118] M. E. Fisher, S.-k. Ma, and B. G. Nickel, Phys. Rev. Lett. **29**, 917 (1972).

[119] J. Sak, Phys. Rev. B **8**, 281 (1973).

[120] A. Theumann, Phys. Rev. B **21**, 2984 (1980).

[121] A. Theumann, Phys. Rev. B **22**, 5441 (1980).

[122] J. A. Hertz and P. Sibani, Physica Scr. **1985**, 199 (1985).

[123] P. Sibani and J. A. Hertz, J. Phys. A **18**, 1255 (1985).

[124] G. J. Rodgers and A. J. Bray, J. Phys. A. **21**, 2177 (1988).

[125] S. Franz, T. Jrg, and G. Parisi, J. Stat. Mech. **2009**, P02002 (2009).

[126] M. Castellana, A. Decelle, S. Franz, M. Mézard, and G. Parisi, Phys. Rev. Lett. **104**, 127206 (2010).

[127] M. Castellana and G. Parisi, Phys. Rev. E **82**, 040105 (2010).

[128] M. Castellana and G. Parisi, Phys. Rev. E **83**, 041134 (2011).